FABRICATION AND MODIFICATION OF IMPLANTABLE MICRO-PROBES FOR NEURO-STUDIES

by

HUNG VIET CAO

Presented to the Faculty of the Graduate School of

The University of Texas at Arlington in Partial Fulfillment

of the Requirements

for the Degree of

DOCTOR OF PHILOSOPHY

THE UNIVERSITY OF TEXAS AT ARLINGTON

May 2012

ProQuest LLC.
789 East Eisenhower Parkway
P.O. Box 1346
Ann Arbor, MI 48106 - 1346

ACKNOWLEDGEMENTS

I would like to express my appreciation and thankfulness to my supervising professor Dr. Jung-Chih Chiao. His support and encouragement have enlightened me to finish this work and inspired me to follow a bright research life ahead. My sincere appreciation also extends to Dr. Peng (co-adviser), Dr. Bredow, Dr. Davis and Dr. Iqbal to be on my comprehensive exam committee. I also want to thank my collaborators Dr. Mohanty and Dr. Gu in Physics Department; Ai-Ling in Dr. Peng's lab; and Dr. Gerhardt at University of Kentucky for his precious discussions.

I appreciate UTA Nanofab center and UTD cleanroom research laboratory for giving me excellent facilities and good working environments. All of my work could not be done without the hi-tech equipment and help from the staff. A special thank is sent to the CONTACT program which brought a chance to me to do fabrication at UTD. I am also thankful to my research group members; especially those who worked with me in the neurotransmitters and sensors projects; and all of my friends for giving me suggestions and information to finish this work.

I would like to express my gratitude to my wife Trang and my kids Son and Phong for being here and supporting me all the time. Furthermore, I would like to thank my father and my sister. Their academic success is a great inspiration for my endeavors.

March 25, 2012

ABSTRACT

FABRICATION AND MODIFICATION OF

IMPLANTABLE MICRO-PROBES

FOR NEURO-STUDIES

Hung Viet Cao, PhD

The University of Texas at Arlington, 2012

Supervising Professors: Dr. Jung-Chih Chiao and Dr. Yuan Bo Peng

In this work, different types of implantable probes fabricated on Si and polyimide substrates for sensing neurotransmitters, recording extracellular action potentials and stimulating the neurons have been developed. Several electrode configurations have been designed for implantation at various locations in the central nervous system. Each probe contains a multi electrode array (MEA) of 3, 5, 7 or 16 metal electrodes (Au or Pt) fabricated by electron-beam evaporation and lift-off processes.

For sensing purpose, as a proof-of-principle, dopamine (DA) and L-glutamate sensors have been implemented. The surface of electrodes was modified with nanostructures by different methods appropriate to the substrate and electrode material to enhance the performance of the sensors. Self-referencing technique and selective

membrane deposition were also used to get better selectivity and limit of detection (LOD). A reference electrode was implemented in the same probe with the working electrodes, which presented an integrated, compact and robust system. A Ag/AgCl thin film reference electrode was used as the traditional method and pseudo-reference electrodes using IrO_x film were also developed to solve the biocompatibility issue. Cell and animal experiments were carried out to prove the performance.

A method to modify the working electrode with nanowires using the vapor-liquid-solid (VLS) mechanism was realized with Si based probes containing an MEA of Pt, in order to increase the sensitivity of the electrochemical neurotransmitter sensors. The sensor probes were manufactured from a 300 μm thick 4-inch silicon (Si) wafer and then tailored into individual probes. The surfaces of electrodes were observed and characterized by scanning electron microscopy (SEM) and cyclic voltammetry (CV). With polyimide substrate, the probes were fabricated from a 125 μm thick Kapton sheet (*Dupont*). The flexibility of the probe helps to prevent scar forming in tissues aiming for long-term *in vivo* monitoring. A comparison between Au and Pt thin films was conducted by cyclic voltammetry. Several low-temperature processes were tried to modify the electrode surfaces with nanoparticles. The complete devices were made and used to demonstrate the enhancement in performance contributed by nanostructures in the enzyme-based electrochemical sensing of L-glutamate and DA. Comparison between electrodes with and without nanostructures modification was conducted showing that the modification methods were better to improve the performance of electrochemical sensors. *In vivo* experiments were also

carried out to demonstrate the capability of the sensor with the live animals. A pain study was followed with approved protocols to prove that the sensor could distinguish different levels of excitations.

Those probes were also tested to record action potentials.

For stimulation, the above-mentioned probes could be used to electrically stimulate the neurons like the traditional approaches. Beside, a specially-configured probe was designed for optical stimulation as well. The probe was implemented to have three action potential recording electrodes and two bigger pads to mount a commercially available micro-LED for generating the stimulation light. Transgenic mice with visual cortex expressing channelrhodopsin-2 (ChR2) were used to test the performance of the integrated probes. The result was compared with that recorded by a conventional tungsten electrode. Data showed that the device was capable of stimulating as well was recording the neuron activities.

TABLE OF CONTENTS

ACKNOWLEDGEMENTS iii

ABSTRACT iv

LIST OF ILLUSTRATIONS xi

Chapter Page

1. INTRODUCTION 1

1.1 Neuroscience 1

1.2 Neurons and Disorders 2

1.3 Action Potentials and Neurotransmitters 4

1.4 Conventional Methods 5

1.4.1 Action Potentials 5

1.4.2 Neurotransmitters 6

1.5 Neuron Stimulation 7

1.6 Proposed Approaches 8

2. NANOWIRE MODIFICATION TO ENHANCE THE PERFORMANCE OF NEUROTRANSMITTER SENSORS 10

2.1 Introduction 10

2.2 Fabrication 13

2.3 Characterization 14

2.4 Sensor Preparation and Experiment Setup 16

2.4.1 Sensor Preparation 16

2.4.2 Experiment setup 17

2.5 Results and Discussions 18

2.6 Conclusions 20

3. A FULLY-INTEGRATED FLEXIBLE IMPLANTABLE L-GLUTAMATE SENSOR 22

3.1 Introduction 22

3.2 Fabrication 23

3.3 Device Characterization 26

3.4 Reference Electrode 28

3.4.1 Ag/AgCl reference electrode 28

3.4.2 IrO_x pseudo-reference electrode 29

3.4.2.1 Solution preparation 30

3.4.2.2 Process 31

3.4.2.3 Stability test 32

3.4.2.4 Biocompatibility test 34

3.5 Sensor Preparation 34

3.5.1 Dopamine and H_2O_2 calibrations 34

3.5.2 Enzyme-based L-glutamate sensor 36

3.5.2.1 Meta-Phenylenediamine selective membrane 37

3.5.2.2 Self-referencing technique 37

3.6 L-glutamate Calibration Results and Discussions 39

3.6.1 Using Ag/AgCl reference electrode 39

3.6.2 Using IrO_x as reference electrode 41

3.7 Flexibility 42

3.8 Conclusions 43

4. A MICRO-LED INTEGRATED PROBE FOR OPTOGENETICS STIMULATIONS 44

4.1 Introduction 44

4.2 Materials and Methods 47

4.2.1 Optrode design 47

4.2.2 Animal preparation 50

4.2.3 In vivo Stimulation and Recordings using μLED-optrode 52

4.2.4 Histological Evaluation 53

4.3 Results and Discussions 55

4.3.1 μLED-intensity Dependent Neuronal Spiking Recorded by Optrode 55

4.3.2 μLED-intensity Dependent Neuronal Spiking Recorded by Tungsten Electrode 55

4.3.3 μLED-frequency Dependent Neuronal Spiking in Visual Cortex Measured by Optrode 57

4.4 Conclusions 60

5. OTHER DEVICES 61

5.1 Dopamine Sensors 61

5.2 Long Probes for Monkey Studies 63

5.3 Using Thermal Actuator to Control the Penetration Depth of the Implantable Probes 63

5.4 Simple Nanostructures Modification 65

5.5 Au Nanoparticles Modification by Using Cysteamine 67

5.6 Au Nanoparticles Modification by Electrodeposition 68

5.7 3D MEA 70

6. SOME CASE STUDIES 72

6.1 Pain Management 72

6.1.1 Motivation and background 72

6.1.2 Rat model experiments 74

6.2 Addiction Studies 77

7. FUTURE WORK 80

7.1 Long-term Implant 80

7.2 Correlation of Signals 82

7.3 LED Arrays 84

7.4 Future Work Summary 85

APPENDIX

A. ENZYME COATING PROCEDURES 86

B. REFERENCE ELECTRODE PROCEDURES 89

C. H&E STAINING 92

REFERENCES 94

BIOGRAPHICAL INFORMATION 104

LIST OF ILLUSTRATIONS

Figure Page

1.1 Sketch of a neuron. Adapted from [1.2]……1

1.2 Signaling mechanism of a neuron. Adapted from [1.1].....3

1.3 A carbon fiber electrode (left) [1.3] and a 3D Utah-type electrode array (right), adapted from [1.4]...……..……...5

2.1 Fabrication processes: A. Thermal oxidation.
B. Pattern Au/Ti layers by lift-off.
C. Grow the Si-nanowires by the VLS method.
D. Pattern the Pt/Ti layer by lift-off.
E. Pattern SiO_2 as the insulation layer.
F. Machining the probe by laser……..12

2.2 (a) Electrode configurations.
(b) An SEM image showing the probe tip.
(c) Two probing devices with different lengths of probes.
(d) The complete probing system with connections to the recorder ready for implantation……...……..14

2.3 An SEM image of the Si-nanowires modified surface……...15

2.4 SEM images of (a) a Pt thin film on a Si substrate without surface modification and (b) a Pt thin film on the Si-nanowires modified silicon wafer…….……...15

2.5 CV for the electrodes with and without nanowires modification……...16

2.6 Experiment setup for calibration…….17

2.7 Sensor responses at different concentrations of L-glutamate for sensors (a) without and (b) with Si-nanowires modification on the sensing electrodes……18

3.1 Fabrication processes……..23

3.2 (a) SEM image of the probe tip and
(b) a photo of the assembled devices……..……24

3.3 Cyclic voltammetry plots: (a) Pt thin film versus an Ag/AgCl
electrode in N_2-bubbled 1 M H_2SO_4 at 100 mV/s and
(b) Au thin film versus an Ag/AgCl electrode in
0.1 M PBS at 50 mV/s……..……..25

3.4 Optical microscope photos of thin films Pt/Cr/PI, Pt/Cu/Cr/PI
and Pt/Au/Cr/PI (left to right)..……...27

3.5 SEM images show the comparison between Pt/Au/Cr film (left)
and Pt/Cr film (right)..……27

3.6 Energy-dispersive X-ray analysis of the electroplated
Ag/AgCl thin film electrode..……29

3.7 SEM images of the IrO_x film deposited on Au electrode with
different electrodeposition parameters (a) fixed potential 0.8 V
(b) CV in 15 minutes at 50 mV/s in 0-0.9 V
(c) CV in 15 minutes at 50 mV/s in 0-0.8 V
(d) CV in 15 minutes at 50 mV/s in 0-0.7 V..……30

3.8 The potential measurement between IrO_x electrode and
Ag/AgCl commercial reference electrode..……32

3.9 Biocompatibility tests with IrO_x, AgCl and Au (as control).
(a) and (b) are day 1 and day 3 results respectively.……...33

3.10 H_2O_2 calibrations using commercial Ag/AgCl reference electrode
and IrO_x reference electrode (blue curve).……34

3.11 DA calibration comparison between Ag/AgCl
and IrO_x reference electrodes.……..35

3.12 (a) Cross section of the modified surface electrode and
(b) an SEM image of the protein matrix..……36

3.13 L-glutamate responses for the probes: (a) with mPD-coated electrodes
and (b) using the self-referencing technique…….38

3.14 Comparison of limit of detection, sensitivity, linearity and variability……39

3.15 L-glutamate response of the Kapton sensor probe with integrated IrO_x pseudo-reference electrode..……41

3.16 Flexibility of the integrated probe……42

4.1 (a) Principle of optogenetics.
(b) Direct versus indirect activation……46

4.2 Fabrication processes……..48

4.3 (a) Image of the optrode assembled on a printed circuit board, compared to a US dime. The probe shaft was implantable with the circuit board outside the body to connect to a wearable module for animal experiments. The circuit board was made larger than necessary for the convenience of handling and connecting during experiments.
(b) SEM image of the optrode showing the μLED.
(c) Side-view photo in which a photo-polymerized lens was formed on the μLED.
(d) Light generated by the optrode at a forward bias of 2.9 V…….……...50

4.4 (a) Schematic of the optrode-based stimulation/recording experimental setup. (b) Photo of the experimental setup.
(c) Raw electrical recordings for 20 s from two electrode channels in the optrode…….……..51

4.5 (a) Coronal and (b) Sagittal histological sections of the mice brain. Arrows point to the optrode insertion site. Scale bar: 400 μm.
(c) Confocal fluorescence image of cortical brain region in the slice. Scale bar: 100 μm……..…….53

4.6 (a) Rate-histogram of spikes measured by the microelectrode at the tip of the optrode, from two light-responsive units stimulated by different intensities of the optrode-μLED at a frequency of 10 Hz.
(b) Corresponding inter-spike intervals as a function of time with varying intensities of stimulation in the optrode-μLED…….54

4.7 (a) Rate-histogram of spikes measured by a separate tungsten electrode, from two light-responsive units stimulated by different intensities of the optrode-μLED at a frequency of 10 Hz. (b) Corresponding inter-spike intervals as a function of time with varying intensities of stimulation by the optrode-μLED…….……..56

4.8 (a) Raw electrical recording from visual cortex using the microelectrode at the tip of the optrode, in response to optrode-μLED stimulation at varying frequencies. (b) Rate-histogram of spikes from neurons stimulated by optrode-μLED with different frequencies at a power density of 0.7 mW mm^{-2}. (c) Corresponding inter-spike interval as a function of time with varying frequencies of stimulation by the optrode-μLED…..…….58

5.1 An SEM image and dopamine response from our CFE……..62

5.2 Effect of excessive Nafion on a Pt electrode……..63

5.3 A 65-mm long probe in comparison with others……64

5.4 The conceptual design of using thermal actuator to control the probe……...65

5.5 Nanoparticles concentration processes. (a) Original solution. (b) After centrifugation. (c) Two after ultrasonication (left) Compared with the original one (right)……66

5.6 SEM images of (a) the Au nanoparticle-modified surface and (b) the Ag nanostructures on the electrode surface.……67

5.7 Concept and a demonstration of Au nanoparticles modification by using Cysteamine. Adapted from [5.1]……..68

5.8 SEM images of the nanomodification electrodeposition method……...69

5.9 3D electrode probe by stacking single ones……70

6.1 (a) The flexible sensor probe was inserted into the L3 region of the spinal cord.(b) The recorded signals show the L-glutamate releases in response to graded stimuli in the leg……75

6.2 AP recordings at the thalamus with respect to pressure stimuli using (a) Au electrode and (b) Pt electrode..……77

6.3 DA responses in NAcc with respect to injection to the thigh of (a) 0.3 ml morphine and (b) 0.25 ml cocaine…..…….79

7.1 Photo of the stained slices at the implantation sites……80

7.2 A stained brain slice showing the damages caused by the probes……..81

7.3 Our future probe with different sensors and AP recording electrodes.
The size is 10×10 μm^2…….82

7.4 Different LED arrays designs. The yellow square shows
the electrodes to record the AP...……84

CHAPTER 1

INTRODUCTION

1.1 Neuroscience

Neuroscience has been known as the scientific study of the nervous system and considered as a branch of biology. Nevertheless, nowadays it is an interdisciplinary field that attracts the attention of various majors such as chemistry, computer science, engineering, mathematics, medicine, philosophy, physics, and psychology. The overall objective of neuroscience is to study all aspects of the nervous system, including molecular, cellular, developmental, structural, functional, evolutionary, computational, and medical ones. Traditionally, there are five experimental trends in neuroscience: Anatomy, Embryology, Physiology, Pharmacology, and Psychology. Basically, Anatomy is about nerve cells (neuron), Embryology is about dendrites and axons, Physiology is about electrical signal produced by neurons (action potential), Pharmacology is about receptors and chemicals released by neurons (neurotransmitters), and Psychology is about behavior studies. This dissertation is mainly focused on Pharmacology and slightly goes through Physiology by discussing the implementation of implantable devices to detect neurotransmitters and action potentials for neuroscience studies [1.1-1.2]. Neurons stimulation is also mentioned by proposing and implementing a newly developed method named optogenetic stimulation in which light was used instead of electrical pulses to make the cells depolarized.

1.2 Neurons and Disorders

There are two major cell types in the nervous system, neurons and glial cells (or glia). While neurons enable the nervous system to carry out all the complex functions, glial cells support them to work optimally. Typically, a neuron consists of cell body (soma), dendrites, axon and presynaptic terminals. The cell body contains the nucleus, which stores the genes of the cell and the endoplasmic reticulum where the cell's proteins are synthesized. Dendrites receive the incoming signals from other neurons. These inputs converge and are integrated in the soma. Axon conveys information in the form of action potentials along its length from the soma to the presynaptic terminals where neurotransmitters can be released to communicate with adjacent neurons. These are illustrated in Fig. 1.1.

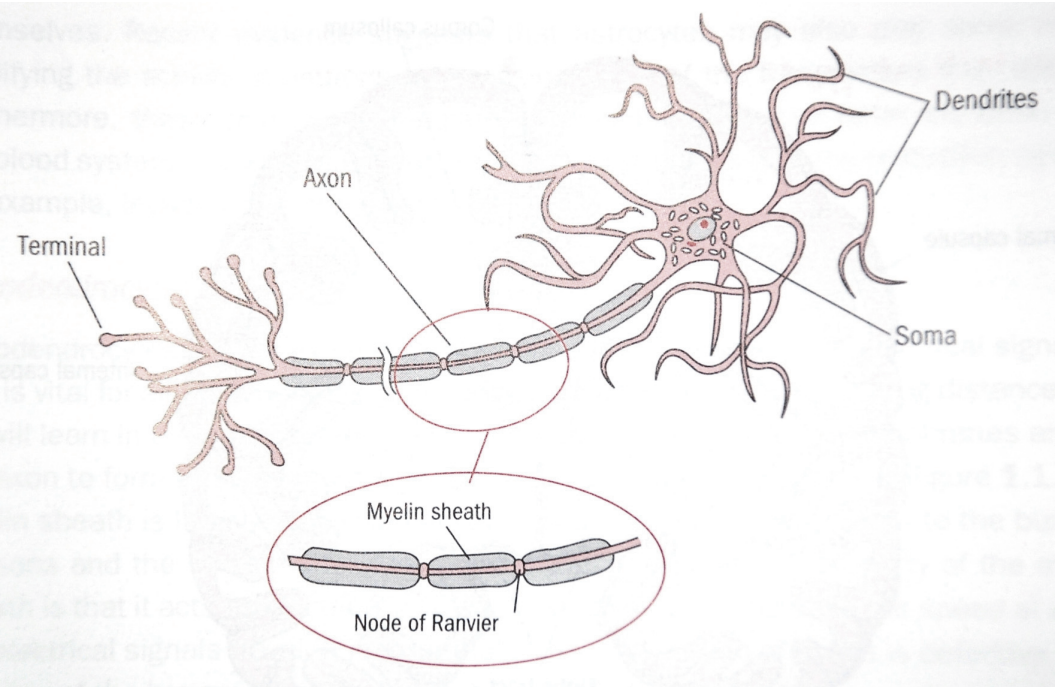

Figure 1.1 Sketch of a neuron. Adapted from [1.2].

Myelin sheath is the fatty insulation layer made of glia wrapped around the axon to increase the speed of the propagated action potentials. The node of Ranvier is like a repeater station which regenerates the action potentials to keep their amplitude [1.1-1.2].

Neuro-disorders could be any malfunctions in the neurons. It could be caused by genes, aging, accident, etc that affect the operation of neurons. Since neurons are fundamental units that control all of the body activities, studying their functions and problems is extremely important.

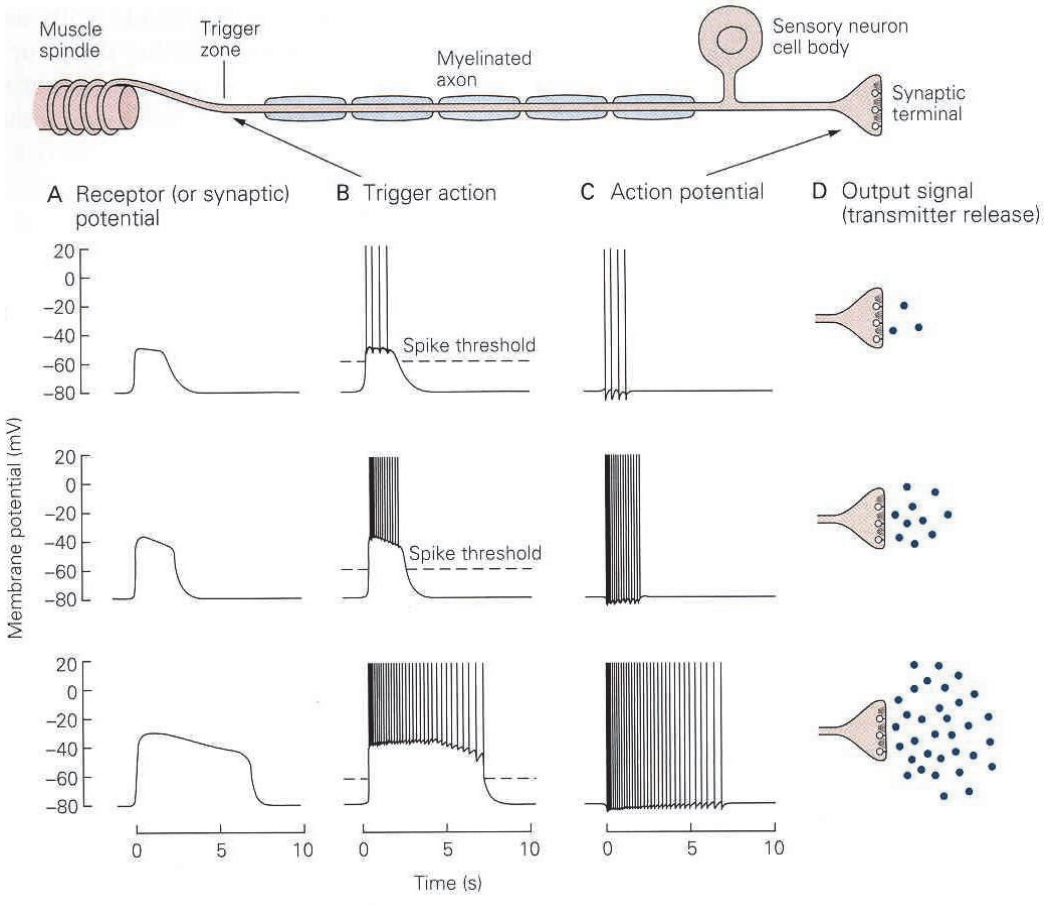

Figure 1.2 Signaling mechanism of a neuron. Adapted from [1.1].

1.3 Action Potentials and Neurotransmitters

Action potentials are the signals by which the brain receives, analyzes and conveys information. They are rapid and transient; with amplitude of 100 mV and duration of about 1 ms. The information carried by an action potential is determined not by the form of the signal but by the pathway of it in the brain. Action potentials are initiated at a special region at the origin of the axon called axon hillock, and then they are conducted along the axon at rates of 1-100 m/s.

Corresponding to the action potentials which carry signals inside neurons, neurotransmitters are the chemicals used for inter-neuron communications. Typically, the intensity of the action potentials and the concentrations of neurotransmitters are proportional. These are shown in Fig 1.2.

There are a lot of different chemicals that act as neurotransmitters in the nervous system but there are three main categories:

- Amino acids, such as L-glutamate, gamma-aminobutyric acid (GABA), glycine, etc.
- Neuropeptides, such as vasopressin, somatostatin and neurotensin.
- Monoamines, such as dopamine, serotonin, acetylcholine, etc.

Action potential is unique but neurotransmitter has different types depending on the neuron. A neuron which releases L-glutamate is termed glutamatergic, and similar things are applied with GABA (GABAergic) and dopamine (dopaminergic) ones, and etc. Both action potentials and neurotransmitters are important factors to study the

operation of neurons and a correlation of these two would give a much better understanding about neuronal activities.

1.4 Conventional Methods

1.4.1 Action potentials

The conventional devices that have been used to record the extracellular action potentials are the single tungsten probe, the single and bundle carbon fiber electrodes and the Utah-type 3D electrode array. These could be inserted into the brain or spinal cord to record the action potentials in an experiment or implanted for long-term recordings. Nevertheless, the single-electrode ones lack the capability to record multiple signal simultaneously and when they are bundled, the distances among electrodes are not controllable. The silicon base 3D electrode array is not biocompatible for long-term implants. Some of the conventional electrodes are shown in Fig. 1.3.

1.4.2 Neurotransmitters

Monitoring concentrations of neurotransmitters extracellularly in a mammalian

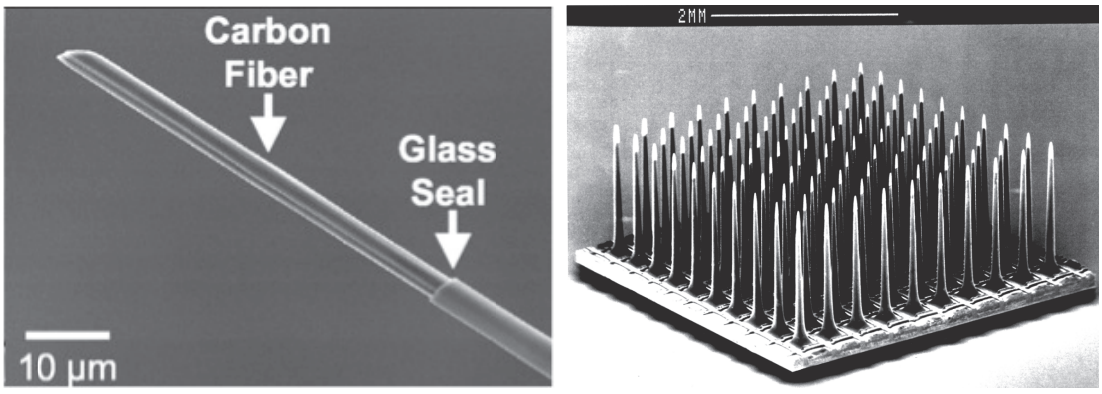

Figure 1.3 A carbon fiber electrode (left) [1.3] and a 3-D Utah-type electrode array (right), adapted from [1.4].

CNS helps to understand their roles associated with numerous neurological disorders, such as Parkinson's disease, Alzheimer's disease, depression, addiction, chronic pain, etc. The technique of using microdialysis probes enables the monitoring of neurotransmitters and other molecules in interstitial tissue fluid. The principle underlying microdialysis is based on the fact that substances move from an area of higher concentration to an area of lower concentration. Since 1960, using this technique, people have successfully sampled almost all neurotransmitters. Those approaches using microdialysis probes have good sensitivity and selectivity, but they provide poor temporal and spatial resolutions [1.5-1.7]. These issues made microdialysis an unattractive option for *in vivo* uses in monitoring neurotransmitters.

Other approaches have been studied and used for the last few decades including optical [1.8-1.9] and electrochemical [1.10-1.20] methods. Optical systems usually are not only costly and bulky but also less reliable. The concept of *in vivo* neurotransmitter analysis by electrochemical approach was pioneered by Ralph Adams in the 1970s [1.21] and developed rapidly during the 1990s using carbon fiber electrodes (CFEs) with numerous techniques such as high-speed chronoamperometry (HSC), fast-scan cyclic voltammetry (FSCV) and fast cyclic voltammetry (FCV), etc. Dopamine (DA), serotonin (5-HT) and norepinephrine (NE) releases and uptakes have been measured in second-by-second basis with these methods [1.22-1.32].

Microwires (made of metal such as Pt or Ir) and CFEs have been used as the electrode materials to sense L-glutamate (Glu), DA, 5-HT, and NE. However, even

though they can be bundled into arrays, it iss very difficult to arrange them precisely in space for desired locations in tissues to monitor and correlate neural signals locally. For high counts of electrodes, the bundles increase the size of the inserted lead and thus cause more damage to the tissues. This issue can be addressed with multi electrodes arrays (MEAs) fabricated by microfabrication techniques. Using MEAs, multifunctional sensing capability to sense different neurotransmitters simultaneously in a single probe by proper enzyme deposition have been demonstrated [1.16-1.18] [1.20].

1.5 Neuron Stimulation

Neurostimulation therapies have been used to treat psychiatric disorders for years. Electric current and magnetic field were deployed with patients using various techniques, such as vagus nerve stimulation, transcranial magnetic stimulation, deep brain stimulation, treatment and major depression [1.33]. However those aforementioned methods stimulate all neurons within a given volume, including cells that are not implicated in the disease state, thus leading to unwanted side-effects and even reduced efficacy.

The probes are discussed in this thesis could be used for electrical stimulation since they contain a multi electrode array. A current source with the proper pulse could be applied to a pair of electrodes to deliver the desired stimulation. Beside, a specially-configured probe was also designed and implemented to obtain for the emerging technique called optogentic stimulation. This method will give precise stimulation with minimal invasion.

1.6 Proposed Approaches

In this thesis, various types of probes are proposed, implemented and discussed aiming for long-term implantable neurotransmitter sensors and integrated action potential recording and reference electrodes. Some nano-scale structures modification methods are also carried out and described in order to enhance the performance of the sensor. A micro-LED integrated probe for optogenetic stimulation and recording was also developed and investigated in a mice model.

There are two main types of probes in this work, which are silicon (Si) based probes and polyimide based probes. The Si ones give better performance and can stay in high temperature processes but they are not flexible and biocompatible. The polyimide ones are flexible and biocompatible; therefore they are suitable for long-term uses *in vivo* and give more comfort in operation. However, they cannot sustain high temperature and are difficult to fabricate.

Based on the characteristic of each type of probe, different fabrication and modification methods have been considered and selected. The following were features of these devices:

- The size of probe is small enough for implant and stiff enough to penetrate the tissue.
- Each probe has a MEA of Pt or Au. The fully-integrated ones will have a Ag/AgCl reference electrode or IrO_x pseudo-reference electrode.

- Each electrode in the probe can be modified with proper enzymes to sense different analytes. The original form can be used to detect electro-active substances or record action potentials.
- There are probes with different lengths in order to use with different animals and cases.
- Standard PCBs and connection pins were designed and made for all type of probes.
- The flexibility of the polyimide probes prevents the scar-forming in the tissue, thus increases the implantation time.
- The Si based probes can be nanowire modified with vapor-solid-liquid (VLS) mechanism which requires high-temperature processes.
- The polyimide based probes are suitable for low-temperature processes. They are modified with Au nanoparticles by several methods.
- Micro-LED integrated probes have two big pads to mount the LED and also three normal electrodes to record the electrophysiology signals.

CHAPTER 2

NANOWIRE MODIFICATION TO ENHANCE THE PERFORMANCE OF NEUROTRANSMITTER SENSORS

2.1 Introduction

The ultra weak sensor signals (electric currents in the range of pA) in electrochemical approaches using MEA could cause difficulties in recording and interpreting, which has been a technical challenge in existing acquisition systems. Therefore, increasing the signal levels in both baseline and sensitivity, while maintaining the small dimensions of the sensor probes, becomes important.

The reduction or oxidation current recorded in electrochemical sensors can be described by [2.1]

$$i = nFAC_bM \tag{2.1}$$

where i is the electrical current measured, n is the number of electrons for the specific chemical reaction, F is the Faraday constant of 96,500 $Cmol^{-1}$, A is the active surface area, C_b is the bulk solution concentration of the analyte, and M is a term about mass transport of the analyte to the electrode surface. For a particular analyte, the current response can be raised by increasing the active surface area. Without physically increasing the 2-dimensional area, the roughness of the electrode surface can be changed by nanowires modification as they increase the active surface in the third dimension, resulting in a gain of the total current output.

Numerous surface modification approaches have been applied for electrochemical sensors [2.2-2.10] to increase the surface area of working electrodes, which in return gives a raise in the current outputs. Carbon nanotubes [2.3-2.4] [2.7-2.8] [2.10], nanoparticles and nanowires [2.2] [2.5-2.6] [2.9] were used in surface modifications. Among those nanostructure modification approaches, VLS has been reported as one of the most prolific and simple methods to grow nanowires [2.11-2.12].

The VLS mechanism was initiated by Wagner and Ellis in 1964 to grow Si nanowires [2.11]. In this method, metal nano-droplets are created on a surface (Si, SiO_2, metals) and then the gas that carries the source material, which generally is silane (SiH_4) or tetrachlorosilane ($SiCl_4$), is introduced into the chamber maintained above the eutectic temperature [2.11-2.12]. The nano-droplets which are liquid will be the preferred sites for the vapor to deposit. The carrier gas then reacts to form liquid eutectic particles as following:

$$SiH_4 \longrightarrow \text{metal catalyst-Si(liquid)} + 2H_2\,\text{(gas)} \qquad (2.2)$$

$$SiCl_4 \longrightarrow \text{metal catalyst-Si(liquid)} + 2HCl\,\text{(gas)} \qquad (2.3)$$

Growing nanowires on top of the electrode surface will change its active area and consequently increase the sensitivity in an electrochemical sensor. Furthermore, the immobilization of enzyme on working electrodes for an enzyme-based sensing approach could benefit from the physical nanostructures which will play a role to enhance the enzyme adhesion on the surface of electrodes.

In this chapter, a method to grow nanowires using the VLS mechanism in a conventional PECVD system to enhance the performance of our Si-based neurotransmitter sensors has been proposed and implemented. The surfaces of electrodes were observed and characterized by SEM and cyclic voltammetry. The complete devices were made and used to demonstrate the enhancement in performance contributed by nanowires in the enzyme-based electrochemical sensing of L-glutamate which is the most abundant excitatory neurotransmitter. Comparison between electrodes

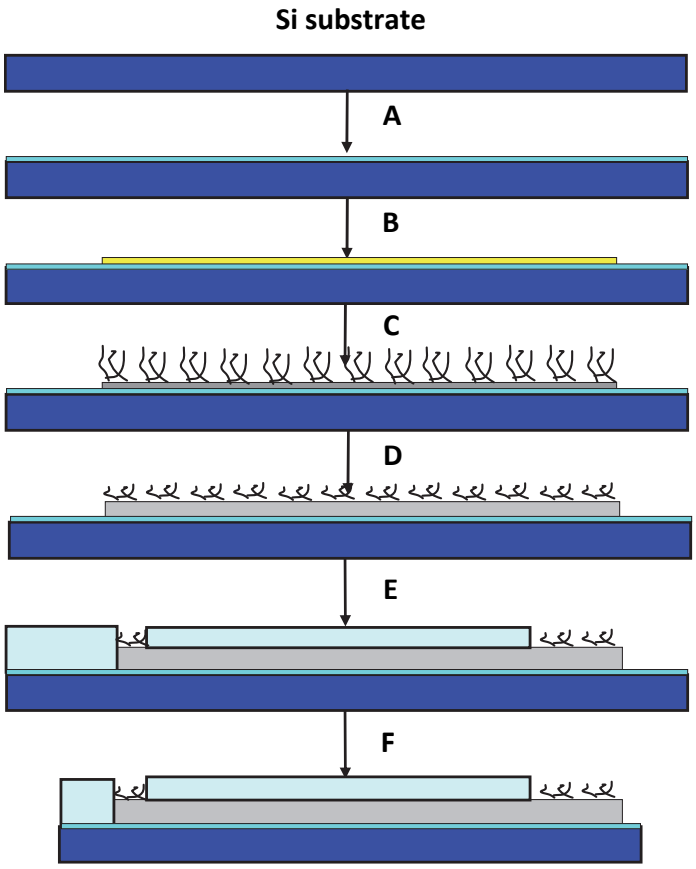

Figure 2.1 Fabrication processes: A. Thermal oxidation. B. Pattern Au/Ti layers by lift-off. C. Grow the Si-nanowires by the VLS method. D. Pattern the Pt/Ti layer by lift-off. E. Pattern SiO_2 as the insulation layer. F. Machining the probe by laser.

with and without nanowire modification was conducted showing that the modification method was a good option to improve the performance of electrochemical sensors.

2.2 Fabrication

The sensor probes were fabricated on a 300 μm thick 4-inch Si wafer and later released. A 500 nm thick layer of SiO_2 was formed by dry thermal oxidation to be used as insulation, followed by a lift-off process to pattern a double layer of 1 nm thick gold (Au) on 50 nm thick titanium (Ti). The wafer was then placed into a PECVD chamber for the VLS process under a pressure of 1100 mTorr, temperature of 420^{o}C and 30 sccm premixed SiH_4/Ar for 5 minutes. Another lift-off process was performed with the same photomask to obtain a layer of 150 nm thick Pt on 50 nm thick Ti. A 300 nm thick layer of SiO_2 was patterned with openings on the electrode areas and contact pads. Finally, the micro sensor probes were tailored by the laser micromachining system with precise alignment. The fabrication procedures are illustrated in Fig. 2.1. PCBs and standard electronic pins were used for easy assembly. Figure 2.2 shows the electrode configurations, an SEM image of the probe tip, assembled probes with two different lengths, and the complete device ready for implantation. The electrode area was 50×100 μm^2 while the complete probes were 400 μm wide with different lengths of 7, 12 and up to 65 mm for various requirements in animal experiments.

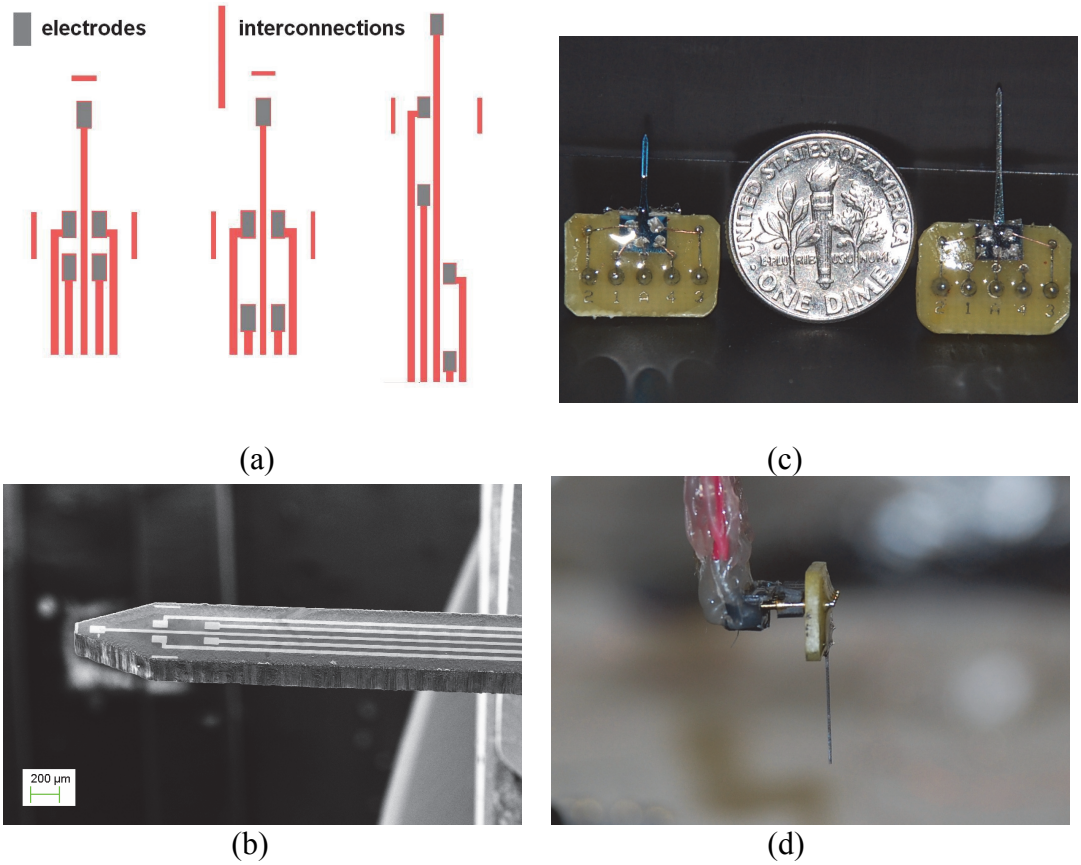

Figure 2.2 (a) Electrode configurations. (b) An SEM image showing the probe tip. (c) Two probing devices with different lengths of probes. (d) The complete probing system with connections to the recorder ready for implantation.

2.3 Characterization

Figure 2.3 shows an SEM image of the Si-nanowire modified surface. The deposition time for the nanowires was limited in order to get a less dense surface so it is easier to observe the configuration and shapes of nanowires. Figure 2.4 shows SEM images of surfaces for (a) a Pt thin film deposited on a Si substrate and (b) a Pt thin film coated on the Si-nanowire modified Si substrate. It was shown that nanowires collapsed after the deposition of Pt; however, the surface roughness did change drastically. A

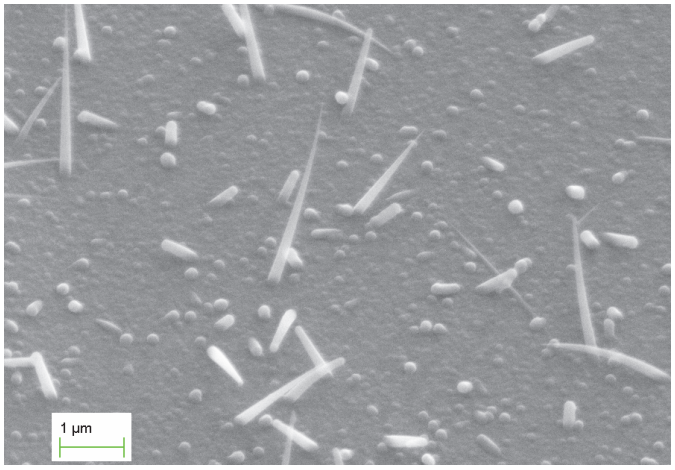

Figure 2.3 An SEM image of the Si-nanowires modified surface.

cyclic voltammetry experiment was conducted to quantitatively analyze the surfaces of electrodes. The CV plots of the Pt electrodes with and without nanowire-modification are shown in Fig. 2.5. It can be seen apparently that the nanowire-modified electrode has a much larger value in the graphical integral. The data analysis indicated that the roughness factors of electrodes without and with nanowire modification are in the ranges of 30–60 and 400–500, respectively. The active area was increased by about ten times.

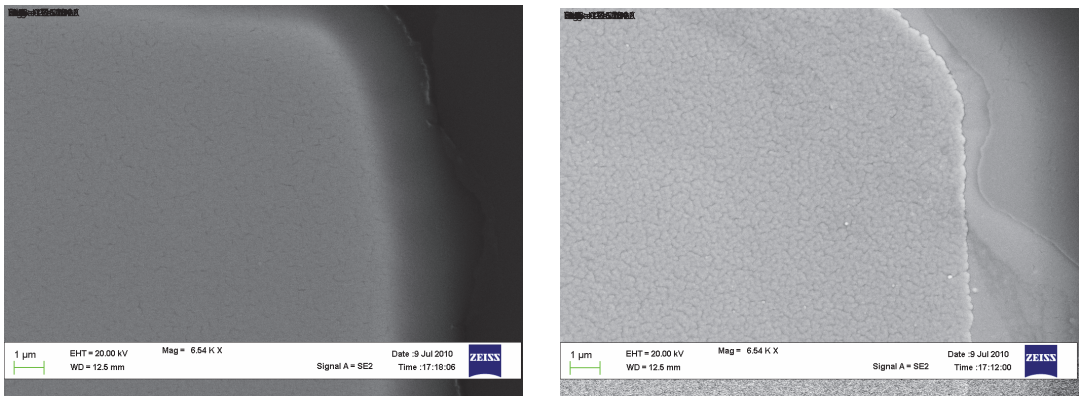

(a) (b)

Figure 2.4 SEM images of (a) a Pt thin film on a Si substrate without surface modification and (b) a Pt thin film on the Si-nanowires modified silicon wafer.

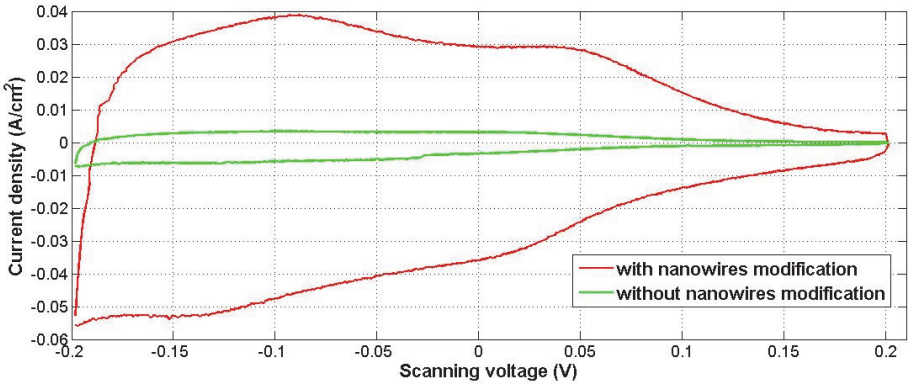

Figure 2.5 Cyclic voltammogram for the electrodes with and without nanowires modification.

2.4 Sensor Preparation and Experiment Setup

2.4.1 Sensor preparation

The chemicals used in the enzyme preparation were L-glutamate oxidase (GluOx) (G4001-01, from *USBio*), bovine serum albumin (BSA) (A-3059, from *Sigma*) and glutaraldehyde (Glut) (G-5882, from *Sigma*). The electrodes were first cleaned in iso-propanol alcohol (IPA) followed by air drying. GluOx was dissolved in deionized (DI) water with a ratio of 1 unit of GluOx to 2 µl of water. Then 2 µl of the solution was mixed with 9 µl of a cross-linking agent containing 1% BSA and 0.125% glutaraldehyde. The mixture of the enzyme solution was securely deposited onto the electrode surface under a stereomicroscope with a 10 µl Hamilton syringe. After several minutes, the enzyme mixture would become dry and the same procedure was repeated three to five times. The sensor probes were kept at room temperature for three days to cure the protein matrix before calibration to prevent the enzyme from being dissolved in

solution. This process is described in detail in Appendix A. The L-glutamate sensor operates based on the following chemical reaction:

$$\text{L-glutamate} + O_2 + H_2O \rightleftharpoons \text{2-oxoglutarate} + NH_3 + H_2O_2 \quad (2.4)$$

The produced peroxide (H_2O_2) was then oxidized releasing electrons which form an electric current proportional to the concentration of L-glutamate. This is based on the following reaction:

$$H_2O_2 \rightarrow O_2 + 2H^+ + 2e \quad (2.5)$$

2.4.2 Experiment setup

The measurement was performed in a beaker containing 20 ml of 0.05 M phosphate-buffered saline (PBS) at a constant temperature of 37°C with a magnetic rod stirring constantly at the bottom of the beaker. The probe tip was dipped into the solution along with a glass Ag/AgCl reference electrode. The bias voltage between the working and reference electrodes was set at 0.7 V and the electric current was

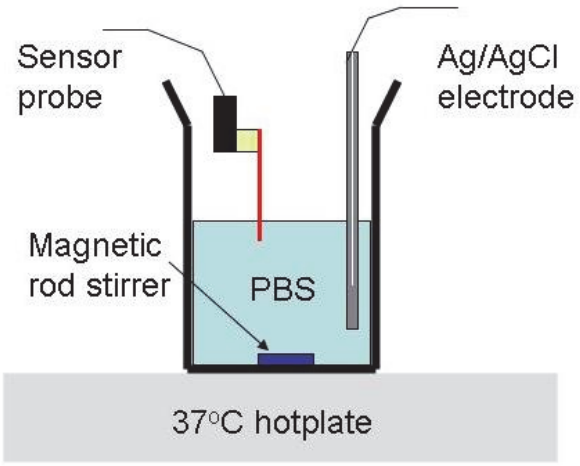

Figure 2.6 Experiment setup for calibration.

continuously recorded by a potentiostat (*Pinnacle* 3104). Typically, it took 30 minutes for the signals to reach the baseline, and then different amounts of L-glutamate were added in steps. Figure 2.6 shows the experiment setup.

2.5 Results and Discussions

Figure 2.7 shows the responses of sensors to L-glutamate concentrations without and with Si-nanowire modification. It is clear that the sensor with Si-nanowire modified electrodes has a much higher baseline and sensitivity slope. The baseline rose from 0.4

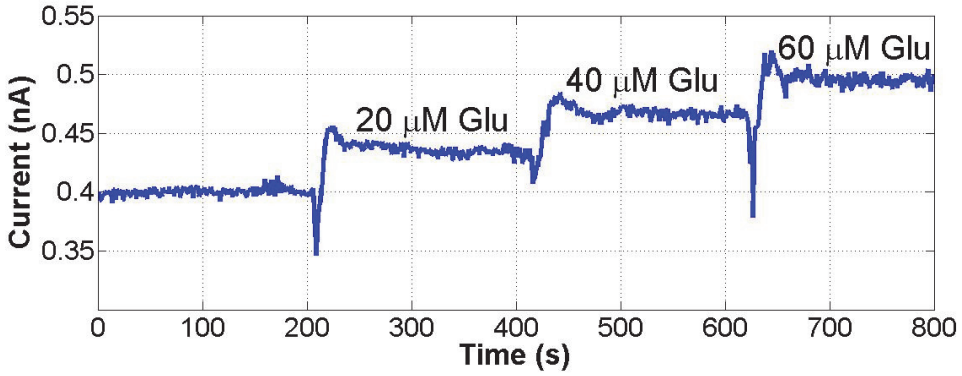

(a)

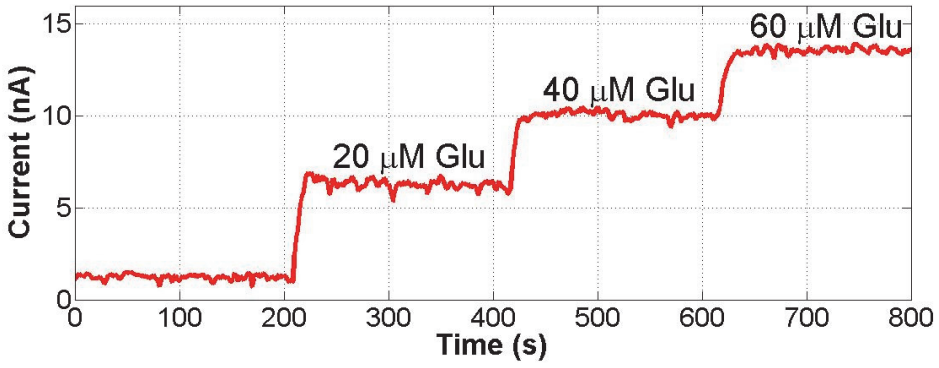

(b)

Figure 2.7 Sensor responses at different concentrations of L-glutamate for sensors (a) without and (b) with Si-nanowires modification on the sensing electrodes.

to 1.3 nA for the sensors without and with nanowire modification, respectively. The slopes of responses for electrodes without and with nanowire modification are 0.0016 and 0.2044 nA/μM, while the linearity coefficients (R^2) are 0.9951 and 0.9924, respectively. The critical specification for the sensitivity of such a sensor is the limit of detection (LOD). Assuming the noises during measurements are mainly Gaussian noises, the detection level could be estimated as three times the standard deviation of the baseline [2.3-2.4]. With this consideration, LODs are estimated as 4.8 and 1.7 μM for sensors without and with nanowire modification, respectively. The LOD enhancement is not remarkably great when compared with the significant change of the active surface area. This is because the nanowire modification not only increases the electrical current output of signals but also takes in more noise. Thus, the signal to noise ratio does not vary much. However, even if the LOD stays the same, raising the baseline provides a benefit to simplify the recording instrument configuration since it will not require a highly sensitive low-noise instrumentation amplifier. This will reduce the complexity, power consumption, size and cost of the implant electronics. Based on the same reason, I have determined that there is no need to maximize the active surface area. The active surface area will be much larger if the deposition time for the VLS process is increased significantly. However, since the signal to noise ratio will not increase dramatically, I decided that as long as the baseline is raised to a level that suits the design requirements for low cost electronics, the surface area is then sufficient. This also provides a benefit of reducing fabrication and material costs in the VLS process. Furthermore, conducting the VLS process longer with a higher flow rate of the gas

source will give denser nanowires, but this also can induce cross-talk among the electrodes that causes signal interferences.

The LODs obtained were not greatly enhanced because the noise level was high in the experiments. The ambient noise in the non-specific laboratory which was not designed for highly sensitive experiments, the noise from the electro-magnetic stirrer, and the noise in the data acquisition system contribute as non-Faradaic terms adding up to the total current output in Eq. (2.1) as

$$i_{TOTAL}=(i_{F1}+ i_{F2}+\ldots+ i_{Fn}) + (i_{nonF1}+ i_{nonF2}+\ldots+ i_{nonFm}) \qquad (2.4)$$

where i_{Fj} represent the Faradaic components from analytes in the solution and i_{nonFk} represent noise components. With Si-nanowire modification, the baselines in both electrodes were enhanced, but the noise levels were also increased. This could be addressed using the self-reference technique. I will discuss this in the next chapter.

2.6 Conclusions

A fabrication technique using conventional PECVD to modify the surface property of neurotransmitter sensor probes with Si-nanowires has been carried out. The improvement was demonstrated by comparing the characteristics of surface roughness with cyclic voltammetry and performance of the electrodes in sensing L-glutamate electrochemically without and with nanowire modification on the sensing surfaces. The nanowire modification increased the baseline of sensing and sensitivity significantly, which made the L-glutamate sensor probe suitable for integration with low-cost and

portable electronics that are essential for medical implants. The probe device architecture allowed an array of electrodes, which all could be modified with nanowires to increase the active surface areas, in a single probe. Many different molecules such as Choline (Ch), Acetylcholine (ACh), γ-Aminobutyric acid (GABA), etc, can be sensed simultaneously. The electrodes in the probe without enzyme coating can be used to record the action potentials fired by neurons near the area of interest providing the possibility of correlating action potentials and neurotransmitters in studies.

CHAPTER 3

A FULLY-INTEGRATED FLEXIBLE IMPLANTABLE L-GLUTAMATE SENSOR

3.1 Introduction

L-glutamate which is the most abundant excitatory neurotransmitter in the CNS has been studied with probes on different types of substrates [1.16-1.18] [1.20] with good results. However, most of the existing sensor probes are not either flexible [1.17-1.18] [1.20] or biomechanically compatible [1.16-1.18] for long-term uses *in vivo*. They are also not integrated systems [1.16-1.18] [1.20] as they need an additional Ag/AgCl reference electrode for measurements. These call for a need of a biocompatible neural microprobe with an integrated reference electrode. Furthermore, correlations between the firing of action potentials and neurotransmitter concentration variations, or correlations among various neurotransmitters in a small local area have not been thoroughly studied together *in vivo* to further understand neuro-activities due to the lack of an integrated probe.

In this chapter, a fully-integrated implantable probe on a flexible substrate to sense neurotransmitters has been proposed and developed. The probe was also capable of recording action potentials. The integrated reference electrode was developed by using a conventional Ag/AgCl thin film or an IrO_x film to solve the biocompatibility issue. IrO_x thin film which has been demonstrated in sensing pH [3.1-3.2] presented a

fairly stable potential in a normal biological environment with a slight variation in pH level. Thus it could be used as a pseudo-reference electrode. Enzyme-based electrochemical L-glutamate sensors were developed and reported to demonstrate the principle. The assembled sensors were calibrated and tested at various concentrations of L-glutamate with the presence of interfering molecules showing good sensitivity and selectivity.

3.2 Fabrication

Our sensor probes were fabricated on a 125 μm thick polyimide film monolithically and later tailored into individual probes. The film was first cut to a 100 mm diameter to fit on a silicon wafer. The film was cleaned by isopropyl alcohol (IPA).

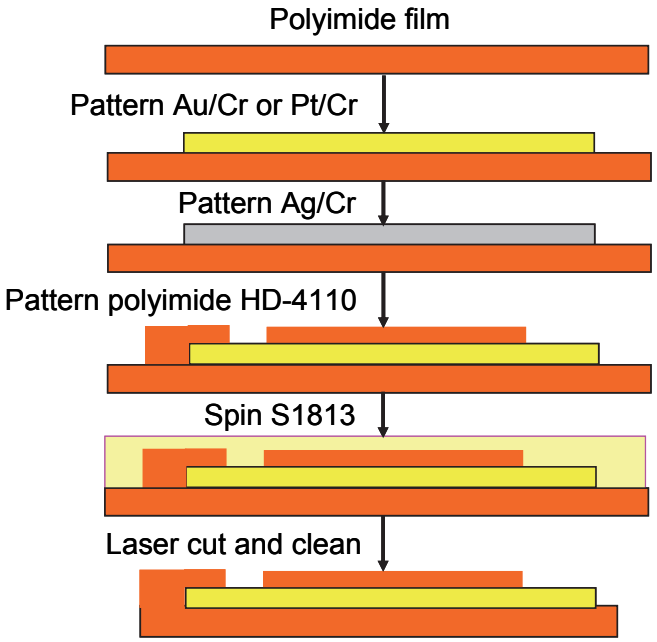

Figure 3.1 Fabrication processes.

Lift-off processes were performed to pattern a double layer of 150 nm thick Au on 20 nm thick Cr as the working electrodes. Pt was used to replace Au on another batch. For Ag/AgCl integrated probes, a second lift-off process was carried out to form a layer of 150 nm thick Ag on 30 nm thick Cr patterns for the Ag/AgCl reference electrode. A 300 nm thick insulation layer of polyimide (mixture 1:1 of HD-4110 and T-9039, from *HD Microsystems*) was spun on the samples followed by a photolithography process to open the electrode windows and contact pads. They were then cured inside a temperature-programmable inert gas oven for 12 hours polyimidization. A layer of photoresist S1813 (*Microchem Corp.*) was spun to protect the surface of electrodes, then a programmable laser micromachining system (*Oxford Lasers*) was used to tailor the sample into individual probes. The protection layer was released in acetone and the probes were cleaned and dried. The fabrication processes are illustrated in Fig. 3.1. A printed circuit board (PCB) was designed to mount the probe. Connections from leads in PCB to contact pads of the probe were made with silver epoxy. Standard electronic

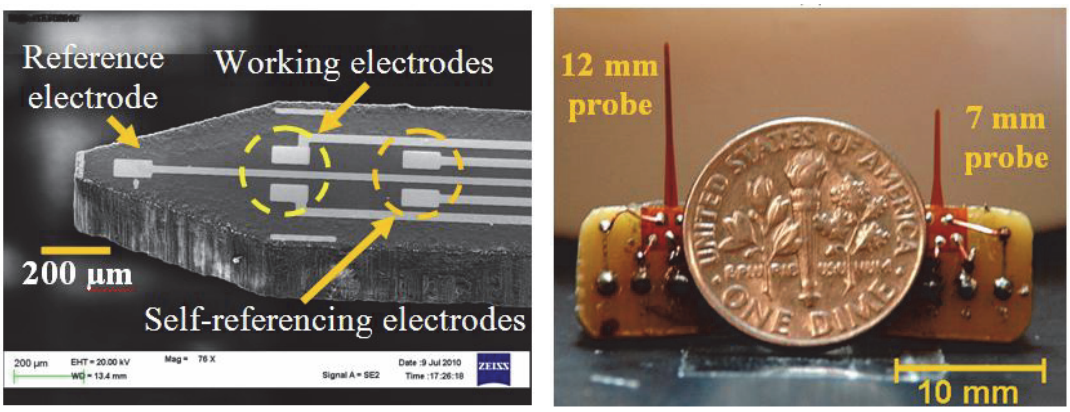

(a) (b)

Figure 3.2 (a) SEM image of the probe tip and (b) a photo of the assembled devices.

pins were soldered to the PCB. Figures 3.2 (a) and (b) show an SEM image of the probe tip and a photo of the assembled probes with two different probe lengths, respectively.

3.3 Device Characterization

The mismatches in physical properties between metals and polyimide made the microfabrication process difficult which affected the film quality. A method to

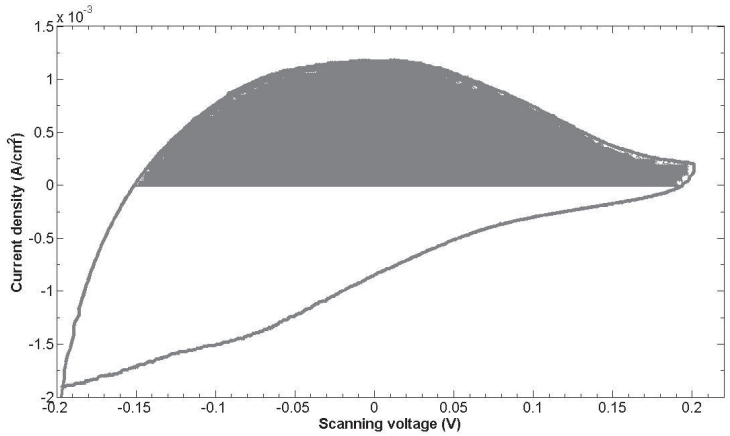

(a)

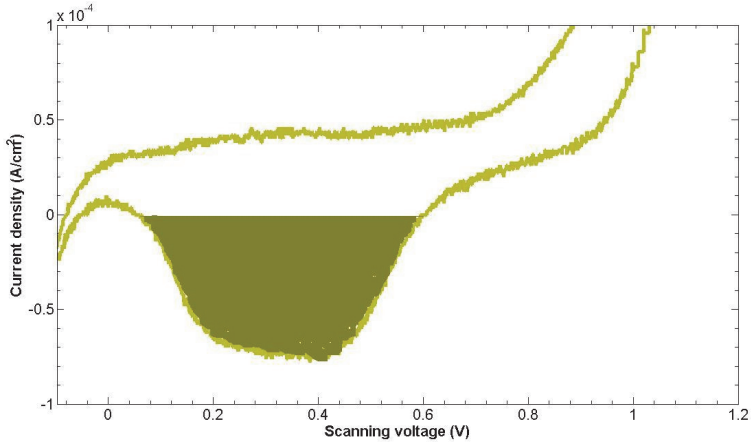

(b)

Figure 3.3 Cyclic voltammetry plots: (a) Pt thin film versus an Ag/AgCl electrode in N_2-bubbled 1 M H_2SO_4 at 100 mV/s and (b) Au thin film versus an Ag/AgCl electrode in 0.1 M PBS at 50 mV/s.

quantitatively analyze the surface of electrodes would help to estimate the performance of the device. Cyclic voltammetry (CV) experiments were conducted to compare the roughness of Pt and Au thin films deposited by e-beam evaporation on polyimide. The roughness factor, which is the ratio of the microscopic (active surface for reaction) area to the geometric area, can be calculated by taking the integral in a CV plot [3.2-3.3].

The relation can be expressed as:

$$\rho = A_m / A_g \tag{3.1}$$

$$A_m = Q_H / Q_H^* \tag{3.2}$$

where ρ is the roughness factor, A_m is the microscopic area, A_g is the geometric area, Q_H is the total charges obtained from the CV plot and Q_H^* is the charges per unit area for a single layer of molecules to be adsorbed/desorbed on the metal thin film surface. The charges per unit area (Q_H^*) needed to desorb hydrogen (210 μC/cm^2) and adsorb oxygen (386 μC/cm^2) can be used with Pt and Au, respectively, according to literature [3.1-3.2].

The experiment was performed with Pt by varying the potentials on the Pt electrodes within the hydrogen window potential of –0.2 to +0.2 V versus a glass Ag/AgCl reference electrode in a nitrogen-bubbled 1 M H_2SO_4 solution at a scanning

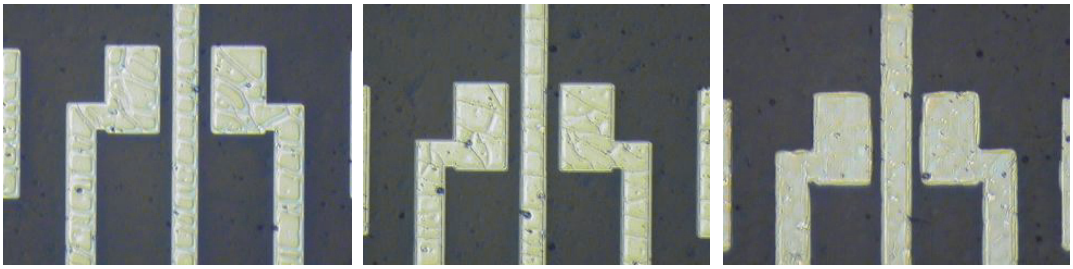

Figure 3.4 Optical microscope photos of thin films Pt/Cr/PI, Pt/Cu/Cr/PI and Pt/Au/Cr/PI (left to right).

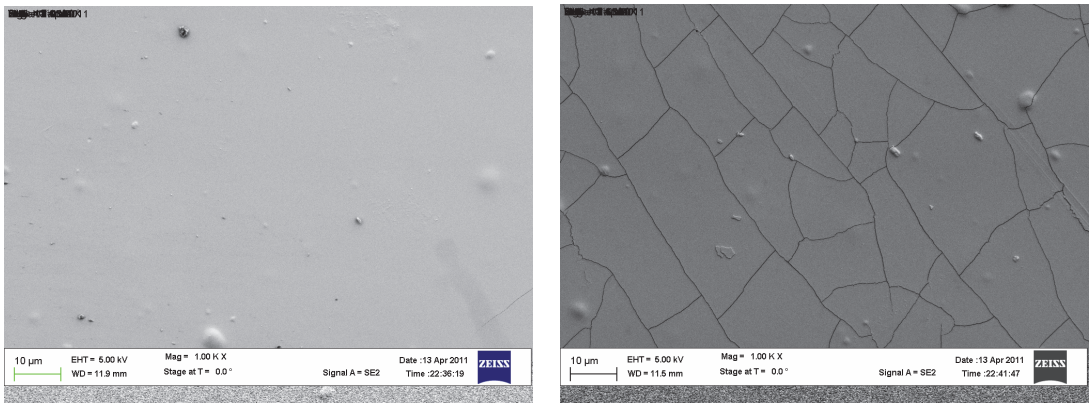

Figure 3.5 SEM images show the comparison between Pt/Au/Cr film (left) and Pt/Cr film (right).

rate of 100 mV/s. With Au, the CV was conducted in the potential window of –0.1 to +1.2 V in 0.1 M phosphate buffered saline (PBS) with a scanning rate of 50 mV/s. Figure 3.3 shows the CV plots where shaded areas were taken into integrals.

The results indicated that the roughness factors of Pt and Au thin films were 12 and 2, respectively. The numbers agreed with direct observation under an optical microscope showing cracks in the Pt thin film.

This is expected since Au is the most malleable and ductile metal. Cracks appeared in the Pt thin film will obviously affect the electrical and electrochemical performance of the sensor. In order to obtain good quality of Pt thin film deposited by electron-beam evaporation, a buffer layer of Cu or Au was tried and results were compared. Figure 3.4 shows the optical microscope photos of thin films Pt/Cr/PI, Pt/Cu/Cr/PI and Pt/Au/Cr/PI. It is obvious that using Au as a buffer layer has improved

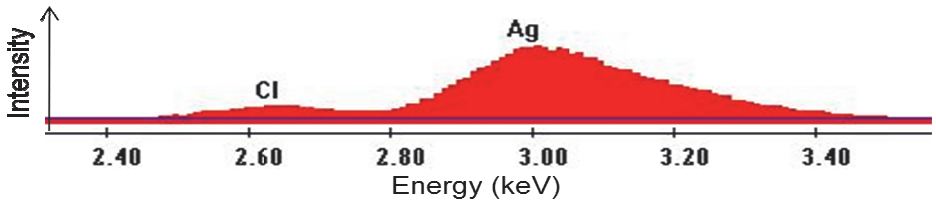

Figure 3.6 Energy-dispersive X-ray analysis of the electroplated Ag/AgCl thin film electrode.

the film quality. Figure 3.5 shows the comparison in SEM images of the thin films Pt/Au/Cr/PI and Pt/Cr/PI.

3.4 Reference Electrode

3.4.1 Ag/AgCl reference electrode

A solution of 0.1 M HCl with saturated NaCl was used for electroplating the reference electrode. With an applied voltage of +0.5 V between the Ag pad and a Pt wire electrode, the electroplating process was performed in 10 seconds. The probe was then soaked in a 3 M NaCl solution, then cleaned and kept dry in a dark chamber to prevent reaction with light. The electrode color changed from white to gray and energy-dispersive X-ray analysis (EDAX) verified the composition of silver and chlorine as shown in Fig. 3.6.

3.4.2 IrO_x pseudo-reference electrode

IrO_x could be formed by various methods such as sputtering, sol-gel and electroplating [3.5-3.6]. The IrO_x film has been used to sense pH level in a wide range of applications due to the advantages in sensitivity, repeatability and stability [3.5-3.6].

Since the pH level in biological environment does not change much (in a range of pH 6.8-7.4), IrO_x has been used as the pseudo-reference electrode in biosensor applications owing to its biocompatibility compared with the traditional Ag/AgCl reference electrode. However, with the output current in the pA range, using IrO_x as a reference electrode is still a challenge since it requires an extremely stable potential. Furthermore, the micro size of the probe also prohibits the development of such a device.

In this work, I have chosen the electroplating method to create an IrO_x thin film on a Au or Pt electrode in order to use it as a pseudo-reference electrode in our

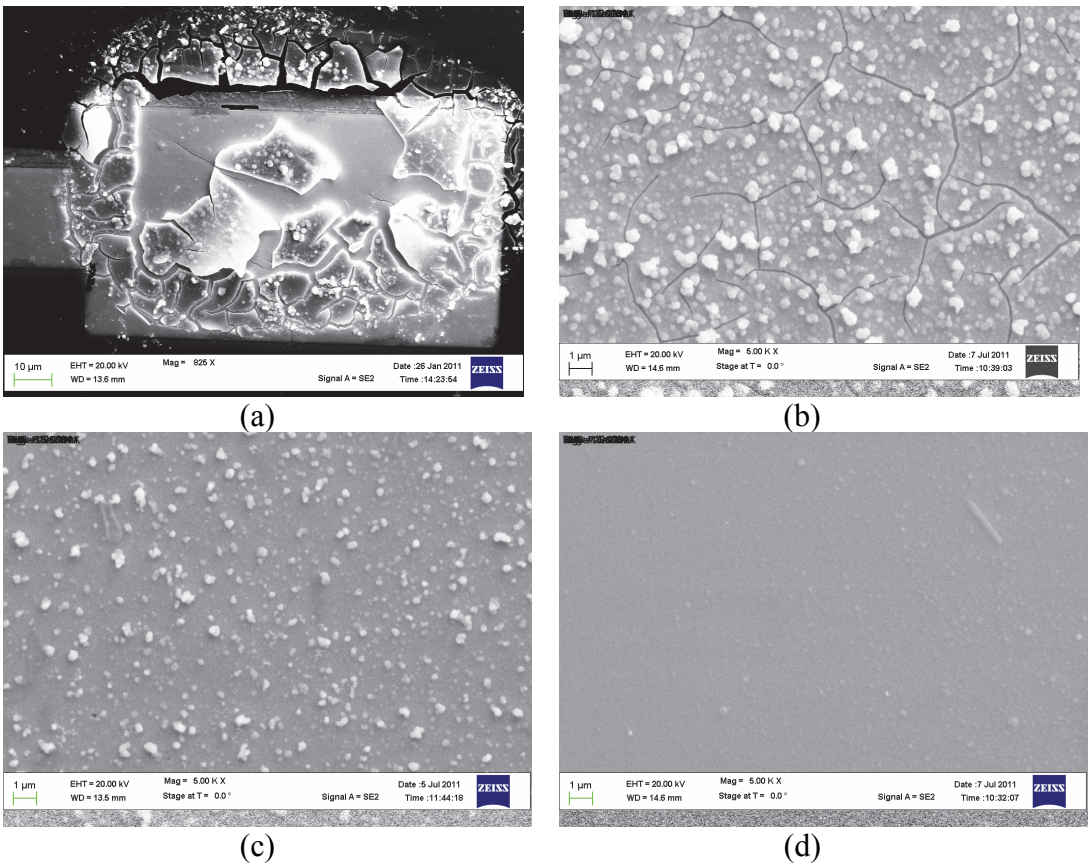

(a) (b)

(c) (d)

Figure 3.7 SEM images of the IrO_x film deposited on Au electrode with different electrodeposition parameters (a) fixed potential 0.8 V (b) CV in 15 minutes at 50 mV/s in 0-0.9 V (c) CV in 15 minutes at 50 mV/s in 0-0.8 V (b) CV in 15 minutes at 50 mV/s in 0-0.7 V.

amperometric neurotransmitters sensors. The formation of IrO_x film was done with fixed potential electrodeposition and then by using cyclic voltammetry to enhance the film quality. The biocompatibility of the film was verified by both *in vitro* and *in vivo* experiments.

3.4.2.1 Solution preparation

The electrodeposition solution was prepared by dissolving 0.075 g powder $IrCl_4.H_2O$ 99.9% into 40 ml DI water. The solution was stirred by a magnetic rod for 30 minutes before adding 0.5 ml 30% H_2O_2 and 10 ml $H_2C_2O_4.2H_2O$. After 10 minutes stirring, the solution's color changed from dark purple to light yellow-green. The solution had a pH level around 1.5 when measured by a *HANAH* pH meter. Then, K_2CO_3 powder was added into the solution in order to increase the pH of the solution to 10.5. The anodic electrodeposition solution was set aside for two days for stabilization.

3.4.2.2 Process

The IrO_x pseudo-reference electrode was formed by an anodic electrodeposition using the above-mentioned solution onto a Au or Pt electrode. For fixed potential deposition, a bias of around 0.6-0.9 V versus a Pt wire electrode was used to obtain the electroplating current density at around 2 A/m^2. Nevertheless, the film was not usually uniform due to the excessive amount of deposited IrO_x. Therefore a cyclic voltammetry approach was developed and optimized to obtain better quality. Various bias ranges, time, and scanning rates have been used to pick up the most suitable one. SEM images were used to judge the quality of the film. Figure 3.7 shows SEM images of the IrO_x

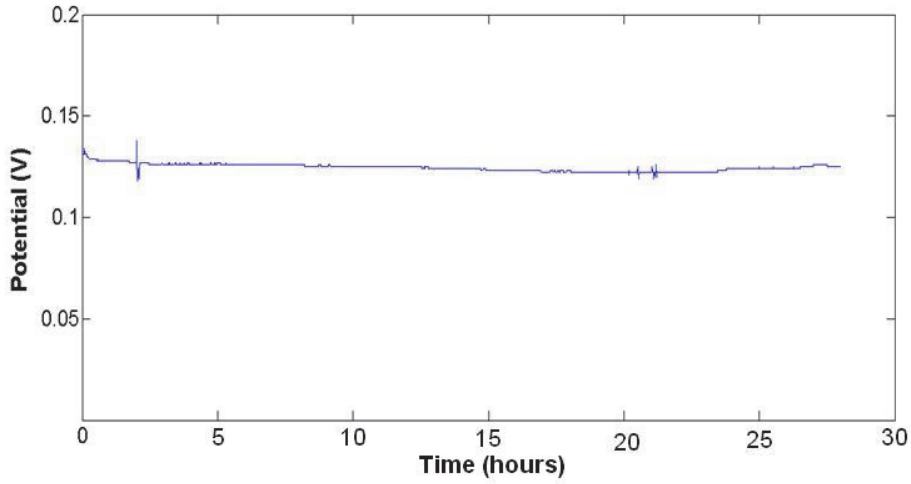

Figure 3.8 The potential measurement between IrO_x electrode and Ag/AgCl commercial reference electrode.

film obtained with different electroplating parameters, fixed potential 0.8 V (a), CV at 50 mV/s for 15 minutes with potential windows of 0-0.9 V (b), 0-0.8 V (c) and 0-0.7 V (d) onto a 50×100 μm^2 Au electrode. The experiments have shown that, the smoother the film, the more stable and the less noise the electrode would have. Therefore, I finalized with choosing the CV process at a rate of 50 mV/s in 15 minutes, and the potential window with Au and Pt electrodes are 0-0.7 V and 0-0.65 V, respectively.

3.4.2.3 Stability test

Sensitivity, repeatability and hysteresis characteristics have been examined in our previous work [3.5-3.6]. However, the most important thing for a reference electrode is whether its potential would shift in the environment or not. An experiment was carried out to investigate the electroplated IrO_x electrode. The difference in potential versus a commercial Ag/AgCl electrode was recorded for hours. While not

recording, the IrO_x electrode was immersed in 0.05M PBS solution. Figure 3.8 shows the result. It is clear that for a period of nearly a day, the potential of the IrO_x film

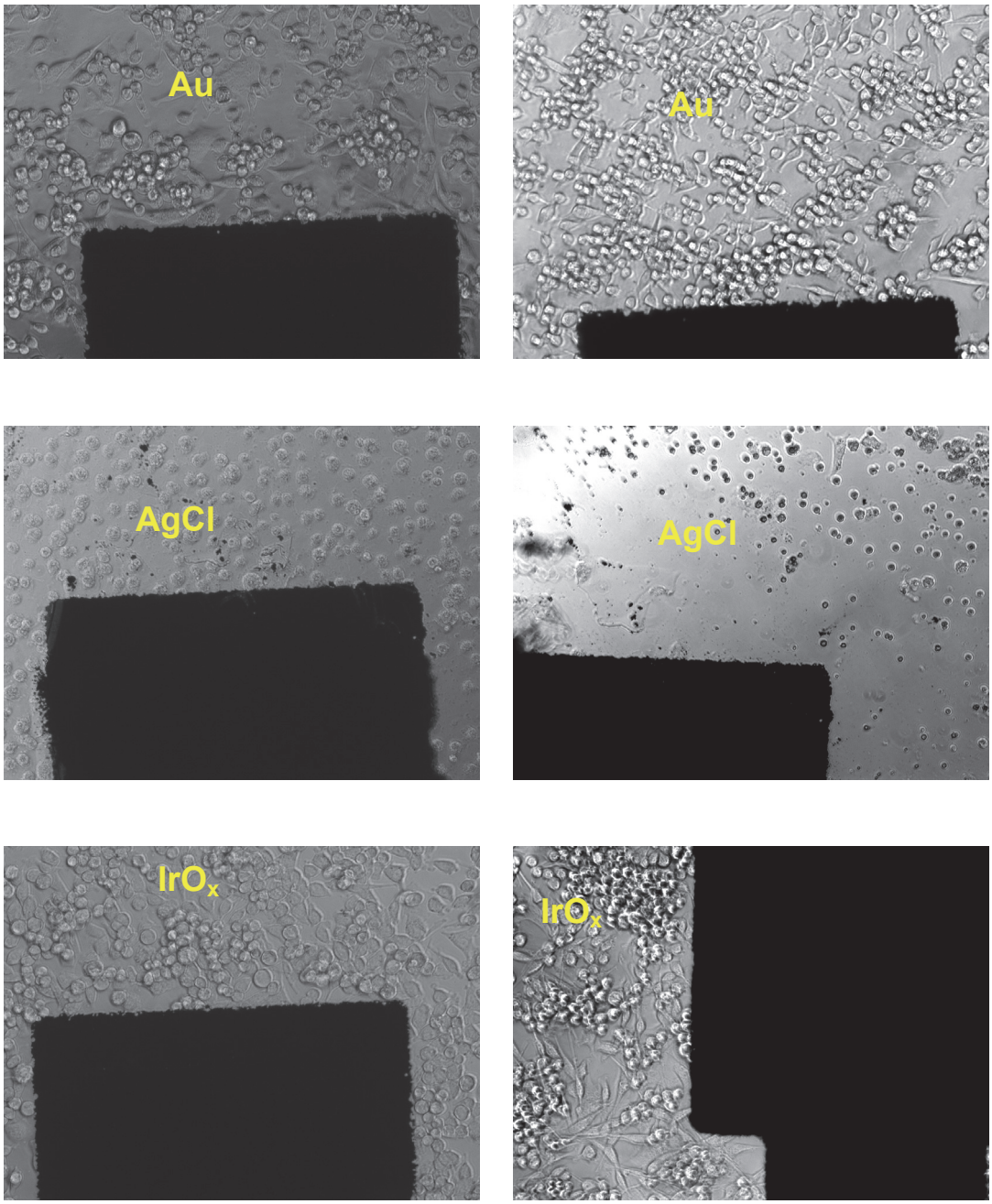

(a) (b)

Figure 3.9 Biocompatibility tests with IrO_x, AgCl and Au (as control). (a) and (b) are day 1 and day 3 results respectively.

stayed stable compared with the conventional reference electrode. Further experiments would be required to verify whether it could be really used as a reference electrode in amperometric neurotransmitter sensors or not.

3.4.2.4 Biocompatibility test

Due to availability, PNT1-A cells (prostate cells) were chosen to test the biocompatibility of reference electrodes *in vitro*. The cells were seeded in 3 PDMS wells on glass slides with AgCl, IrO_x and Au (as control) electrodes in the bottom. The cells were the observed in 3 days. Figure 3.9 shows the photos of the cells at different wells at day 1 and day 3. It is clear that the cell survived with the presence of IrO_x but they all died near the AgCl electrode. This also indicated our fabricated IrO_x film was biocompatible.

3.5 Sensor Preparation

3.5.1 Dopamine and H_2O_2 calibrations

The blank probes could be tested to demonstrate the sensing capabilities with H_2O_2 or electroactive neurotransmitters, such as dopamine (DA), serotonin (5-HT), etc.

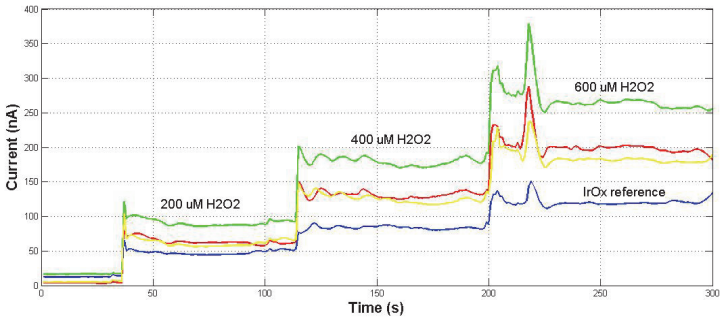

Figure 3.10 H_2O_2 calibrations using commercial Ag/AgCl reference electrode and IrO_x reference electrode (blue curve).

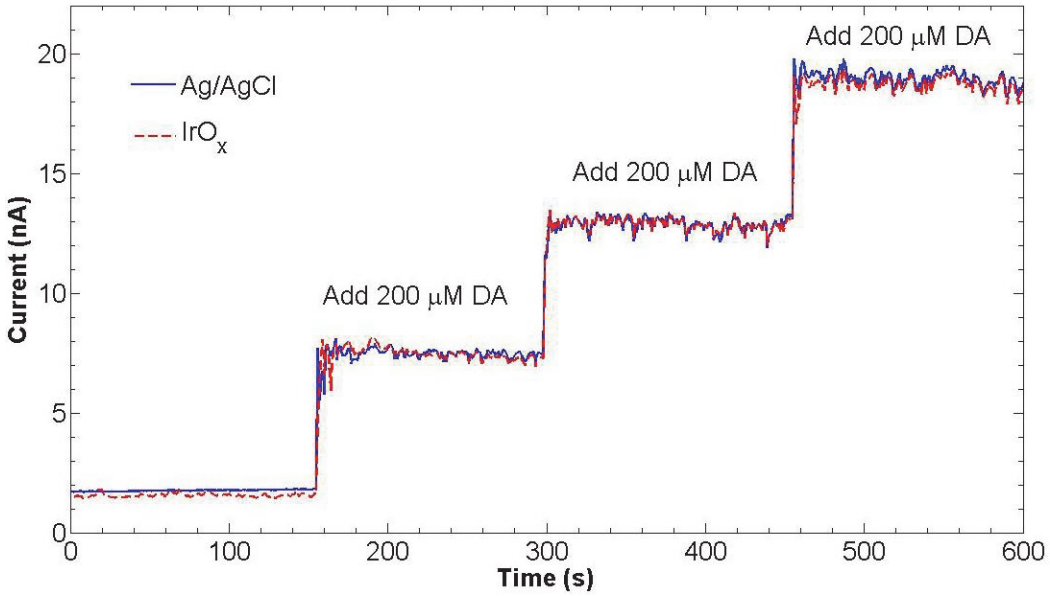

Figure 3.11 DA calibration comparison between using Ag/AgCl and IrO_x reference electrodes.

Due to its availability and importance, DA was chosen. Figure 3.10 shows the comparison between the H_2O_2 calibrations of the Kapton probes using commercial Ag/AgCl electrode and IrO_x pseudo-reference electrode. It is obvious that the IrO_x pseudo-reference electrode worked well in this calibration compared with the standard one.

Figure 3.11 shows DA calibrations of the Kapton probe using integrated Ag/AgCl (blue) and IrO_x (red) reference electrodes. The almost identical results indicated that IrO_x could be used as an alternative for Ag/AgCl in the role of being a reference electrode.

3.5.2 *Enzyme-based L-glutamate sensor*

The enzyme coating procedures are the same as mentioned in the previous chapter and can be found in details in Appendix A. The experiment setup was the same as mentioned in chapter 2; however an extra reference electrode was not necessary. In order to do further experiments with live animals, the sensors needed to be selective with L-glutamate. Thus, a selective membrane and a technique called self-referencing were investigated.

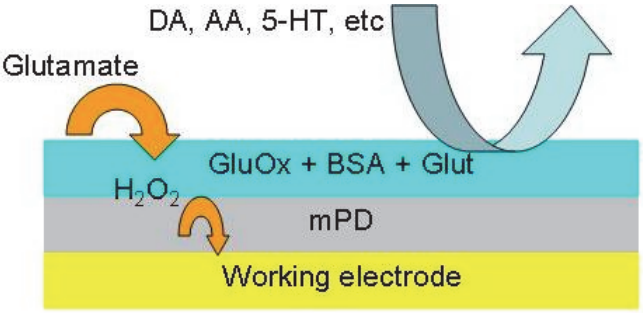

(a)

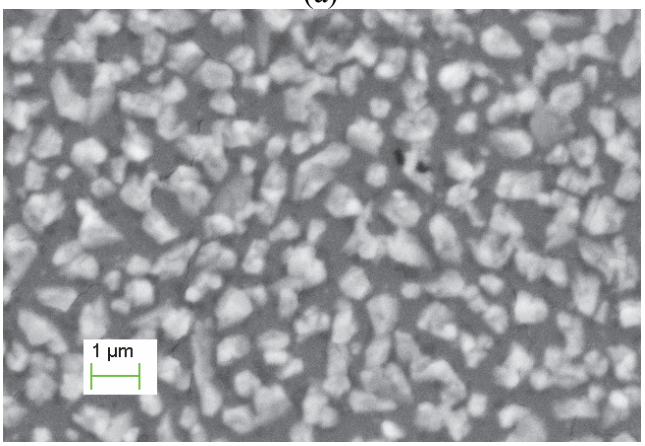

(b)

Figure 3.12 (a) Cross section of the modified surface electrode and (b) an SEM image of the protein matrix.

3.5.2.1 Meta-Phenylenediamine selective membrane

Meta-Phenylenediamine (mPD) has been used widely on top of the working electrode to form a selective membrane to block big molecules, such as ascorbic acid (AA), DA, and 5-HT [1.17-1.18] [3.3-3.4]. A solution of 5 mM mPD was prepared by first purging 0.05M PBS with nitrogen to deoxygenate and then dissolving mPD to prevent oxidation. The mPD electropolymerization process was done by a cyclic voltammetry between the working and Ag/AgCl reference electrodes in the potential window of 0.2 to 0.7 V at a 50 mV/s scanning rate for 15 minutes. The probe was then rinsed in DI water and kept at room temperature for 24 hours prior to calibration. The configuration for the electrode surface after modification is shown in Fig. 3.12 (a). Figure 3.12 (b) shows an SEM image of the cured protein matrix on top of the working electrode. It is obvious that the cured protein matrix is porous so that mPD could be electropolymerized on the working electrode surface.

3.5.2.2 Self-referencing technique

A self-referencing electrode which had identical dimensions and metal composition was located close to the working electrode on the probe. Unlike the working electrode being coated with the mixture of ($GluO_x$+BSA+Glut), only (BSA+Glut) was coated on the surface of the self-referencing electrode which thus would be able to sense all the electro-active chemicals except L-glutamate. The working principle is that the self-referencing electrode receives the same ambient noise as the working electrode does, temporally and spatially. Therefore, noise can be subtracted to

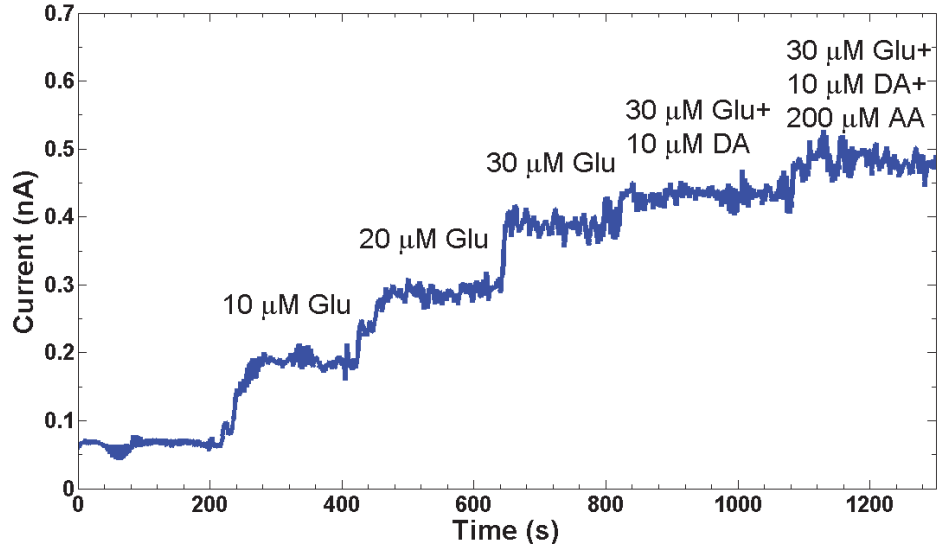

(a)

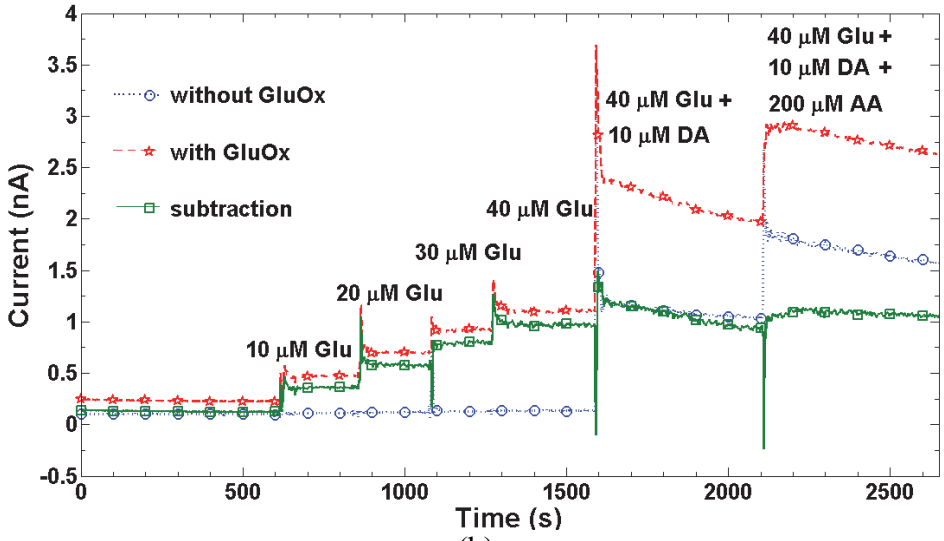

(b)

Figure 3.13 L-glutamate responses for the probes: (a) with mPD-coated electrodes and (b) using the self-referencing technique.

produce higher signal-to-noise ratios [1.17] [3.3-3.4]. From Eq. (2.4), this can be expressed as

$$I_{WORKING} = i_{Glu} + (i_{F1} + i_{F2} + \ldots + i_{Fn}) + (i_{nonF1} + i_{nonF2} + \ldots + i_{nonFm})$$

$$I_{SELF\_REF} = (i_{F1} + i_{F2} + \ldots + i_{Fn}) + (i_{nonF1} + i_{nonF2} + \ldots + i_{nonFm})$$

Therefore $i_{Glu} = I_{WORKING} - I_{SELF\_REF}$

3.6 L-glutamate Calibration Results and Discussions

3.6.1 Using Ag/AgCl reference electrode

The response of the probe with mPD-coated electrodes is shown in Fig. 3.13 (a) and that of the probe with a self-referencing electrode is shown in Fig. 3.13 (b). Figure 3.13 (a) shows that DA and AA were blocked as 10 μM DA added less than 6% additional current, while 10 μM DA and 200 μM AA together added 28% additional current in the signal of 30 μM L-glutamate. The noises recorded during measurements were relatively high. The low signal-to-noise ratio restricts the limit of detection (LOD) and consequently brings difficulty for *in vivo* recording and neuro-activity recognition.

The response of the probe with the mPD-coated electrode is shown in Fig. 3.13 (a), while Fig. 3.13 (b) shows the performance for using the self-referencing probe. Figure 3.14 shows the comparison of limit of detection, sensitivity, linearity and

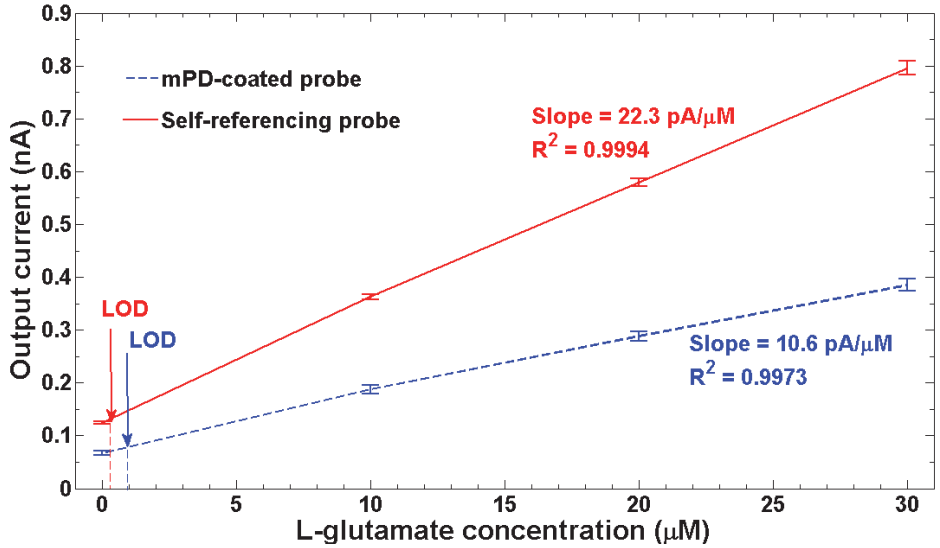

Figure 3.14 Comparison of limit of detection, sensitivity, linearity and variability.

variability of those two techniques. Figure 3.13 (a) shows that majority of the DA and AA were blocked by mPD as 10 μM DA as interference added less than additional 6% of electrical current while 10 μM DA and 200 μM AA together added additional 28% of electrical current in the signal produced by 30 μM L-glutamate. The noise recorded during measurements, as the fluctuations in the signals, were relatively high restricted the limit of detection (LOD). Consequently, this makes difficulties for *in vivo* recording neuro-activity recognition.

Figure 3.13 (b) indicates that the signal subtraction between the (GluOx+BSA+Glut)-coated working electrode and (BSA+Glut)-coated self-referencing electrode rejected the interference from AA and DA more effectively. The contribution of 10 μM DA added less than 0.1% of additional electrical current while while 10 μM DA and 200 μM AA together added nearly 4% of electrical current in the signal produced by 40 μM L-glutamate. The self-referencing technique did not only address the sensor selectivity, but also improve the signal quality and, therefore, enhanced the LOD. Assuming a Gaussian noise environment, LOD usually could be estimated as three times the standard deviation of the baseline [3.3] [3.4]. Based on the results, the LODs before and after signal subtraction in Fig. 3.13 (b) are 0.43 and 0.25 μM for L-glutamate, respectively. This demonstrated that the spatially and temporally correlated noises between the two electrodes could be reduced.

The sensitivity slopes of mPD-coated and self-referencing probes were measured at 10.6 and 22.3 pA/μM, respectively, with LODs of 0.9 and 0.25 μM, as shown in Fig. 3.14. This indicates that mPD was electropolymerized excessively on the electrode surface so it did not only block the interference molecules but also affected the response with L-glutamate. Thus it had a lower sensitivity. The mPD coating could not block the noise and therefore had a higher LOD compared with the one using self-referencing technique. The self-referencing probe was then chosen for animal experiments.

3.6.2 Using IrO_x as reference electrode

The IrO_x integrated probes were also modified with enzyme in order to detect L-glutamate. Although its capability had been demonstrated in calibrations with H_2O_2 and DA, issues still existed. The quality of the sensor after enzyme coating was not stable.

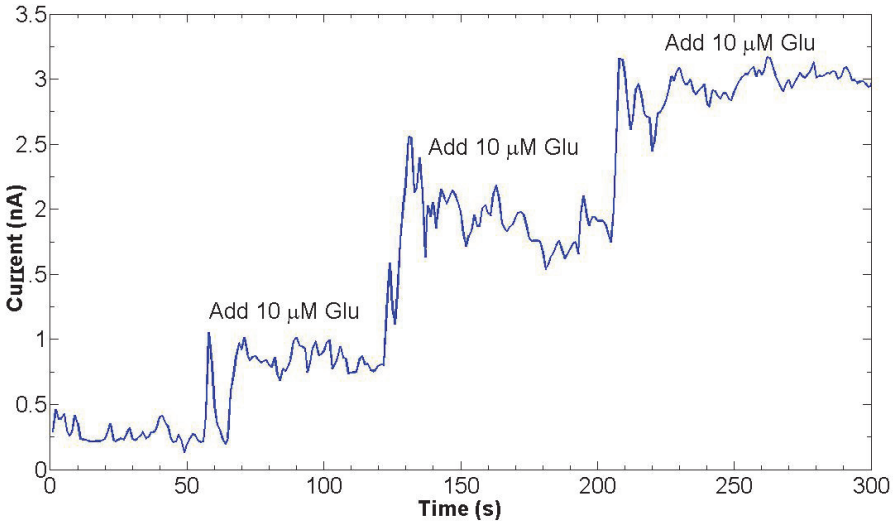

Figure 3.15 L-glutamate response of the Kapton sensor probe with integrated IrO_x pseudo-reference electrode.

Figure 3.15 is a typical example. Although, it showed the response with L-glutamate significantly, but the noise level was too high prohibiting us from carrying out a lot of animal studies that required high precision. More experiments should be spent to investigate this issue.

3.7 Flexibility

The implantable probe needs to be small, flexible but rigid enough to penetrate the tissue. The flexibility also gives ease in operation since those conventional probes such as Si or ceramic ones are very brittle. Figure 3.16 shows the flexibility of the integrated neurotransmitter sensor probe. The sensor probes can be bent in one-dimension considerably without affecting electrode performance or signal connection line conductivity. The sensor lead yet is stiff enough to be inserted into tissues.

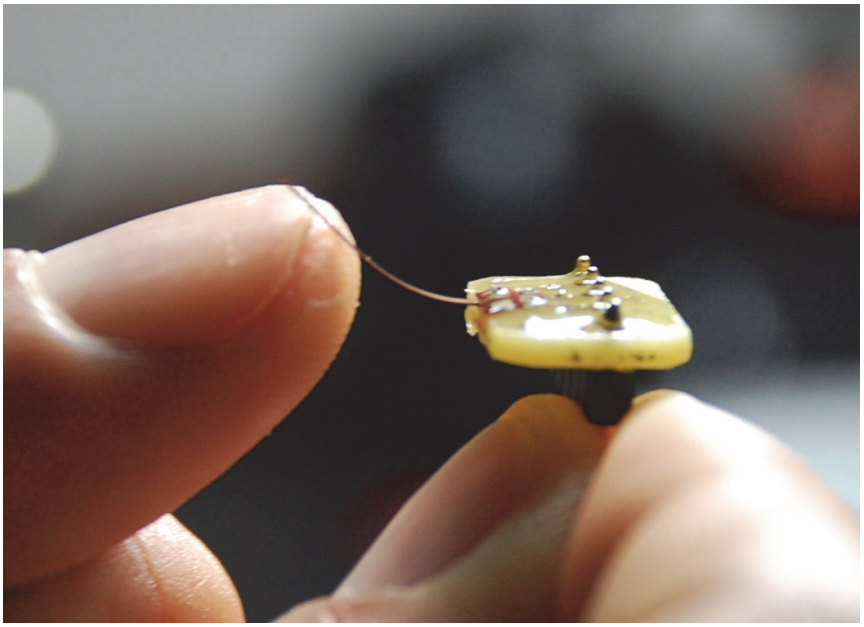

Figure 3.16 Flexibility of the integrated probe.

3.8 Conclusions

A compact, flexible, implantable integrated probe for studies of neurotransmitters has been developed. The integrated reference electrode makes it simpler for *in vivo* experiments by eliminating implantation of multiple electrode leads. The multi-electrode probe allows integration of self-referencing electrodes to enhance sensor selectivity and signal quality. The electrode without enzyme can be used for action potential recording while nearby electrodes coated with specific enzymes can sense the respective neurotransmitters. This enables studies to accurately correlate the functionalities of individual neurotransmitters with neurons firing in animal or human models *in vivo*. The flexibility of the sensor probes will enhance biomechanical compatibility to tissues and probe longevity. As the proof of concept, an enzyme-based electrochemical L-glutamate sensor has been demonstrated with good performance. Using proper oxidases, similar techniques can be applied for sensing other neurotransmitters with the same demonstrated advantages.

CHAPTER 4

A MICRO-LED INTEGRATED PROBE FOR OPTOGENETICS STIMULATIONS

4.1 Introduction

Point-of-care technologies have significant potential for effective diagnostics as well as therapeutic impact in personalized medicine. For several decades [4.1-4.3], simultaneous electrical stimulation and recording has been realized for treatment of brain disorders while monitoring neural activities. However, there is also convincing evidence that points to the deleterious effect of electrically stimulating neurons. Moreover, it has been technically difficult to experimentally induce the depolarization of specific types of neurons. For example, existing electrode-based deep brain stimulation methods indiscriminately stimulate all neurons within a given volume, including cells that are not implicated in the disease state, thus leading to unwanted side-effects and even reduced efficacy as opposing excitatory and inhibitory cell types are affected by the electrodes. In the past, light has also been used to control neuronal cells primarily by photothermal means [4.4-4.5] or by uncaging chemically-modified signaling molecules [4.6] (e.g. glutamate). However, these methods have poor spatial resolution and none of these can have selectivity for cell types in a 3D tissue volume. In contrast, optical stimulation of genetically-targeted neurons (so-called optogenetic stimulation) has enabled highly selective activation of chemically identical neurons

(Fig. 4.1). Promoter-specific genetic insertion allows cell-specific expression of natural light-sensitive proteins to allow light-activation. Since the first demonstration of optogenetic stimulation of neurons, new microbial opsins and their structural modification have been developed for highly-precise light activation or silencing of neural circuits [4.7-4.8]. Among these, channelrhodopsin-2 (ChR2) and halorhodopsin (NpHR) are being widely used to enable investigation of function of neural circuitry in a cell-type-specific, temporally accurate manner [4.8-4.11]. While ChR2 is a cation channel that allows cations to enter the cell following exposure to blue light (~470 nm) causing depolarization [4.9-4.12], NpHR [4.11] is a chloride pump that activates upon illumination with yellow light (~580 nm) resulting in cellular hyperpolarization. As the activation maxima of these two proteins are over 100 nm apart, they can be controlled independently to either drive firing of action potential or to suppress neural activity in intact neural tissue or together can modulate neuronal synchrony. Both proteins have fast temporal kinetics, on the scale of milliseconds, making it possible to drive reliable trains of high frequency action potentials in vivo using ChR2 and suppress action potentials using NpHR [4.11][4.13]. Optogenetic stimulation eliminates the highly challenging requirement of placing electrode arrays for stimulation and thus is minimally invasive [4.14]. Furthermore, it allows rapid reversibility [4.9] (unlike other optical stimulation method such as glutamate uncaging), high throughput (with multiple beam stimulation), and electrical noise reduction.

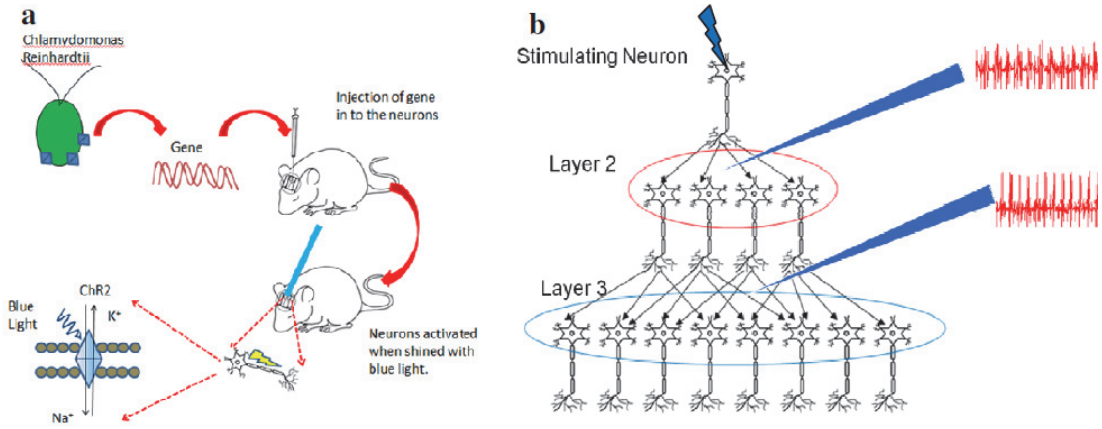

Figure 4.1 (a) Principle of optogenetics. (b) Direct versus indirect activation.

Light for optogenetic stimulation can be delivered deep into the brain using either an optical fiber [4.15] coupled to a laser beam or directly by µLED (micro-scale light-emitting diode) [4.16]. The very low electrical power requirement as compared to laser and compact size of µLED is advantageous for development of implantable neural prosthetic. On the other hand, µLEDs will provide greater control on spatio-temporal stimulation patterns for applications such as restoration of audio-visual functions. While light can optogenetically stimulate specific neurons in native circuitry, continuous sensing of neuronal activity in the vicinity of the activation site is required for: (i) testing the efficacy of stimulation for optimization, (ii) providing feedback from stimulated neurons to the stimulating source, and (iii) sensing specific neurotransmitters released subsequent to stimulation. In this respect, the µLED method provides two important advantages of (i) easy on-chip integration with an array of micro-electrodes, and (ii) unconstrained mobility and behaviors of experimental subjects in *in-vivo*

conditions unlike the fiber-based method. Though tungsten electrodes can be stereotactically placed near the μLED, integrated micro-electrode with μLED on a single chip is essential for accurate estimation of location and origin of the neural activity [4.17-4.18]. For example, the inability to see the location of separate electrodes with respect to an LED embedded in tissue may lead to difficulties in discerning direct versus indirect stimulation activity from different layers (Fig. 4.1).

In this chapter, the development of an optrode for optogenetic stimulation by μLED and simultaneous recordings of neural activity using integrated electrodes on a single polyimide substrate is reported. Focusing the light from the μLED was achieved by a photo-polymerized lens batch-fabricated on the same probe. The performance of the optrode for cortical stimulation and recording was investigated on mice visual cortex neurons expressing ChR2. Stimulation intensity and frequency-dependent spiking activities of visual cortex were recorded.

4.2 Material and Methods

4.2.1. *Optrode Design*

Our μLED-integrated probes were fabricated on a 125 μm thick polyimide film by standard semiconductor processes. Polyimide film was first cut into a 100-mm diameter round piece for fabrication. It was cleaned by isopropyl alcohol (IPA) and baked at 100^{o}C for 15 minutes to improve film adhesion. Photolithography was performed to pattern a 1.5 μm thick layer of negative photoresist NR9-1500PY

(*Futurrex, Inc*) followed by an electron-beam evaporation process (*CHA Industries, Inc*) to deposit a layer of 150 nm thick Au on a 20 nm thick Cr layer. The sample was immersed in acetone and ultrasonication was carried out for 5 minutes for a lift-off process to have the desired patterns. After cleaning and baking, a 500-nm thick insulation layer of silicon nitride was patterned by another lift-off process using the same photoresist and sputtering (*AJA International, Inc*) to open the electrodes and contact pads.

A programmable laser micro-machining system (*Oxford Lasers*) was used to precisely tailor the substrate into micro-scale probes which were then cleaned in acetone and dried by nitrogen. A light-emitting diode (μLED) with dimensions of 1000×600×200 μm^3 (Pico LED, *Rohm Semiconductor*) was securely attached onto the pads in the probe using silver epoxy. We chose the commercially available LEDs to

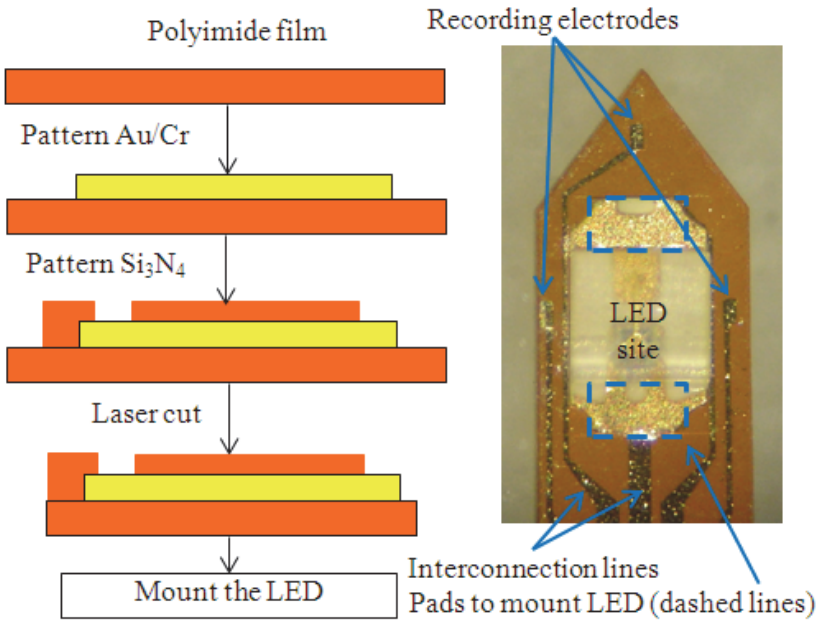

Figure 4.2 Fabrication processes.

demonstrate the feasibility of our design. In the final applications, organic μLEDs can be monolithically fabricated on the same substrate or die-size solid-state μLED could be flip-chip bonded on the probe. Polydimethylsiloxane (PDMS) was used to encapsulate the contacts providing thermal and electrical insulations with respect to surrounding tissues when the probe is used *in vivo*. The fabrication processes are illustrated in Fig. 4.2. Two metal contact pads of 200×400 μm^2 were used for mounting the μLED whilst the three electrodes with the size of 50×100 μm^2 were used for action potential recording. The connection metal lines provided the biasing voltage to the LED or took the neuronal signals back to the connector end. The optrode shaft was 12 mm long and 900 μm wide as shown in Fig. 4.3 (a).

A printed circuit board (PCB) was designed and manufactured to mount the optrode. The probe end was secured on the board with the shaft suspended, and connections were made with silver epoxy. A strip of five standard electronic pins was soldered onto the PCB so that the optrode could be securely and easily connected to a stimulating and recording system during animal experiments. Figure 4.3 (b) shows a SEM (scanning electron microscope) image of the μLED-assembled probe tip. The white color was due to the charge accumulation in the polyimide during SEM imaging. For collimating the divergent light emitted from the top surface of the μLED, a lens was fabricated (Fig. 4.3 (c)) by photo-polymerizing NOA-61 (*Norland Optical Adhesive*) polymer. A micro-droplet (0.4 μl) of NOA-61 was applied on top of the μLED and UV light was utilized to polymerize in 30 seconds. The polymerized lens

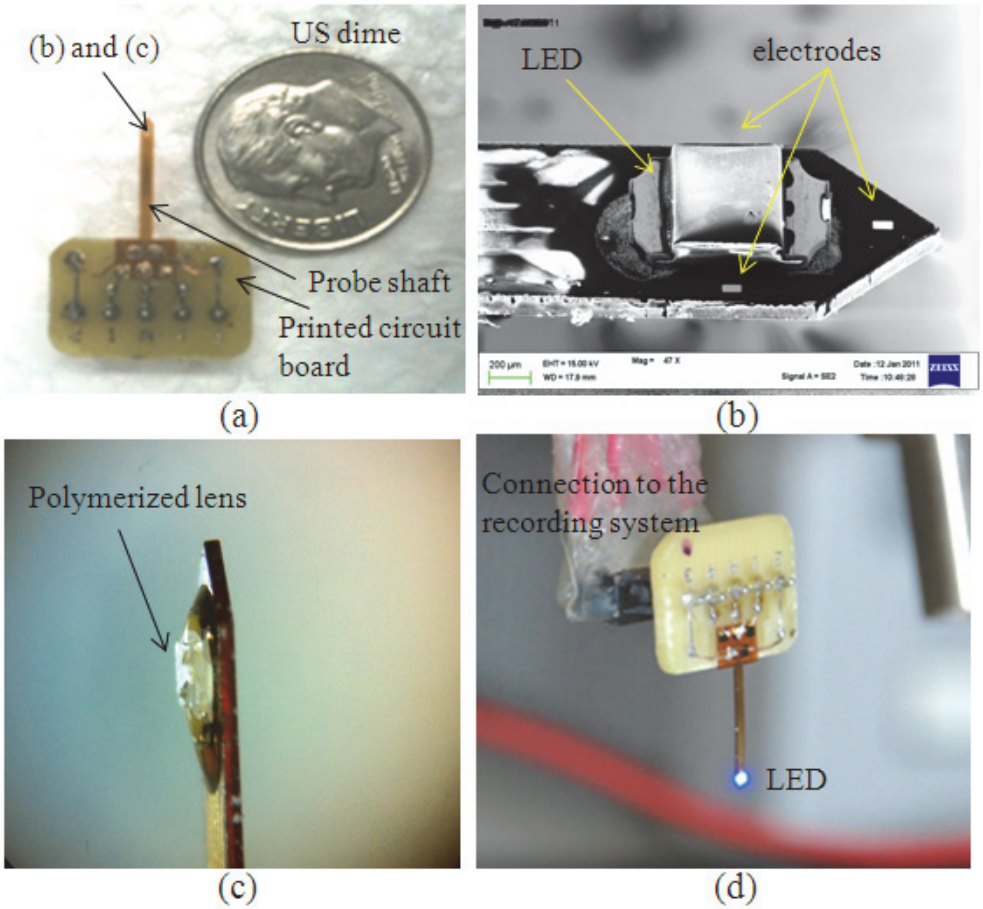

Figure 4.3 (a) Image of the optrode assembled on a printed circuit board, compared to a US dime. The probe shaft was implantable with the circuit board outside the body to connect to a wearable module for animal experiments. The circuit board was made larger than necessary for the convenience of handling and connecting during experiments. (b) SEM image of the optrode showing the µLED. (c) Side-view photo in which a photo-polymerized lens was formed on the µLED. (d) Light generated by the optrode at a forward bias of 2.9 V.

was transparent for the blue light. The device was tested in water to ensure the encapsulation was moisture proof and sterilized in isopropyl alcohol before use. The µLED was operated at a forward bias of 2.9 V and generated blue light at a wavelength of 465 nm as visible by naked eyes, shown in Fig. 4.3 (d). The light could be time-modulated with a function generator.

4.2.2 *Animal preparation*

Adult (25-30 g) mice (B6.Cg-Tg, transgenic with Thy1-ChR2-YFP expression, Jackson Lab) were subjects of these experiments. All aspects of experimental manipulation of the animals have been approved by members of Institutional Animal Care and Use Committee. Mice were maintained on a 12:12 light cycle (lights on at 7:00). Animals were anesthetized with 90 mg/kg ketamine, 10 mg/kg xylazine and placed in a stereotaxic frame (*Leica Microsystems*). A midline scalp incision was made and a 1.5 mm diameter craniotomy was drilled. The optrode was inserted in the right hemisphere at antero-posterior (AP) -3.0 mm, lateral (L) 2.0 mm and dorsoventral (DV) 1.5 mm for the visual cortex (anteromedial and primary) from bregma. The position of

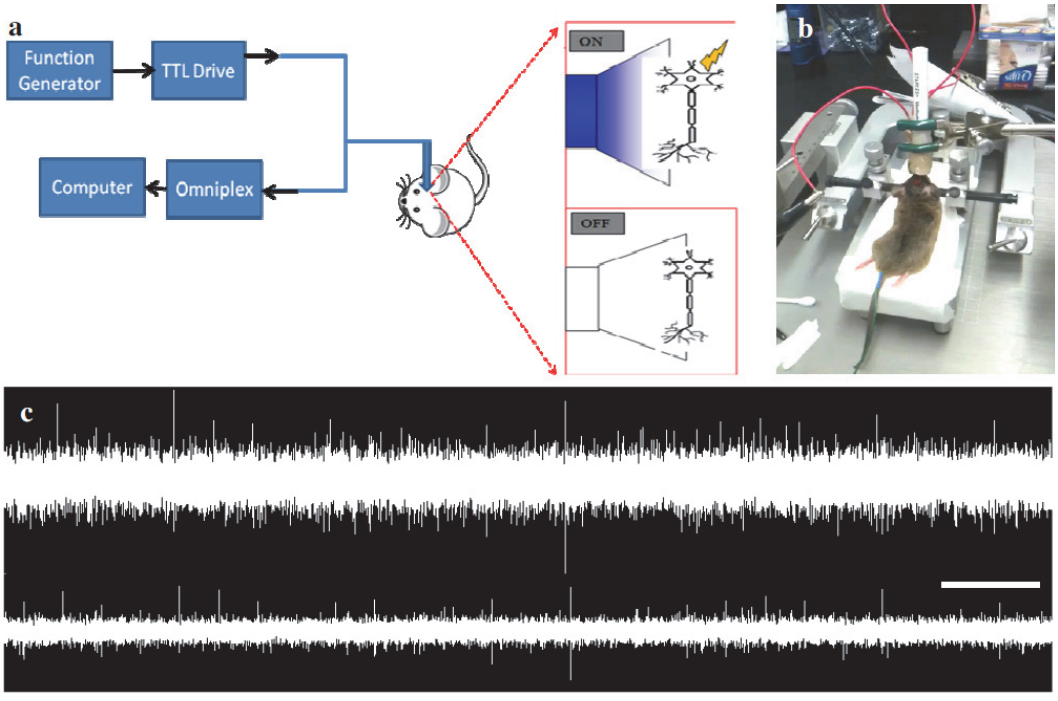

Figure 4.4 (a) Schematic of the optrode-based stimulation/recording experimental setup. (b) Photo of the experimental setup. (c) Raw electrical recordings for 20s from two electrode channels in the optrode.

the optrode was verified histologically after the experiments. The neural activity of three mice were activated and recorded in this experiment.

4.2.3 *In vivo Stimulation and Recordings using µLED-optrode*

To achieve in-vivo stimulation and recording, the optrode was inserted into the craniotomized brain region of the anesthetized mice. Simultaneous optical stimulation and electrical recording of visual cortex was carried out. The eyes of mice were covered and room light was switched off in order to avoid ambient visually evoked spiking. In order to compare the signal recorded by separate electrode, a 1-MΩ 75-µm-diameter tungsten electrode (*A-M systems Inc.*) was stereotactically inserted. Recorded signals were bandpass filtered between 300 Hz and 8000 Hz, AC amplified 5000x (OmniPlex, *Plexon Inc.*) and recorded using Plexcontrol software (*Plexon Inc.*). Plexon Offline Sorter and NeuroExplorer were used for analysis. Light pulses were generated by a function generator and synchronized to OmniPlex. Figure 4.4 (a) shows the schematic of the optrode- based stimulation/recording experimental set up. The actual set up is shown in Fig. 4.4 (b). Light intensity from the µLED was varied from 0.3 to 2.0 mW/mm2 and measured using a light power meter (*Thorlabs Inc.*). Raw electrical recordings from two electrode channels from the optrode are shown in Fig. 4.3 (c).

4.2.4 *Histological Evaluation*

Following electrical recording, mice were deeply anesthetized with pentobarbital and perfused transcardially with phosphate buffered saline (PBS) followed by 4% paraformaldehyde (PFA) dissolved in PBS. Brains were removed carefully and post-fixed in 4% PFA for an additional 24 to 48 hrs. Brains were transferred to 30% sucrose for 48 to 72 hrs before slicing 40 µm sections of the visual cortex region on a cryostat. Slices were then washed and mounted on gelatin-coated slides and stained with 0.25% Thionine stain (*Invitrogen*). Slices were then treated with mounting media (*Fisher Scientific*), and coverslip. Location of the optrode was

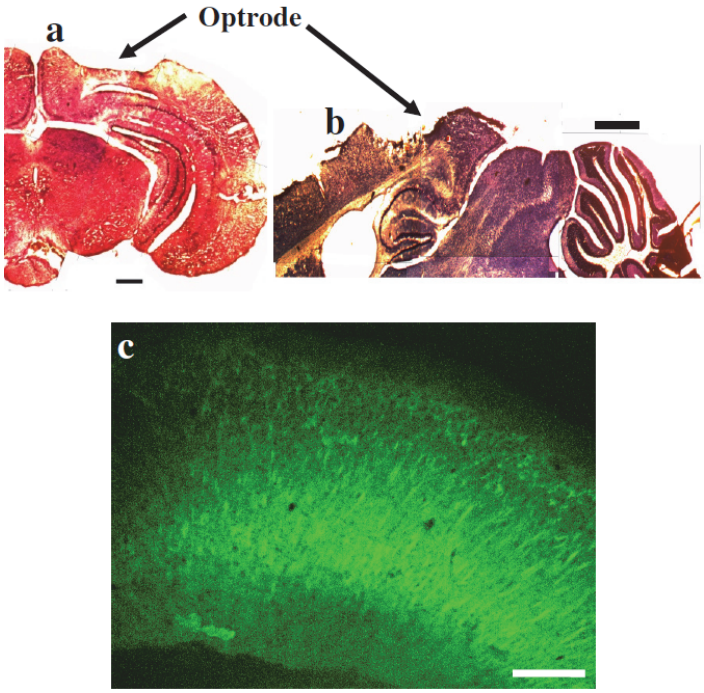

Figure 4.5 (a) Coronal and (b) Sagittal histological sections of the mice brain. Arrows point to the optrode insertion site. Scale bar: 400 µm. (c) Confocal fluorescence image of cortical brain region in the slice. Scale bar: 100 µm.

determined by examining all mice sections using an inverted microscope with a 2.5X objective. The images of sections containing optrode are assembled into coronal and sagittal montage using Adobe Photoshop. Figure 4.5 (a) and (b) respectively shows the coronal and sagittal histological section of the mice brain with inserted optrode-site marked by arrows. For analysis of ChR2-YFP expression, confocal microscopy of cortical slices was performed using 488 nm excitation in a Biorad confocal microscope (*Carl Zeiss Inc*). Figure 4.5 (c) shows confocal fluorescence image of the cortical slice.

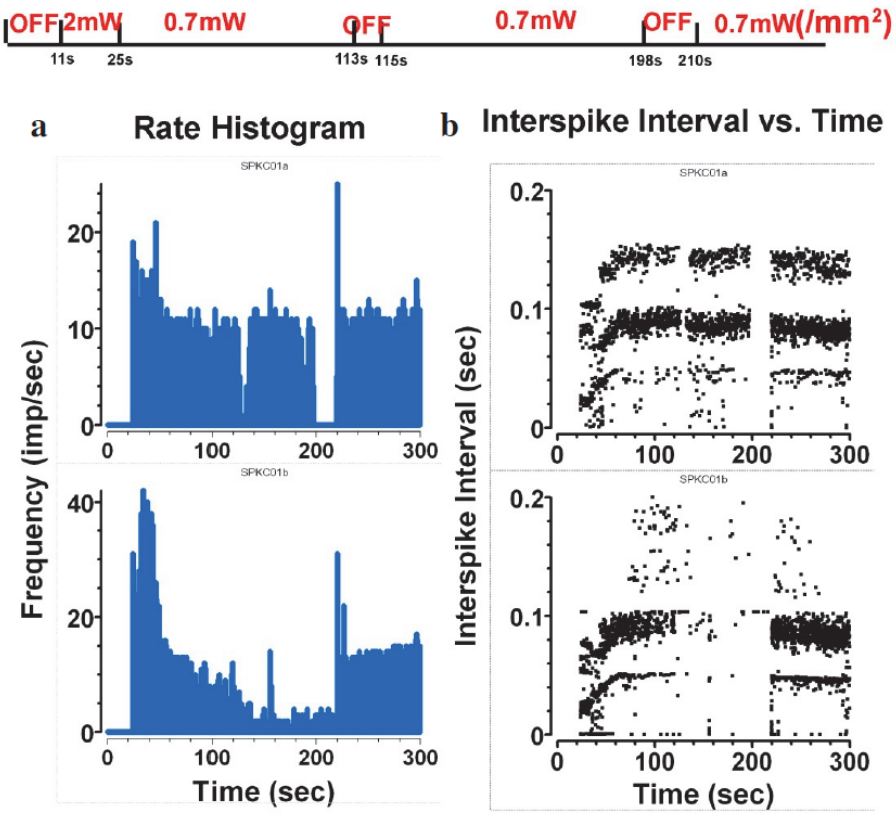

Figure 4.6 (a) Rate-histogram of spikes measured by the microelectrode at the tip of the optrode, from two light-responsive units stimulated by different intensities of the optrode-µLED at a frequency of 10 Hz. (b) Corresponding inter-spike intervals as a function of time with varying intensities of stimulation in the optrode-µLED.

4.3 Results and Discussion

4.3.1 µLED-intensity Dependent Neuronal Spiking Recorded by Optrode

Figure 4.6 shows the µLED-intensity dependent neuronal spiking recorded by the microelectrode at the tip of the optrode. Figure 4.6 (a) shows the measured rate-histogram of spikes, from two light-responsive units stimulated by two different intensities (0.7 and 2.0 mW mm^{-2}) of the optrode-µLED, at a frequency of 10 Hz. The spiking rates from both the recorded units were found to depend on the intensity of light. Corresponding inter-spike intervals as a function of time with varying intensity of stimulation by the optrode-µLED is shown in Fig. 4.6 (b). When the light was turn off (0-11^{th}s, 113^{rd}-115^{th}s, 198^{th}-210^{th}s), the spike rates dropped. The two light-responsive units reacted differently, as expected, while each responded to light intensities coordinately. At least two distinct ISI-distributions can be seen in both the recorded units (Fig. 4.6 (b)). The lowest ISI pattern (high firing rate) was found to have narrowest distribution over period of time.

4.3.2 µLED-intensity Dependent Neuronal Spiking Recorded by Tungsten Electrode

Figure 4.7 shows µLED-intensity dependent neuronal spiking recorded by a separate tungsten-electrode placed in close vicinity (< 1 mm) of the optrode-µLED. Figure 4.7 (a) shows the measured rate-histogram of spikes, from two light-responsive units stimulated by three different intensities (0.3, 0.7 and 2.0 mW mm^{-2}) of the optrode-µLED at a frequency of 10 Hz. Unlike the optrode-electrode recordings, the spiking rate of one of the recorded units (bottom panel of Fig. 4.7 (a)) was found to

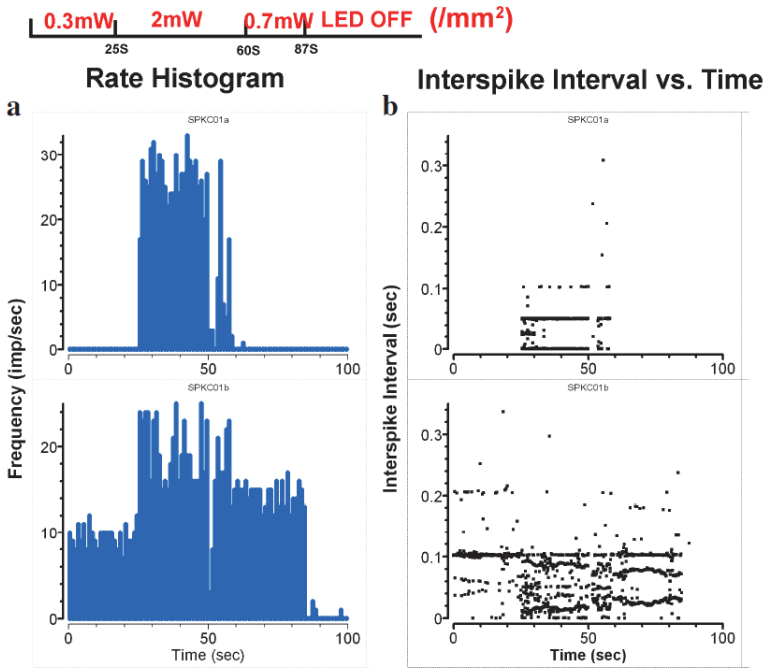

Figure 4.7 (a) Rate-histogram of spikes measured by a separate tungsten electrode, from two light-responsive units stimulated by different intensities of the optrode-µLED at a frequency of 10 Hz. (b) Corresponding inter-spike intervals as a function of time with varying intensities of stimulation by the optrode-µLED.

depend on the intensity of light. The spiking rate of the other unit (top panel of Fig. 4.7 (a)) responded to light intensity >2.0 mW/mm^2. Corresponding ISI as a function of time with varying intensities of stimulation by the optrode-µLED are shown in Fig. 4.7 (b)). As compared to optrode-electrode recordings, the ISI patterns were found to be different (Fig. 4.7 (b)). The distribution of ISI in case of tungsten-electrode recordings was significantly lower (Fig. 4.7 (b)) than the optrode-electrode (Fig. 4.6 (b)), suggesting the fact that these two-types of electrodes are probing different set of neurons in the visual network.

4.3.3 μLED-frequency Dependent Neuronal Spiking in Visual Cortex Measured by Optrode

Figure 4.8 shows the μLED-frequency dependent neuronal spiking in visual cortex measured by our optrode. The raw electrical recordings from visual cortex using microelectrode at the tip of the optrode, in response to optrode-μLED stimulation at varying frequencies are shown in Fig. 4.8 (a). For analysis of this set of experiment, I increased the threshold of spike-detection so as to select a narrower group of neurons. Figure 4.8 (b) shows the rate-histogram of spikes from neurons stimulated by the optrode-μLED at different frequencies. The power density of stimulation was fixed at 0.7 mW mm^{-2} for all these measurements. A duty cycle of 50% was used at all frequencies. Figure 4.8 (c) shows the corresponding inter-spike intervals as a function of time with varying frequencies of stimulation by the optrode-μLED. As it can be seen from the figure, though the rate histogram (Fig. 4.8 (b)) does not show variations of spiking rates with varying frequencies of stimulation over a 1-second binning period, the spiking pattern (Fig. 4.8 (a)) and the inter spike intervals (Fig. 4.8 (c)) show distinct patterns of neuronal spiking in response to varying frequencies of optrode-μLED stimulation. While neurons stimulated with 5 Hz led to two distinct ISI patterns around 60 and 160 ms, both 10 and 20 Hz stimulations led to one distinct ISI pattern around 100 ms (Fig. 4.8 (c)). Interestingly, low frequency (1 Hz) μLED-stimulation also led to one distinct ISI pattern around 60 ms. Further, in this experiment with optrode-electrode recording, all the ISI patterns were found to have narrow a distribution. This can be attributed to analysis being done with high-threshold spikes.

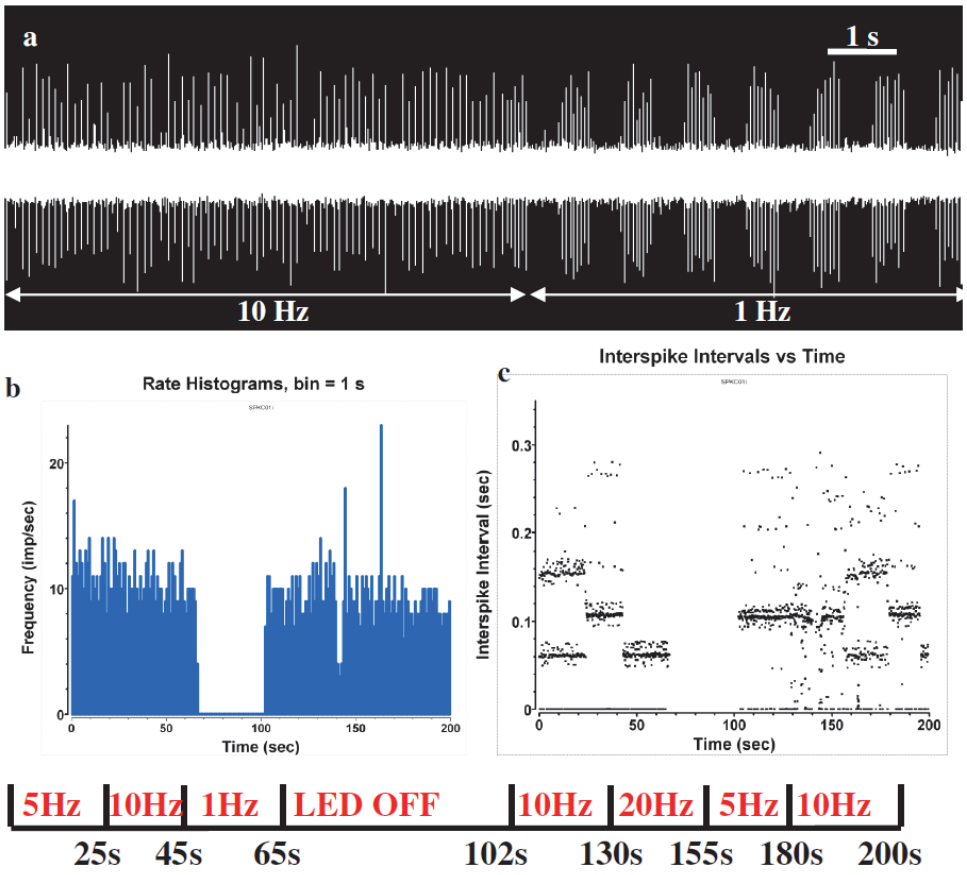

Figure 4.8 (a) Raw electrical recording from visual cortex using the microelectrode at the tip of the optrode, in response to optrode-μLED stimulation at varying frequencies. (b) Rate-histogram of spikes from neurons stimulated by optrode-μLED with different frequencies at a power density of 0.7 mW mm^{-2}. (c) Corresponding inter-spike interval as a function of time with varying frequencies of stimulation by the optrode-μLED.

The ability to control the activity of a defined class of neurons by optogenetics means has the potential to advance clinical neuromodulation. The genetic control makes it possible to develop more precise therapies by restricting the excited or inhibited neurons to the disease-relevant population. Moreover, the ability to simultaneously record electrical activity during optical stimulation without electrical artifacts makes it possible to engage in responsive neuromodulation by dynamically adjusting the

stimulation or inhibition intensity based on feedback from the activity state in the brain. This feature may be especially useful for breaking the neuronal synchronization of electrical activity in diseases such as epilepsy [4.19]. Moreover, optogenetic stimulation of the visual cortex by a μLED array would assist in optogenetic restoration of vision [4.20], in patients having enucleated eye or damaged optic nerve. The combination of electrical-recording and optical-control could also be used to bridge severed connections, for example to relay information from the brain to distal limbs in the case of a severed spinal cord. The optrode provides high spatial resolution and offers necessary millisecond-temporal precision for stimulating neurons.

Previous studies integrated optical fiber with an electrode/electrode array for simultaneous stimulation and recording of neural activities [4.21]. It requires a high power light source and care to mitigate the fragile nature of the fiber and thus, poses difficulty in translating this technology into a wireless device. In contrast, wirelessly-powered μLED has been used for optogenetic stimulation [4.22] though this paper shows a combination with μLED and microelectrodes for the first time. Thus, the μLED based optrode will help in understanding and controlling of in-vivo neuronal circuitry; modulate behavior, and intervene neurological disorders. Use of integrated μLED-electrode and lens array to optogenetically stimulate and visualize the activation process in neuronal circuitry of living organisms, with high spatial and temporal resolution, will help in understanding and intervention of neurological disorders.

4.4 Conclusions

Here, an integrated neural interface for controlled μLED stimulation and recording of neural activities from optogenetically-sensitized visual cortex of mouse models by Au/Cr electrodes has been demonstrated. Furthermore, photo-polymerized lens fabricated on the μLED allowed focusing of light to the neural tissue. Therefore, the integrated polyimide platform for the optrode fabrication has several advantages over the combination of an optical fiber to deliver light and a conventional tungsten recording electrode, including its integrated functionalities, compactness, flexibility, and robustness as an implantable device. Further work needs to be carried out to develop a compact and light weight wireless head-mountable μLED-based optrode for its use in free-behaving animals. The μLED-based optrode technology can be translated for point-of-care optogenetic prosthetic devices where optogenetic intervention of non-functional neurons can be achieved based on the feedback from the electrical recording.

CHAPTER 5

OTHER DEVICES

5.1 Dopamine Sensors

Dopamine is a catecholamine neurotransmitter activating five types of dopamine receptors D_1, D_2, D_3, D_4, and D_5. Dopamine is produced in several areas in the brain including the subtantia niagra and the ventral tagmental area. It is also a neuro-hormone release by the hypothalamus. Dopamine has many important functions in the brain including cognition, motor activity, motivation and reward, sleep, mood, attention, learning, etc. Lack of DA-containing neurons can cause Parkinson's disease, Schizophrenia, etc [1.1].

Dopamine is electrochemically active and therefore it can be sensed directly. In this work, both carbon fiber electrodes and MEAs were used to calibrate with DA in the beaker amperometrically. The bias voltage for CFEs is 0.35 V while that for a Pt thin-film electrode is 0.25 V. DA was added in steps of 10 μM and the current was recorded continuously by a potentiostat. A Nafion membrane was used to protect the electrode from the interference of 250 μM AA.

Nafion (5%, *Sigma-Aldrich*, Catalog #27,470-4) was aliquoted into 500 μl centrifuge tube. The tip of the probe was immersed half way into the tube for five seconds and then baked in an oven at 170^{o}C for 5 minutes. A thin layer of Nafion film

covered the electrode areas. This would help to propel all the molecules with negative charge [1.17].

Figure 5.1 shows an SEM image and the response of a home-made CFE with DA. The LOD was calculated as 100 nM. Figure 5.2 shows the effect of coating Nafion onto Pt electrodes. The film was deposited excessively so it did not only block AA but also somehow stopped all of others.

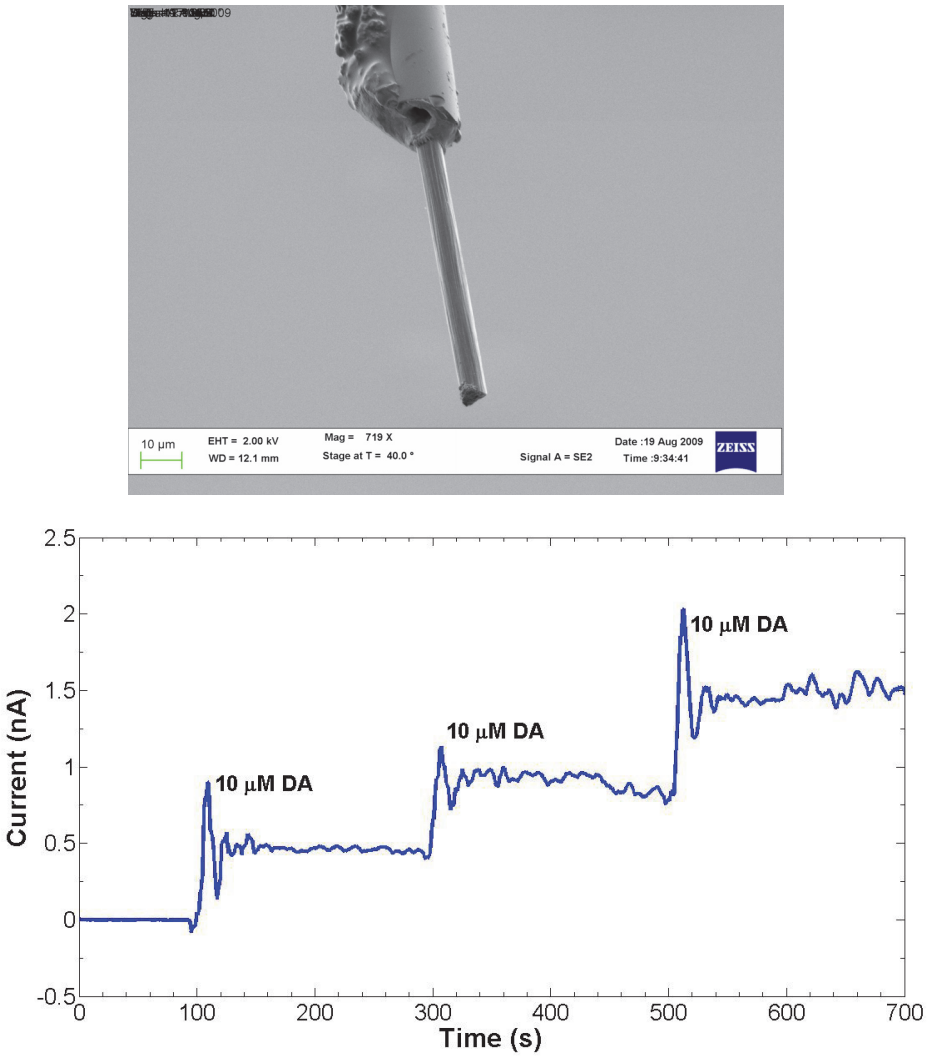

Figure 5.1 An SEM image and dopamine response from our CFE.

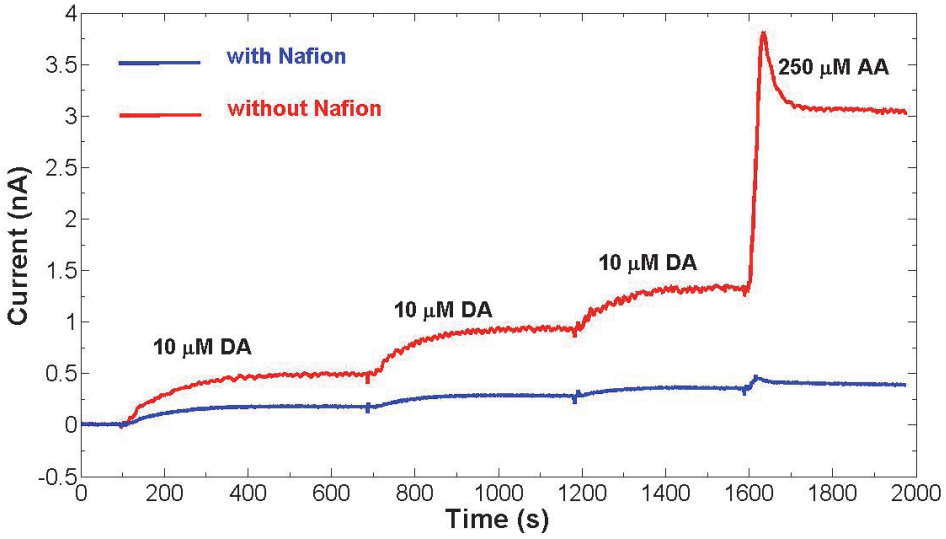

Figure 5.2 Effect of excessive Nafion on a Pt electrode.

5.2 Long Probes for Monkey Studies

For monkey studies, longer probes are needed. A 65-mm long probe was designed and fabricated. Since Si is brittle and polyimide film might be too soft, another solution of using a Ti shim as a probe material was also carried out. First, a 125 μm thick Ti shim was coated with a thin layer of SiO_2 by PECVD or a thin layer of polyimide by spin coating as an insulation layer and then same fabrication processes are repeated. Figure 5.3 shows a 65-mm long probe (middle).

5.3 Using Thermal Actuator to Control the Penetration Depth of the Implantable Probes

For long term implants, it is important to control the locations of the probe electrodes precisely in tissue in order to receive the signals. Therefore a system using a metal thermal actuator to control the penetration depth of the implantable probes was

proposed. The thermal actuators with dimensions of 10×1.4 mm^2 and 15×2 mm^2 were designed. The thermal actuators were fabricated with our laser system, which provided a cost-effective process. Our MEA probe based on polyimide substrate was attached vertically on the cold arm of the actuator by heat resistant epoxy. The required force and penetration depth could be precisely achieved by controlling the electric current flowing through the thermal actuator. Experimental results have shown a vertical movement of 1

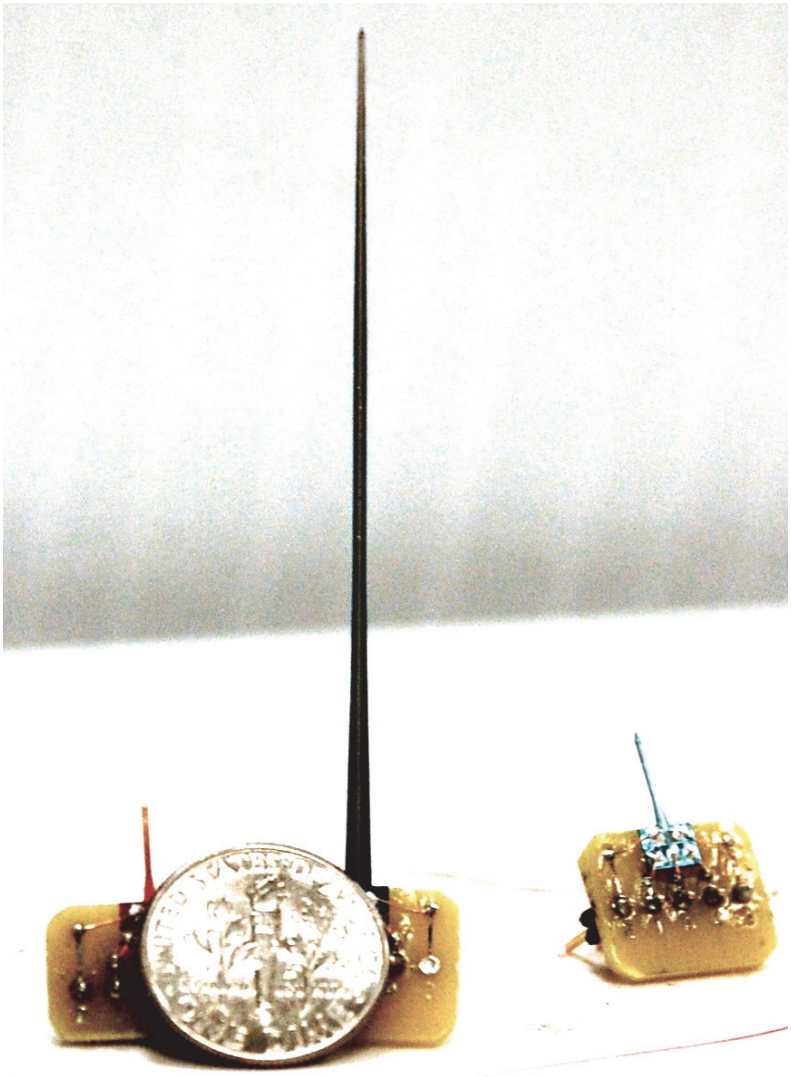

Figure 5.3 A 65-mm long probe in comparison with others.

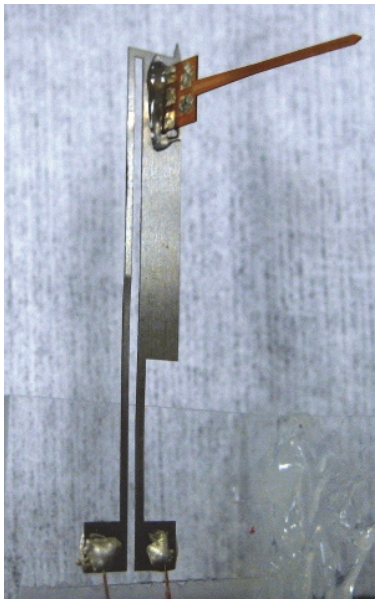

Figure 5.4 The conceptual design of using thermal actuator to control the probe.

mm at a current of 1.2 A, indicating this system can be used to control the penetration depth for implantable probes. Figure 5.4 shows the probe is on a thermal actuator.

5.4 Simple Nanostructures Modification

The modification on the polyimide-based probes was done by applying concentrated gold (Au) or silver (Ag) colloid solutions onto the electrode surfaces with a Hamilton syringe under a stereo microscope. After drying, the nanostructures will stay on the electrode surfaces securely, preliminarily for several experiments. The longevity of the nano-scale structures on the electrode surface could be enhanced by a post process to cover the electrode area with a permeable polymer film. Nafion was used for this purpose. The coating procedures were discussed earlier in this chapter.

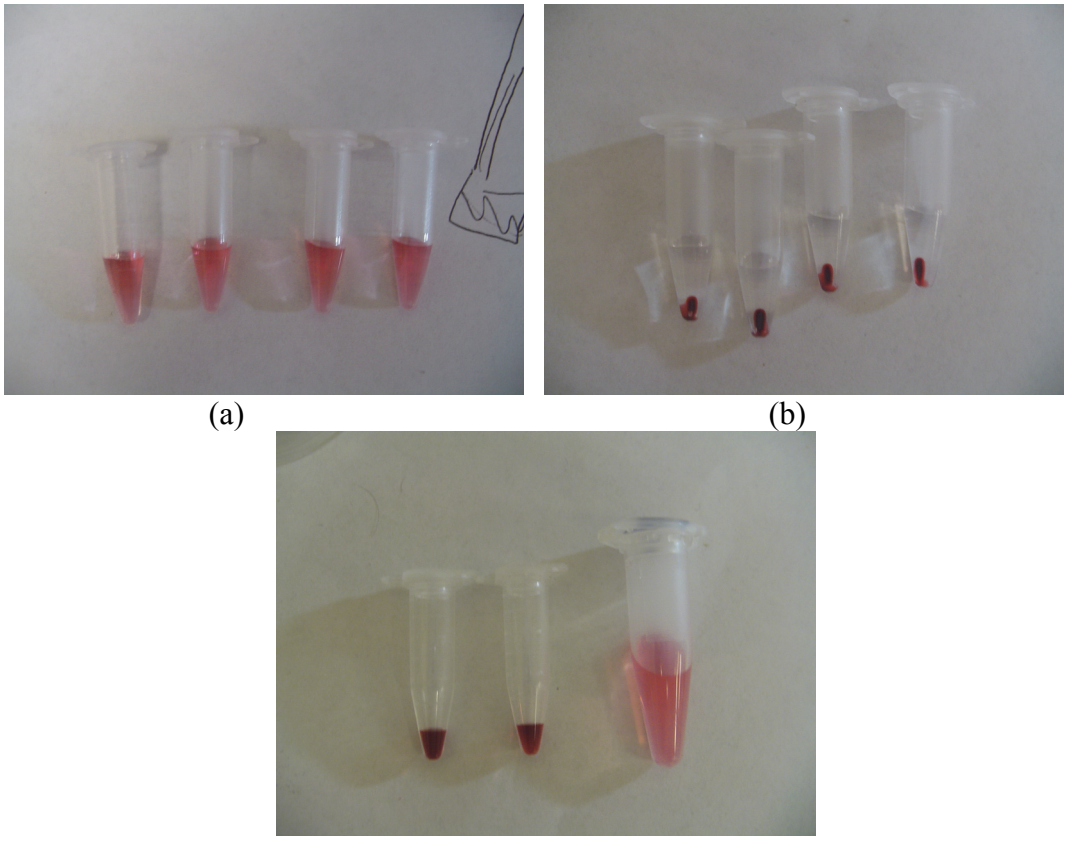

Figure 5.5 Nanoparticles concentration processes. (a) Original solution. (b) After centrifugation. (c) Two after ultrasonication (left) compared with the original one (right).

Gold colloid solutions (*Ted Pella, Inc.*) were concentrated using a micro-centrifuge. First, original solutions were dispensed into centrifuge tubes and a centrifugation process was carried out at 7000 rpm for 5 minutes. The nanoparticles were concentrated in the bottom of the tubes and a certain amount of carrier solution was extracted depending on the desired target concentration. The centrifuge tubes were put into an ultrasonic bath to disperse the nanoparticles evenly. These steps were repeated in order to obtain higher concentration colloid solutions. Various

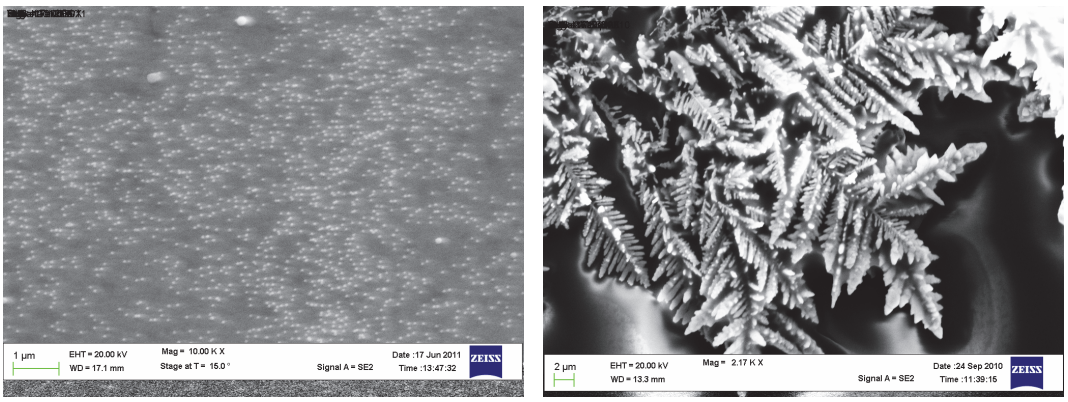

(a) (b)

Figure 5.6 SEM images of (a) the Au nanoparticle-modified surface and (b) the Ag nanostructures on the electrode surface.

concentrations in tubes are shown in Fig. 5.5. In Fig. 5.5 (c), the concentrated solutions were shown to be darker than the original one.

Silver nanostructures were created by the chemical reaction between copper film and silver nitrate ($AgNO_3$) as $Cu + 2AgNO_3 \rightarrow Cu(NO_3)_2 + 2Ag$, followed by ultrasonication to obtain the colloidal solution. It was also concentrated by the same processes. Figure 5.6 shows SEM images of (a) the Au nanoparticle-modified surface and (b) the Ag nanostructures on the electrode surface.

5.5 Au nanoparticles Modification by Using Cysteamine

Cysteamine is a chemical with an –SH (thiol) group and an $–NH_2$ (amine) group. Therefore, it can be bonded to a Au film by thiol groups to form a monolayer which then can bind to Au nanoparticles by the amine groups. This concept and an SEM image of the electrode modified by this method are presented in Fig 5.7 [5.1].

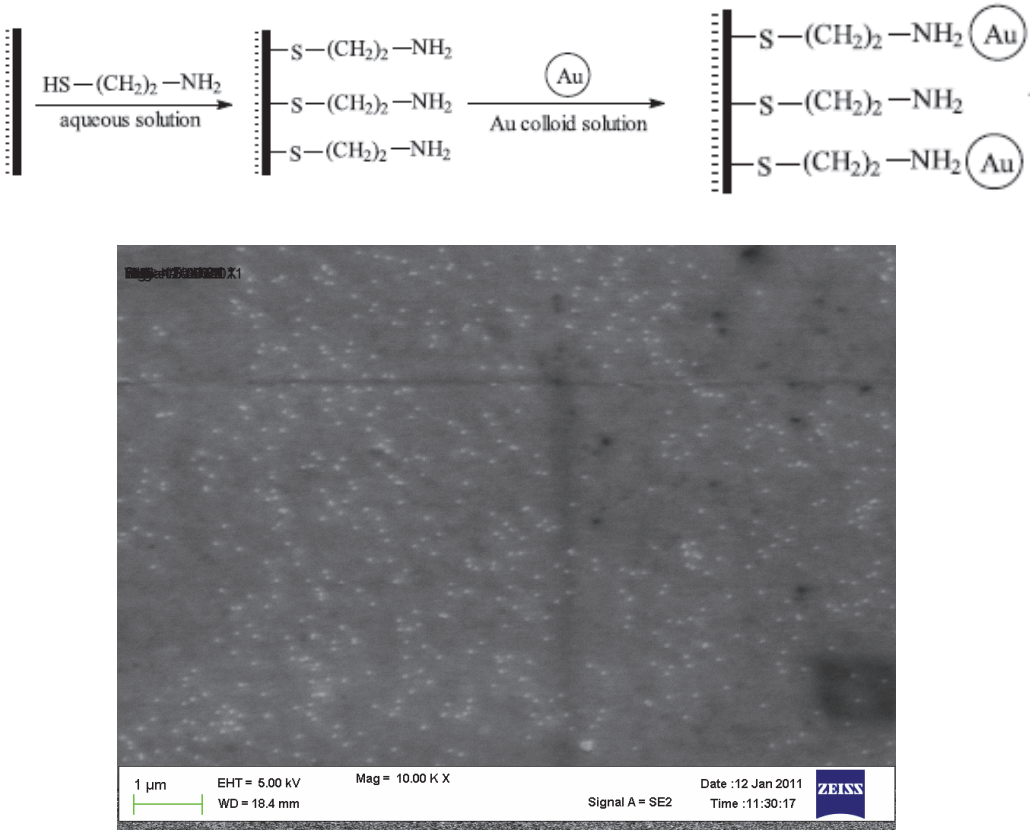

Figure 5.7 Concept and a demonstration of Au nanoparticles modification by using Cysteamine. Adapted from [5.1].

5.6 Au nanoparticles Modification by Electrodeposition

Here, a new role of electrochemically evolved hydrogen bubbles: serving as reducing agents for electroless depositions to produce hollow metallic Au nanoparticles on the electrode surface was demonstrated. This approach introduces a new concept of bubble template modification, and it has the potential to become a general route to modify the surface of electrode with Au nanoparticles.

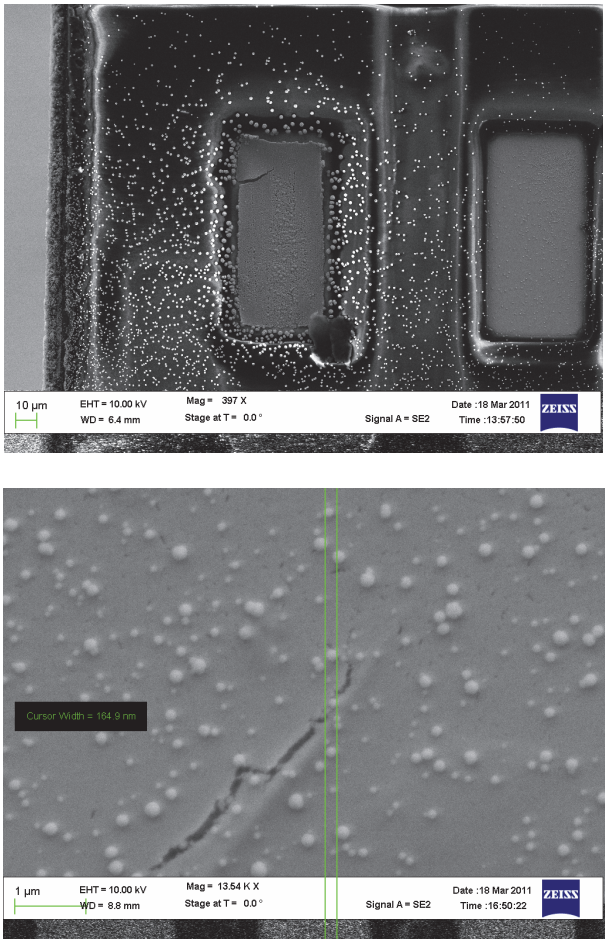

Figure 5.8 SEM images of the nanomodification electrodeposition method.

The electrolytes for electrodeposition were prepared with 0.4 M of Ni sulfamate tetrahydrate mixed with commercial gold(I) sulfite solution (*TECH-GOLD* 25 ES RTU) with volume ratio 1 to 4 to reach the pH of around 6.0.

The electrodeposition experiments were conducted potentiostatically using a typical three-electrode cell with a Ag/AgCl electrode in 3 M NaCl solution as the reference and a platinum mesh as the counter electrode. Potentials were applied to the working electrode using a *Princeton Applied Research* 273A Potentiostat/Galvanostat.

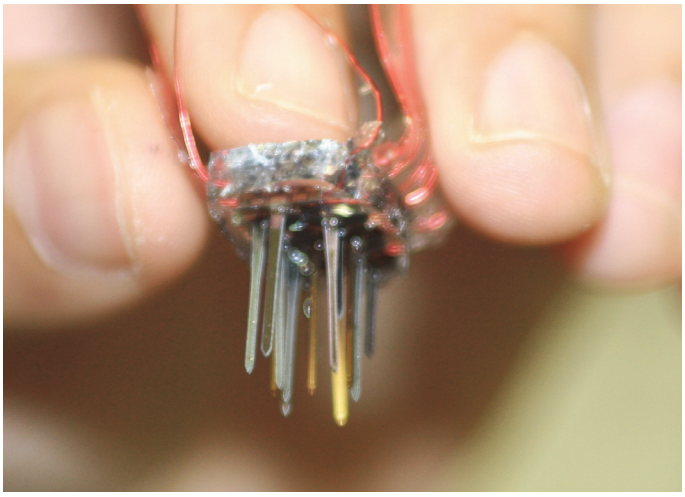

Figure 5.9 3D electrode probe by stacking single ones.

All experiments were conducted at room temperature [5.2]. Figure 5.8 shows some results of the nanoparticles formed on the electrode surface.

5.7 3D MEA

The MEA probe can be securely placed in stacks to the the 3D MEA. That type of device could be used to record the signals in a region in the brain with less missing information. Each individual electrode can be modified to sense various analytes while some of them would be used for recording action potential. This will be like an Utah-type 3D electrode but instead of detecting only electrophysiology signals, it is capable of sensing pharmacology signals as well. Furthermore, different sensors can be achieved in one shaft, which can give more local information for correlation. Figure 5.9 shows the 3D electrode.

CHAPTER 6

SOME CASE STUDIES

6.1 Pain Management Study

6.1.2 Motivation and background

Chronic pain is a significant national health problem. It is the most common reason individuals seek medical care, with 40 million medical visits annually, costing the American public more than $100 billion each year [6.1]. Several major approaches have been used to ease pain, including (a) medication, the most common route to relieve pain; (b) surgery to correct the pathological site; (c) physical rehabilitation; (d) alternative medicines; and (e) surgical implantation of neurostimulators as the last resort.

Neurostimulation of the spinal cord or primary motor cortex delivers low levels of electrical currents directly to nerve fibers or neurons to affect the neuronal membrane excitability, in turn to suppress pain signals by opening and closing of ion channels through releasing various kinds of neurotransmitters [6.2-6.5]. This form of therapy is attractive because it is selective for pain and has few side effects [6.6] compared to other approaches. Neurostimulation reduces or blocks a pain signal rather than eliminating it. Therapeutic studies have shown when used on carefully selected chronic pain patients, neurostimulation could significantly improve pain relief and reduce use of narcotic medications [6.7-6.10].

Pain is a complicated mechanism involving many of our body activities which requires a lot of knowledge in biology, neurology and several other areas to understand. In this section, however, only a general background of the pain mechanism in a simple way necessary to understand the work in this thesis will be provided. More details can be found in [6.11]. In short, the feeling of pain can be explained roughly in a few steps. First, the sensory fibers convey the pain information to the spinal cord from the place where noxious stimuli are presented. The fibers terminate on neurons in the dorsal horn area of the spinal cord. Then APs are fired from the neurons and transmitted to the brain by releasing neurotransmitters. This mechanism is a part of the body's protection systems to notify the brain that there are noxious stimuli. It is at this point that we feel uncomfortable and respond by trying to stop the pain if possible. The pain pathway or the spinothalamic pathway includes the dorsal horn in the spinal cord, the thalamus and the somatosensory cortex. In those areas, pain signals could be detected by analyzing the recorded AP or neurotransmitter release.

Recording AP has been used in our lab in a closed-loop system to detect and treat pain by electrical pulses wirelessly. However, there have been some challenges in data processing to interpret the pain signals and the inhibition signals. This will lengthen the response time and reduce the accuracy. If there is a sensing system that can detect the excitatory (L-glutamate) and inhibitory (GABA) neurotransmitters, it would be clearer to tell if the pain is initiated and when it is relieved. The concentration of those neurotransmitters will tell the level of the pain and pain relief. The neural probes which were mentioned earlier in this thesis are capable of doing so with proper enzyme

modifications. In order to show a proof of principle, a rat model was created and L-glutamate sensors were used to record the L-glutamate release in the dorsal horn of anesthetized rat with respect to graded stimuli in the leg.

6.1.3 Rat model experiments

Male Sprague–Dawley rats (300-400 g) were used in the experiments. All surgical procedures were approved by the University of Texas at Arlington Institutional Animal Care and Use Committee. The procedures were in accordance with the guidelines published by the Committee for Research and Ethical Issues of the International Association for Study of Pain [3.4]. The rats were anesthetized using sodium pentobarbital (50 mg/kg, i.p.). The spinal cord was exposed by performing a 3–4 cm laminectomy over the lumbosacral enlargement. A cannula was inserted in the trachea for artificial respiration if needed. The anesthesia was maintained by intravenous administration of sodium pentobarbital at a rate of 5 mg/ml per hour. The pupil reflex was monitored periodically to ensure a proper depth of anesthesia. The spinal cord was immobilized in a stereotaxic frame and covered with mineral oil. The end tidal CO_2 was maintained at around 30 mmHg and the body temperature was maintained at 37°C using a feedback controlled heating pad and a rectal thermal sensor probe [3.4].

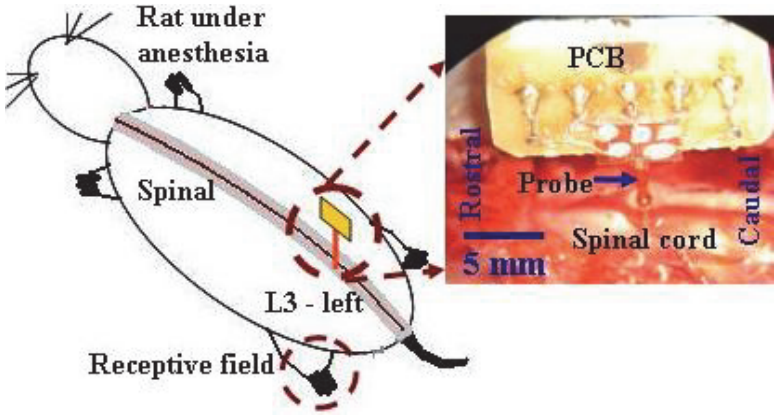

(a)

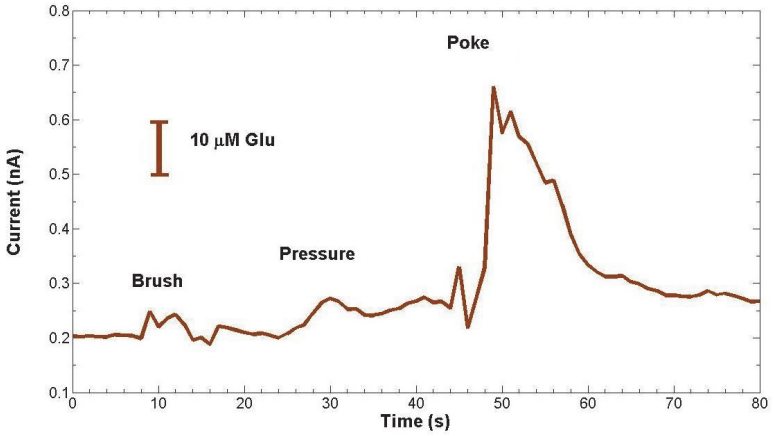

(b)

Figure 6.1 (a) The flexible sensor probe was inserted into the L3 region of the spinal cord. (b) The recorded signals show the L-glutamate releases in response to graded stimuli in the leg.

One of our sensor probes was inserted to the spinal cord dorsal horn, where nociceptive primary afferent fibers terminate [3.4]. The L3 regions were chosen which responded to the rat's legs where the noxious nociceptive signals, indicating pain, would be applied by graded mechanical stimuli. The recording electrodes were about 0.8-1 mm below the tissue surface. The electrical connections were set and currents were

recorded continuously by a potentiostat (*Pinnacle)*. Figure 6.1 (a) shows the probe configuration with respect to the tissue.

After the signal reached the baseline, the timestamp was set at zero and graded mechanical (brush, pressure and poke) stimuli were applied to the receptive fields in the leg. Brush stimulus was applied by a camel hair brush moving over the receptive fields in a rhythmic fashion which was innocuous. Pressure stimulus was applied by a venous bulldog clamp (6 cm long, straight, serrated jaws). The pressure stimulus was between innocuous and noxious. The poke stimulus was applied by a sharp needle as a noxious one [3.4]. Figure 6.1 (b) shows the detection result of local L-glutamate releases when three stimuli were applied sequentially in the leg. The scale shown indicates the relationship between the detected electrical current and the calibrated L-glutamate concentration. The nociceptive signals induced by the mechanical stimuli propagate through peripheral nerve fibers to the spinal cord. The plot was processed by subtracting the signals from the working electrode to the signals from the self-referencing electrode. Therefore, the response was selective to the local L-glutamate releases near the probe. The signals from brush, which is defined as an innocuous stimulus, and poke, as a noxious stimulus, were clearly distinguishable. As indicated in chapter 3, the time response of our sensor toward the equilibrium of L-glutamate solution in a beaker was within 2 s with the help of magnetic stirrer. In Fig. 6.1 (b), the L-glutamate releases in animals toward each stimulus last much longer, between 10 and 18 s. This is due to the L-glutamate diffusion and neuron's uptake time in the spinal cord tissue.

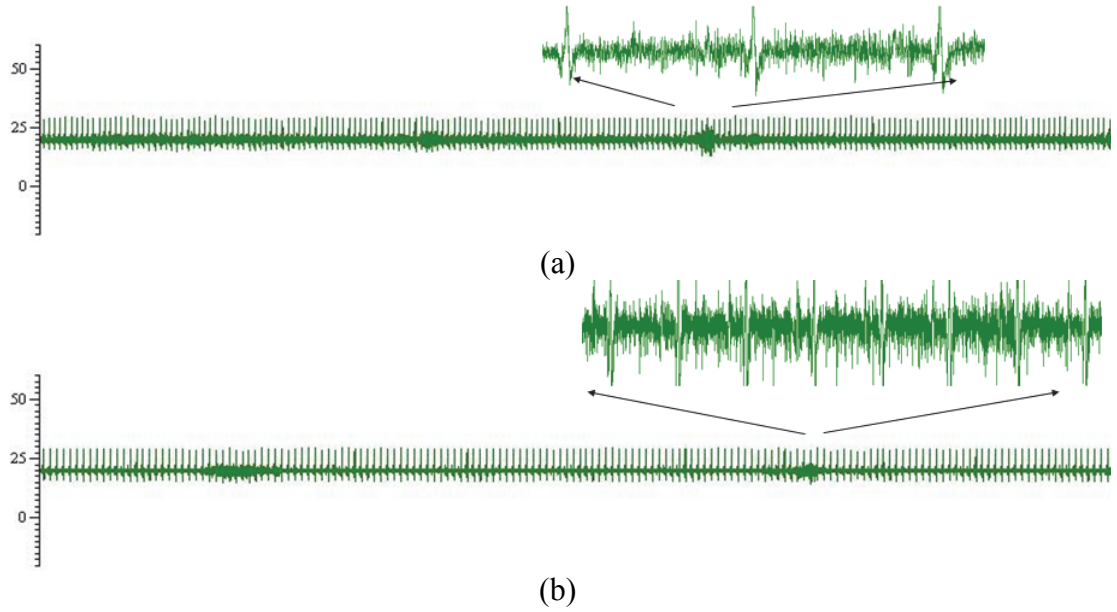

Figure 6.2 AP recordings at the thalamus with respect to pressure stimuli using (a) Au electrode and (b) Pt electrode.

In order to demonstrate the capability of our probe of recording action potentials, an experiment was carried out by inserting it to the thalamus of an anesthetized rat, applying pressure stimuli and recording the signals by a CED 1401Plus system from *Cambridge Electronic Design*. Figure 6.2 shows that the neurons were firing with pressure stimulations and all of those could be observed by the action potentials recorded by either Au or Pt electrodes on our probes.

6.2 Addiction Studies

Addiction of a drug or alcohol is defined as the repeated use of a psychoactive substance or substances, to the extent that the addict is periodically or chronically intoxicated, shows a compulsion to take the preferred substance (or substances). The

addict also has great difficulty in voluntarily ceasing or modifying substance use and exhibits determination to obtain psychoactive substances by almost any means [6.12]. Different neurotransmitters have been believed to be associated with various additive substances, such as DA with cocaine and amphetamine, L-glutamate and GABA with alcohol, etc. Therefore, addictions studies could be investigated using our sensor in real time. The DA information will give us some idea about the state of the addict.

A rat experiment has been designed and carried out to show the proof of principle. A CFE was used to record DA release in the nucleus accumbens (NAcc) which has DA projections from the ventral tegmental area (VTA). These terminals are also the site of action of highly-addictive drugs such as cocaine, morphine and amphetamine, which cause a manifold increase in DA levels in the nucleus accumbens. In addition to cocaine, morphine and amphetamine, almost every recreational drug has been shown to increase dopamine levels in the nucleus accumbens [6.12]. A male Sprague–Dawley rat (~400 g) was used in the experiment. All surgical procedures were approved by the University of Texas at Arlington Institutional Animal Care and Use Committee. The rat was anesthetized using sodium pentobarbital. First, we injected saline to the thigh for control and then the addictive substance was injected at the same location. In the first experiment, 0.3 ml morphine was used and 0.25 ml of cocaine was for the second one. Results are shown in Fig. 6.3a. As we can see from the figures, 0.3 ml morphine caused a small rise in the current output after 10 minutes, but 0.25 ml cocaine gave 2 high peaks after less than 3 minutes. These indicated that cocaine is a stronger addictive substance. It was transferred faster and with much higher effect. The

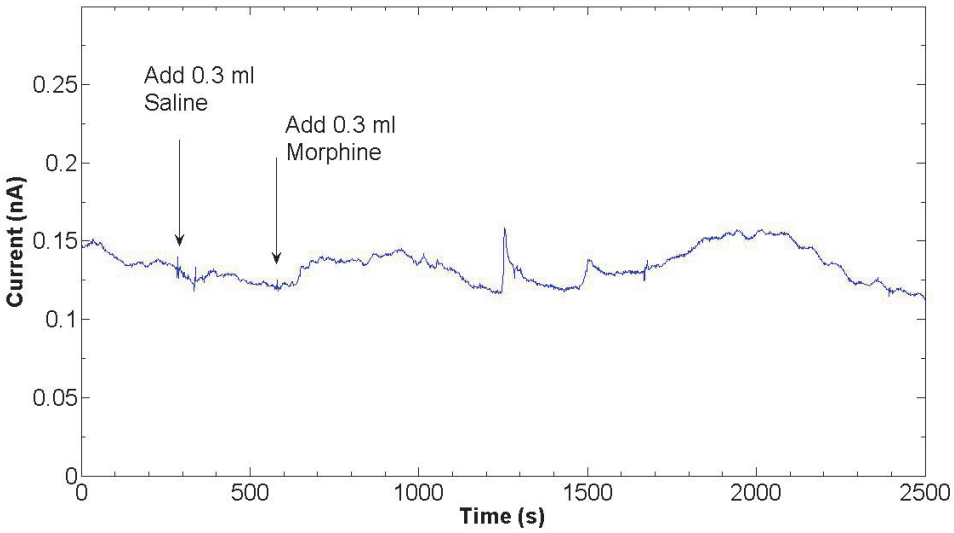

(a)

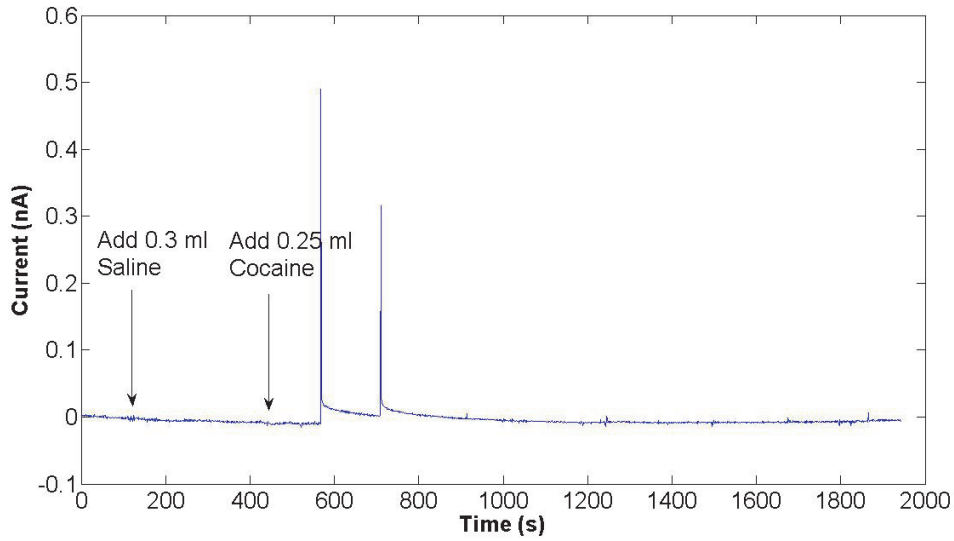

(b)

Figure 6.3 DA responses in NAcc with respect to injection to the thigh of (a) 0.3 ml morphine and (b) 0.25 ml cocaine.

interesting thing was cocaine caused 2 pitches in the nervous system representing by two high peaks and then DA was re-uptaken.

CHAPTER 7

FUTURE WORK

7.1 Long-term Implant

To prove the advantages of our probes, a set of animal experiments to compare those devices is needed. A plan was made to use 8 rats divided into two batches with 4 for each. The first batch (4 rats) will be implanted with 1 AgCl polyimide probe in the left striatum, -0.8 mm from Bregma, 5 mm deep, 3.5 mm from the middle; 1 IrO_x polyimide probe in the right striatum -0.8 mm from Bregma, 5 mm deep, 3.5 mm from the middle; 1 Au polyimide probe in the left striatum +1.7 mm from Bregma, 5 mm deep, 3 mm from the middle and 1 Au silicon probe in the right striatum +1.7 mm from Bregma, 5 mm deep, 3 mm from the middle. This batch will be investigated after one week. The brain will be sliced, stained and compared. The second batch (4 rats) will be done with the same procedure but the rats will be checked after 3 weeks.

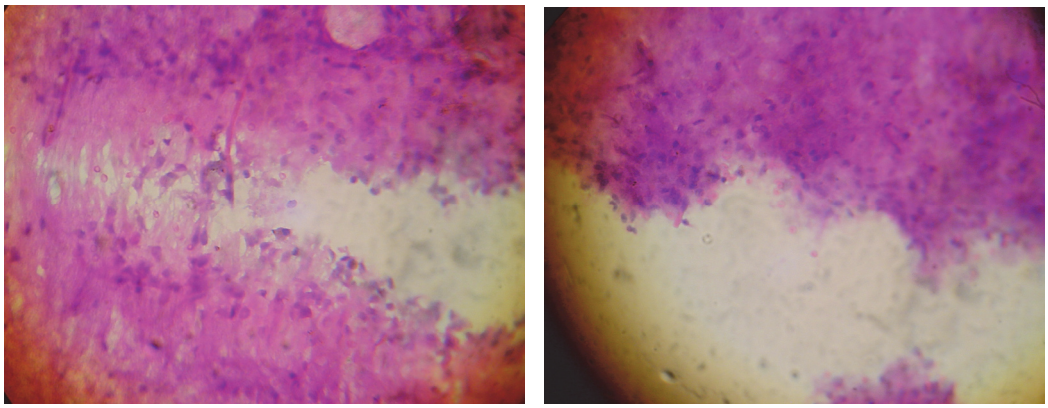

Figure 7.1 Photo of the stained slices at the implantation sites.

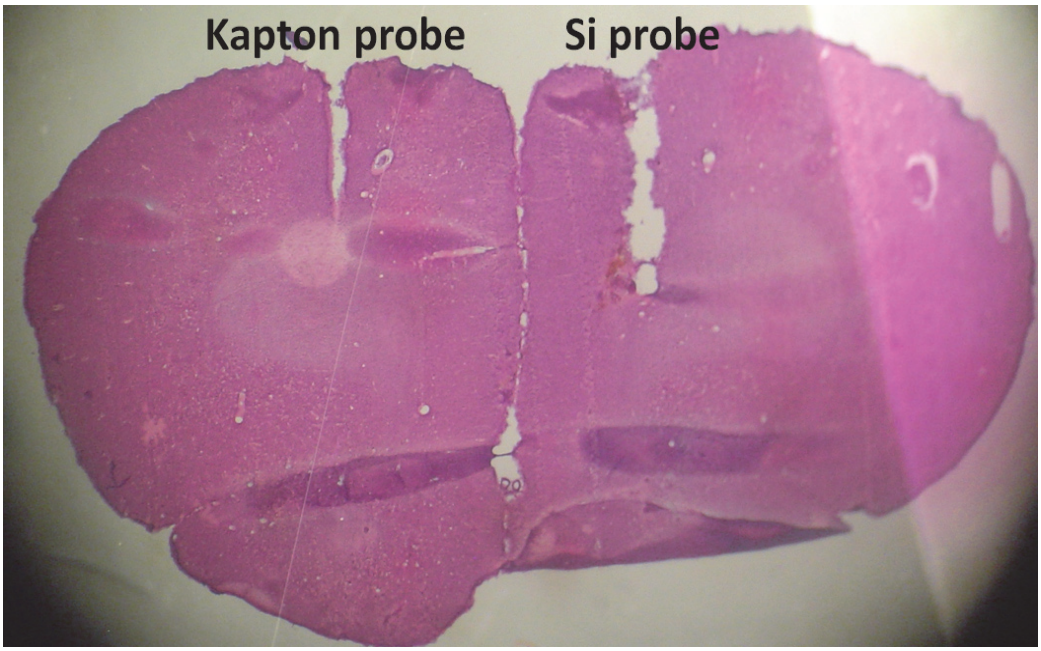

Figure 7.2 A stained brain slice showing the damages caused by the probes.

The H&E (Hematoxylin and Eosin) staining method was chosen due to its simplicity and capability to observe the cell level to check the biocompatibility of the probes. The first rat was taken and tried with the above-mentioned procedures. After 3 days, the rat was perfused with PBS for 5 minutes and then formalin for 15 minutes to harden the brain which was then taken and put into sucrose for 1 day before slicing. At the first time, 40 μm slices were tried due to the equipment limitations. The slices were stained by the steps as described in Appendix C and then observed under microscope. Figure 7.1 shows some photos of the tracks at 40x magnification. It could be seen from the figure that, the slices were too thick to see the cells therefore it is hard to judge the level of damage and inflammation to the animal. Figure 7.2 shows a comparison of the histology insertion tracks between the Kapton probe and the Si probe. It is obvious that

the Si probe caused more damages and a bigger wound than the Kapton one did. This is due to the fact that Si is rigid and not biocompatible.

Further trials with thinner slices and more rats have been prepared. A batch will be investigated after 3 weeks of implantation while the other one will be done after 7 weeks. Other immunohistology methods will be also considered such as GFAP (Glial fibrillary acidic protein) to see the glia, cresyl violet to highlight the neurons and Iba-1 for the microglia.

Enzyme is supposed to work for three weeks and that was confirmed in our lab with the probes placed at room temperature inside the cabinet. Long-term operation should be investigated to see whether the enzyme would degrade faster *in vivo* or some bio-fouling effects would isolate the probe. Furthermore, freely moving animal recording should also be tried.

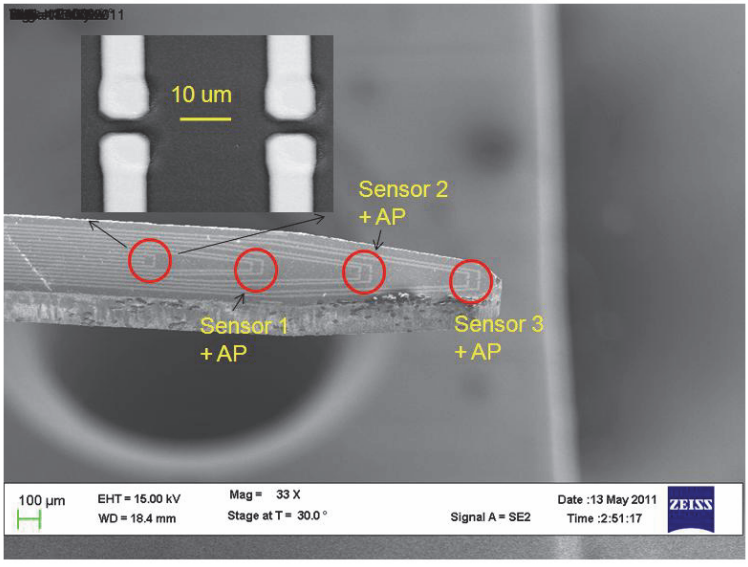

Figure 7.3 Our future probe with different sensors and AP recording electrodes. The size is 10×10 μm^2.

7.2 Correlation of Signals

The correlation of different signals will give better understanding about the CNS. While simultaneously detecting different neurotransmitters is possible to carry out, there are still some challenges with the correlation of AP and sensing neurotransmitters amperometrically in real time. Since the potentiostat used to record the amperometric current in neurotransmitter sensors does not have a ground (it uses virtual ground) while the AP recording system uses the animal body as the ground, there has been always some unknown crosstalk. Since electrochemical amperometric sensors require a continuous current recording, the idea of using a switch to separate those two is not feasible. However, this could be alternatively solved by doing AP recording and neurotransmitters sensing at different places of a same pathway. For example in case of pain management study, a probe would be used to record AP at the spinal cord while the other one is sensing L-glutamate at the thalamus, or vice versa. A single electronic instrument which can do all of these simultaneously would be of great interest in neuroscience research. Figure 7.3 show the future ultimate goal of my research of which we have a microprobe with an MEA consisting a high count of multi-modality electrodes.

7.3 LED arrays

As reported in the chapter 4 with a single micro-LED integrated with 3 recording electrodes in a single probe, it would be useful if it's possible to optogenetically stimulate and record more signals in a bigger area. A 2D array with

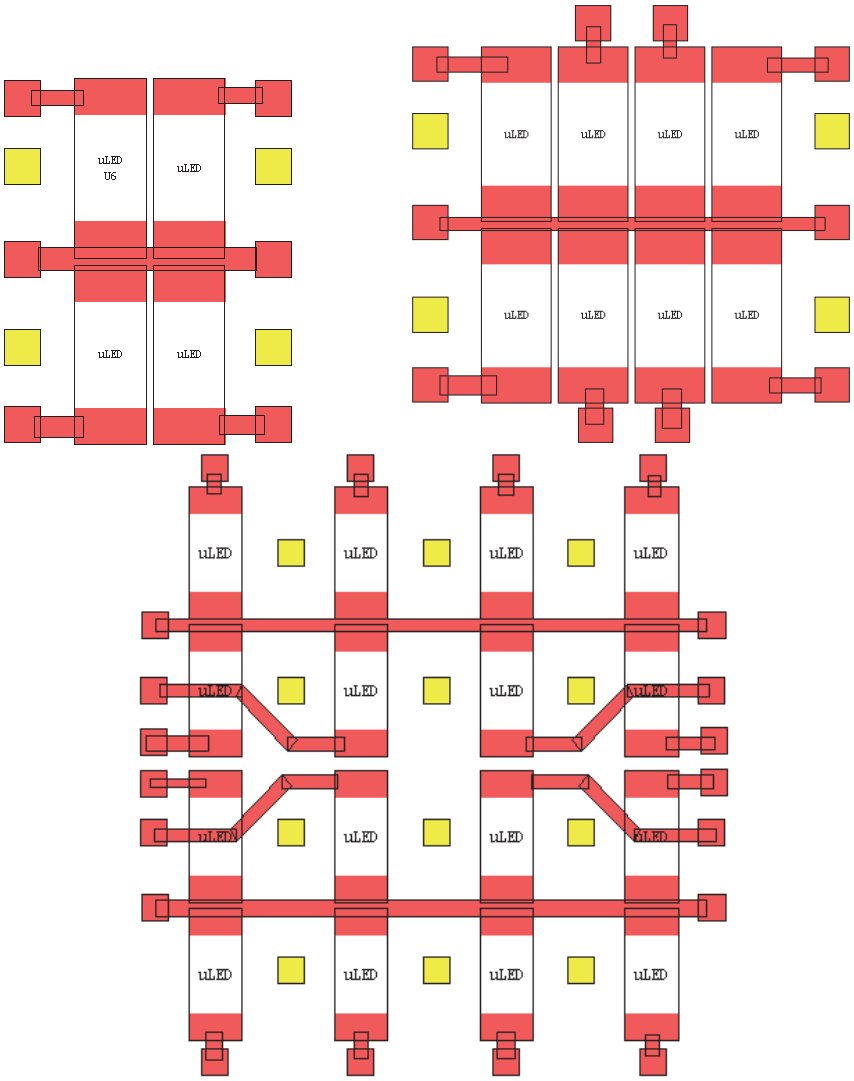

Figure 7.4 Different LED arrays designs. The yellow square shows the electrodes to record the AP.

micro-LEDs integrated with an MEA would be a good choice. Several designs have been made and implemented to do so with different configurations using 4, 8 and 16 LEDs as shown in Fig. 7.4. These arrays can be used to stimulate and record the AP signals at the cortex, therefore it would be an minimal invasive approach.

7.4. Future Work Summary

These will be done in near future:

- Carry out more animal experiments including long-term implant and freely-moving-animal recordings with the existing working devices for pain management study.
- Since action potential recording and neurotransmitter sensing have been done separately, these should be investigated to do simultaneously to have a better way for neuro-studies.
- Use those LED integrated arrays for animal experiments.
- Apply the devices for different neuro-studies.

APPENDIX A

ENZYME COATING PROCEDURES

1. Cleaning (first time use):

   - 5 minutes in Citrisolv (constant stirring)
   - 5–10 minutes in DI water (constant stirring)
   - N_2 blow and dry at low temperature (105–115°C) in an oven for 10 minutes

   (When reusing electrodes, try stirring 30 minutes in 80°C DI water and continue as above).

2. Enzyme coating:

   a) Chemicals: BSA (*Sigma*, A-3059), glutaraldehyde (Glut) (*Sigma*, G-5882), L-glutamate oxidase (GluOx) - Recombinant (Catalog No: G4001-01, *United States Biological*), mPD (*Sigma*, Cat #235903).

   b) Bring all chemicals to room temp before use.

   c) Dissolve GluOx @ 1 U/µl in DI water.

   d) Weigh 0.01 g BSA in 1.5 ml microcentrifuge tube, then add 985 µl DI water, DO NOT vortex vigorously. Add 5 µl of Glut.

   (Final concentrations: BSA; 1%, Glut; 0.125%).

   e) Transfer 4.5 µl of BSA/Glut into a 500 µl microcentrifuge tube.

   f) Add 1 µl of GluOx.

   g) Apply enzyme solution using a 10 µl *Hamilton* syringe with a dome tip needle.

   h) Draw up ~0.1µl of solution.

   i) Create a bead (drop) of solution at the tip of the syringe.

   j) Under a dissecting stereoscope, apply bead on surface of the electrode, wait 2–3 seconds, then pull tip away.

k) Let dry for a minute, typically 3 applications are enough.

l) Set aside in a clean dry place.

m) Room temp for at least 48–72 hours - time required for full cross-linking of the protein to the surface of the electrode.

3. mPD coating:

   a) Degas 100 ml of 0.05 M PBS with N_2 for 15 minutes.

   b) Dissolve 0.0905 g mPD in 100 ml 0.05 M PBS (5 mM).

   c) Add ~40 ml of 5 mM mPD to a 50 ml beaker.

   d) Lower microelectrode tip into 5 mM mPD solution.

   e) Place glass Ag/AgCl reference electrode into beaker.

   f) Run a CV at 50 mV/s in 15 minutes with the potential window 0.2-0.7 V versus the Ag/AgCl electrode.

   g) Remove microelectrode from 5 mM mPD and rinse tip with DI water.

   h) Cure at room temperature for 24 hours prior to calibration.

4. Self-reference electrode coating: Do from step 2 (h) to 2 (m) with the solution of only BSA and Glut (no enzyme).

APPENDIX B

REFERENCE ELECTRODE PROCEDURES

The cleaning procedures follow Appendix A.

1. Ag/AgCl reference electrode:

a) Wire electrode:

- Plating Solution: 50 g NaCl / 90 ml 1M HCl in a 100 ml beaker (plating bath).
- Bath electrode: Pt wire.
- Preparation of Ag wire, cut a 10-15 cm long piece of Teflon coated silver wire (0.008" bare).
- Clamp “red” (+) wire to prepared Ag wire (reference electrode).
- Clamp “black” (-) wire to Pt bath cathode.
- Plug in DC adapter 9 V.
- Look for correct plating process – Bubbles should appear at bath electrode and reference electrode turns a silver/gray color.
- Plating reaction takes from 2-20 minutes generally.
- Plating reaction: $Ag^{\circ} + Cl^{-} \rightarrow AgCl + e^{-}$

b) Planar microelectrode:

- Repeat the same with DC voltage 0.5-1 V in 30-45 seconds.

2. IrO_x pseudo-reference electrode:

a) Solution preparation:

- 0.075 g $IrCl_4.H_20$ 99% was dissolved in 50 ml DI water.
- Stirring solution for 10 minutes.
- Add 0.5 ml H_2O_2 30% and 0.5 g acid oxalic $C_2H_2O_4.2H_2O$.
- The color of solution changed from dark-purple into light yellow-green.

- Add potassium carbonate K_2CO_2 to increase pH solution up to 10.5.
- The pH value was checked by Hanna pH meter.
- Keep 2 days for stabilization before electro-deposition IrO_x.
- The color changes from yellow-green into dark-blue.
- Should be no precipitation observed.
- Precipitated IrO_x only appeared after 1 month.
- To extend the life time to several months, keep solution at 4^oC.

b) Electrodeposition:

- With Au electrode: Run CV at 50 mV/s in 15 minutes with potential window of 0-0.7 V versus a Pt wire electrode.
- With Pt electrode: Run CV at 50 mV/s in 15 minutes with potential window of 0-0.65 V versus a Pt wire electrode.
- Those are for 50×100 μm^2 planar electrodes.
- Need to change based on the area to obtain a current density as low as 2 A/m^2.

APPENDIX C

H&E STAINING

1. Chemicals:

- 100% EtOH.
- Hematoxylin (Gill's 1X).
- Acid alcohol (1%HCl in 70%EtOH).
- Ammonia water (1ml NH_4OH in 1 l H_2O).
- Eosin Y.

2. Steps:

- Rinse in distilled water.
- Hematoxylin in 5 minutes.
- Rinse in tap water in 5 minutes.
- Acid alcohol 2-3 times.
- Rinse in tap water in 3 minutes.
- Ammonia water 5-6 times.
- Rinse in tap water 5 minutes.
- Eosin Y 1 minute.
- Rinse in tap water 2 minutes.
- EtOH 2 minutes.
- EtOH 2 minutes.
- EtOH 2 minutes.
- Coverslip and ready to observe.

REFERENCES

[1.1] E. R. Kandel, J. H. Schwartz and T. M. Jessell, "Principles of Neural Science", *McGraw-Hill*, Fourth Edition, 2000.

[1.2] D. Richards, T. Clark and C. Clarke, "The Human Brain and Its Disoders", *Oxford University Press*, 2007.

[1.3] http://www.clinchem.org/cgi/content/full/49/10/1763

[1.4] http://www.sci.utah.edu/~gk/abstracts/bisti03/

[1.5] V. I. Chefer, A. C. Thompson, A. Zapata and T. S. Shippenberg, "Overview of Brain Microdialysis", *Current Protocols in Neuroscience*, 7.1.1-7.1.28, Apr, 2009.

[1.6] U. Ungerstedt and A.Hallström, "In vivo Microdialysis - A New Approach to the Analysis of Neurotransmitters in the Brain", *Life Sciences*, Vol. 41(7), 1987.

[1.7] J.B. Justice Jr., "Quantitative Microdialysis of Neurotransmitters", *J. of Neurosci. Methods*, Vol. 48, 1993.

[1.8] J. Cordek, X. Wang, and W. Tan, "Direct Immobilization of Glutamate Dehydrogenase on Optical Fiber Probes for Ultrasensitive Glutamate Detection", *Analytical Chemistry*, 71, pp. 1529-1533, 1999.

[1.9] S. Okumoto, L. Looger, K. Micheva, R. Reimer, S. Smith and W. Frommer, "Detection of Glutamate Release from Neurons by Genetically Encoded Surface-Displayed FRET Nanosensors", *PNAS*, 102(24), pp. 8740-8745, 2005.

[1.10] Niwa, O., Horiuchi, T. and Torimitsu, K., "Continuous Monitoring of l-Glutamate Released from Cultured Nerve Cells by an Online Sensor Coupled with Micro-Capillary Sampling", *Biosensors and Bioelectronics*, 12(4), pp. 311-319, 1999.

[1.11] Ryan, M. R., Lowry, J. P., and O'Neill, R. D., "Biosensor for Neurotransmitter l-Glutamic Acid Designed for Efficient Use of l-Glutamate Oxidase and Effective Rejection of Interference", *Analyst*, 122, pp. 1419-1424, 1997.

[1.12] Kuritaa, R., Tabei, H., Hayashib, K., Horiuchib, T., Torimitsu, K., and Niwa, O., "Improvement in Signal Reliability When Measuring l-Glutamate Released from Cultured Cells Using Multi-Channel Microfabricated Sensors", *Analytica Chimica Acta*, 441(2), pp. 165-174, 2001.

[1.13] Burmeister, J. J. and Gerhardt, G. A., "Self-Referencing Ceramic-Based Multisite Microelectrode for the Detection and Elimination of Interferences from the Measurement of l-Glutamate and Other Analytes", *Analytical Chemitry*, 73, pp. 1037-1042, 2001.

[1.14] Oldenziel, W. H., Dijkstra, G., Cremersb, T. I. F. H. and Westerink, B. H. C., "In Vivo Monitoring of Extracellular Glutamate in the Brain with a Microsensor", *Brain Research*, 1118(1), pp. 34-42, 2006.

[1.15] Hamdi, N., Wang, J., Walker, E., Maidment, N. T and Monbouquette, H. G., "An Electroenzymatic l-Glutamate Microbiosensor Selective against Dopamine", *Journal of Electroanalytical Chemistry*, 591(1), pp. 33-40, 2006.

[1.16] Rutherford, E. C., Pomerleau, F., Huettl, P., Strömberg, I., and Gerhardt, G. A., "Chronic Second-by-Second Measures of l-Glutamate in the Central Nervous System of Freely Moving Rats", *Journal of Neurochemistry*, 102, pp. 712-722, 2007.

[1.17] Hascup, K. N., Hascup, E. R., Pomerleau, F., Huettl, P., and Gerhardt, G. A., "Second-by-Second Measures of l-Glutamate in the Prefrontal Cortex and Striatum of Freely Moving Mice", *The Journal of Pharmacology*, 324(2), pp. 725-731, 2007.

[1.18] Frey, O., Van Der Wal, P., De Rooij, N., and Koudelka-Hep, M., "Development and Characterization of Choline and L-Glutamate Biosensor Integrated on Si Microprobes for In-vivo Monitoring", *IEEE EMBS*, Lyon, France, 2007.

[1.19] Qin, S., Van der Zeyden, M., Oldenziel, W. H., Cremers, T. I. and Westerink, B. H., "Microsensors for *in vivo* Measurement of Glutamate in Brain Tissue", *Sensors*, 8(11), pp. 6860-6884, 2008.

[1.20] Wassum, K. M., Tolosa, V. M., Wang, J., Walker, E., Monbouquette, H. G. and Maidment, N. T., "Silicon Wafer-Based Platinum Microelectrode Array Biosensor for Near Real-Time Measurement of Glutamate *in Vivo", Sensors,* 8(8), pp. 5023–5036, 2008.

[1.21] Kissinger, P. T., Hart, J. B. and Adams, R. N., "Voltammetry in Brain Tissue - A New Neurophysiological Measurement", *Brain Research*, 55(1), pp. 209-213, 1973.

[1.22] Adams, R. N., "In vivo Electrochemical Measurements in the CNS", Progress in Neurobiology, 55(1), pp. 297-311, 1990.

[1.23] Bunin, M. A., and Wightman, R. M., "Quantitative Evaluation of 5-Hydroxytryptamine (Serotonin) Neuronal Release and Uptake: An Investigation of Extrasynaptic Transmission", *Journal of Neuroscience*, 18(13), pp. 4854-4860, 1998.

[1.24] Cass, W. A., Gerhardt, G. A., Mayfield, R. D., Curella, P., and Zahniser, N. R., "Differences in Dopamine Clearance and Diffusion in Rat Striatum and Nucleus Accumbens Following Systemic Cocaine Administration", *Journal of Neurochemistry*, 59(1), pp. 259-266, 1992.

[1.25] Cass, W. A., Gerhardt, G. A., Gillespie, K., Curella, P., Mayfield, R. D. and Zahniser, N. R., "Reduced Clearance of Exogenous Dopamine in Rat Nucleus Accumbens, but Not in Dorsal Striatum, Following Cocaine Challenge in Rats Withdrawn from Repeated Cocaine Administration", *Journal of Neurochemistry*, 61(1), pp. 273-283, 1993.

[1.26] Cragg, S. J., Hawkey, C. R. and Greenfield, S. A., "Comparison of Serotonin and Dopamine Release in Substantia Nigra and Ventral Tegmental Area: Region and Species Differences", *Journal of Neurochemistry*, 69(6), pp. 2378-2386, 1997.

[1.27] Garris, P. A., Christensen, J. R. C., Rebec, G. V. and Wightman, R. M., "Real-Time Measurement of Electrically Evoked Extracellular Dopamine in the Striatum of Freely Moving Rats", *Journal of Neurochemistry*, 68(1), pp. 152-161, 1997.

[1.28] Gerhardt, G. A, "Rapid Chronocoulometric Measurements of Norepinephrine Overflow and Clearance in CNS Tissues", *Neuromethods*, 27, pp. 117-151, 1995.

[1.29] Gerhardt, G. A., Cass, W. A., Hudson, J., Henson, M., Zhang, Z., Ovadia, A., Hoffer, B. J. and Gash, D. M., "In Vivo Electrochemical Studies of Dopamine Overflow and Clearance in the Striatum of Normal and MPTP-Treated Rhesus Monkeys", *Journal of Neurochemistry*, 66(2), pp. 579-588, 1996.

[1.30] Gratton, A. and Wise, R. A., "Drug- and Behavior-associated Changes in Dopamine-related Electrochemical Signals during Intravenous Cocaine Self-administration in Rats", *Journal of Neuroscience*, 14(7), pp. 4130-4146, 1994.

[1.31] Gratton, A., 1996, "In vivo Analysis of the Role of Dopamine in Stimulant and Opiate Self-Administration", Journal of Psychiatry and Neurosciene, 21(4), pp. 264-279.

[1.32] Kawagoe, K. T., Zimmerman, J. B. and Wightman R. M., "Principles of Voltammetry and Microelectrode Surface States", *Journal of Neuroscience Methods*, 48, pp. 225-240, 1993.

[1.33] L. Marangell, M. Martinez, R. Jurdi, H. Zboyan, "Neurostimulation therapies in depression: a review of new modalities", *Acta Psychiatrica Scandinavica*, 116, pp. 174–181, 2007.

[2.1] G. Gerhardt and J. Burmeister, "Voltammetry in vivo for Chemical Analysis of the Nervous System", *Encyclopedia of Analytical Chemistry*, pp. 710-731, 2000.

[2.2] T. Selvaraju and R. Ramaraj, "Electrochemically Deposited Nanostructured Platinum on Nafion Coated Electrode for Sensor Applications", *Journal of Electroanalytical Chemistry*, 585, pp. 290-300, 2005.

[2.3] H. Boo et al, "Electrochemical Nanoneedle Biosensor Based on Multiwall Carbon Nanotube", *Analytical Chemistry*, 78, pp. 617-620, 2006.

[2.4] Y. Ma et al, "Enhanced Sensitivity for Biosensors: Multiple Functions of DNA-Wrapped Single-Walled Carbon Nanotubes in Self-Doped Polyaniline Nanocomposites", *Journal of Physical Chemistry B*, 110, pp. 16359-16365, 2006.

[2.5] M Song et al, "Electrochemical Biosensor Array for Liver Diagnosis Using Silanization Technique on Nanoporous Silicon Electrode", *Journal of Bioscience and Bioengineering*, 103(1), pp. 32-37, 2007.

[2.6] D. Deshpande et al, "Development of a Nanoscale Heterostructured Glucose Sensor Using Modified Microfabrication Processes", *Journal of Micro/Nanolithography, MEMS and MOEMS*, 7(2), 2008.

[2.7] S. Ali et al, "A Nonoxidative Sensor Based on a Self-Doped Polyaniline/Carbon Nanotube Composite for Sensitive and Selective Detection of the Neurotransmitter Dopamine", *Analytical Chemistry*, 79(6), pp 2583–2587, 2007.

[2.8] E. Keefer et al, “Carbon Nanotube Coating Improves Neuronal Recordings”, *Nature Nanotechnology,* 3, pp. 434– 439, 2008.

[2.9] H. Yoon et al, “Aligned Nanowire Growth Using Lithography-Assisted Bonding of a Polycarbonate Template for Neural Probe Electrodes”, *Nanotechnology*, 19(2), 2008.

[2.10] G. Lee et al, “Neurotransmitter Detection by Enzyme-Immobilized CNT-FET“, *Current Applied Physics*, 9, pp. S25-S28, 2009.

[2.11] R. Wagner and W. Ellis, “Vapor-liquid-solid Mechanism of Single Crystal Growth”, *Appllied Physics Letters*, 4, 1964.

[2.12] M. Law, J. Goldberger and P. Yang, “Semiconductor Nanowires and Nanotubes”, *Annual Review of Materials Research*, 34, pp. 83-122, 2004.

[3.1] J. C. Hoogvliet, M. Dijksma, B. Kamp, and W. P. van Bennekom, "Electrochemical Pretreatment of Polycrystalline Gold Electrodes To Produce a Reproducible Surface Roughness for Self-Assembly: A Study in Phosphate Buffer pH 7.4", *Anal. Chem.*, Vol. 72, 2000.

[3.2] A. J. Bard and L. R. Faulkner, Electrochemical methods: Fundamentals and Applications, 2nd Ed., *John Willey & Sons, Inc.*, 2001.

[3.3] H. Cao and J.-C. Chiao, “Nanowire Modification to Enhance the Performance of Neurotransmitter Sensors”, *J. of Nanotech. in Eng. and Med.*, Nov, 2010.

[3.4] Hung Cao; Yuan-Bo Peng and J.-C. Chiao. "An Integrated Flexible Implantable L-glutamate Sensor," *Presented at IEEE sensor conference*, Hawaii, November 2010.

[3.5] W.-D. Huang, H. Cao, S. Deb, M. Chiao, and J.-C. Chiao, “A Flexible pH Sensor Based on the Iridium Oxide Sensing Film,” *Sensors and Actuators, A*, Vol. 169, No. 1, pp. 1-11, Sept. 2011.

[3.6] C. M. Nguyen, H. Cao, W. D. Huang, and J-C. Chiao, "An Electro-Deposited IrOx Thin Film pH Sensor," *BMES Biomedical Engineering Society Annual Meeting*, Hartford, Oct. 12-15, 2011.

[4.1] C. N. Woolsey, T. C. Erickson, and W. E. Gilson, "Localization in somatic sensory and motor areas of human cerebral cortex as determined by direct recording of evoked potentials and electrical stimulation," *Journal of Neurosurgery*, 51(4), 476-506 (1979).

[4.2] J. L. Vitek, "Deep brain stimulation: how does it work?," *Cleveland Clinic Journal of Medicine*, 75(Suppl 2), S59 (2008).

[4.3] K. Kumar, C. Toth, and R. K. Nath, "Deep Brain Stimulation for Intractable Pain: A 15-Year Experience," *Neurosurgery*, 40(4), 736-747 (1997).

[4.4] J. Wells, C. Kao, K. Mariappan et al., "Optical stimulation of neural tissue in vivo," *Opt. Lett.*, 30(5), 504-506 (2005).

[4.5] H. Hirase, V. Nikolenko, J. H. Goldberg et al., "Multiphoton stimulation of neurons," *J. Neurobiol.,* 51(3), 237-247 (2002).

[4.6] E. M. Callaway, and L. C. Katz, "Photostimulation using caged glutamate reveals functional circuitry in living brain slices," *Proc Natl Acad Sci U S A*, 90(16), 7661-5 (1993).

[4.7] B. V. Zemelman, G. A. Lee, M. Ng et al., "Selective Photostimulation of Genetically ChARGed Neurons," *Neuron, 33(1),* 15-22 (2002).

[4.8] G. Nagel, T. Szellas, W. Huhn et al., "Channelrhodopsin-2, a directly light-gated cation-selective membrane channel," *Proc. Nat. Acad. Sci*., 100(24), 13940-13945 (2003).

[4.9] E. S. Boyden, F. Zhang, E. Bamberg et al., "Millisecond-timescale, genetically targeted optical control of neural activity," *Nat Neurosci*, 8(9), 1263-1268 (2005).

[4.10] B. Schobert, and J. K. Lanyi, "Halorhodopsin is a light-driven chloride pump," *J. Biol. Chem*., 257(17), 10306-10313 (1982).

[4.11] X. Han, and E. S. Boyden, "Multiple-Color Optical Activation, Silencing, and Desynchronization of Neural Activity, with Single-Spike Temporal Resolution," *PLoS ONE,* 2(3), e299 (2007).

[4.12] S. K. Mohanty, R. K. Reinscheid, X. Liu et al., "In-Depth Activation of Channelrhodopsin 2-Sensitized Excitable Cells with High Spatial Resolution Using Two-Photon Excitation with a Near-Infrared Laser Microbeam," *Biophys. J.*, 95(8), 3916-3926 (2008).

[4.13] F. Zhang, A. M. Aravanis, A. Adamantidis et al., "Circuit-breakers: optical technologies for probing neural signals and systems," *Nat Rev Neurosci*, 8(8), 577-581 (2007).

[4.14] K. Deisseroth, "Optogenetics," Nat Meth, 8(1), 26-29 (2011).

[4.15] A. Alexander, L.-P. Wang, F. Zhang et al., "An optical neural interface: in vivo control of rodent motor cortex with integrated fiberoptic and optogenetic technology," *J. Neural Eng.,* 4(3), S143 (2007).

[4.16] B. McGovern, R. B. Palmini, N. Grossman et al., "A New Individually Addressable Micro-LED Array for Photogenetic Neural Stimulation," *Biomedical Circuits and Systems, IEEE Transactions on*, 4(6), 469-476 (2010).

[4.17] P. K. Campbell, K. E. Jones, R. J. Huber et al., "A silicon-based, three-dimensional neural interface: manufacturing processes for an intracortical electrode array," *Biomedical Engineering, IEEE Transactions on*, 38(8), 758-768 (1991).

[4.18] M. Maher, J. Pine, J. Wright et al., "The neurochip: a new multielectrode device for stimulating and recording from cultured neurons," *Journal of Neuroscience Methods*, 87(1), 45-56 (1999).

[4.19] R. D. Traub, and R. K. Wong, "Cellular mechanism of neuronal synchronization in epilepsy," *Science*, 216(4547), 745-7 (1982).

[4.20] L. Gu, S. Shivalingaiah, M. Ficinski et al., "Non-viral delivery and optimized optogenetic stimulation of retinal ganglion cells led to behavioral restoration of vision," *Nat. Precedings*, 2012.

[4.21] J. Zhang, F. Laiwalla, J. A. Kim et al., "Integrated device for optical stimulation and spatiotemporal electrical recording of neural activity in light-sensitized brain tissue," *J Neural Eng,* 6(5), 055007 (2009).

[4.22] T. W. Christian, G. B. Jacob, M. Patrick et al., "A wirelessly powered and controlled device for optical neural control of freely-behaving animals," *Journal of Neural Engineering,* 8(4), 046021 (2011).

[5.1] H. Y. Gu, A. M. Yu, and H. Y. Chen, "Direct Electron Transfer and Characterization of Hemoglobin Immobilized on a Au Colloid–Cysteamine-Modified Gold Electrode", *Journal of Electroanalytical Chemistry*, 516, 2001.

[5.2] Huang, C., J. Jiang, E.I. Meletis, M. Lu, L. Sun, and Y. Hao. Capturing electrochemically evolved nanobubbles by electroless deposition - a facile route to synthesis of hollow nanoparticles. *Nano Letters, 9* (12), 429 2009.

[6.1] Medical Data International, Market and Technology Reports, *U.S. Markets For Pain Management Products,* Report RP-821922, June 1999.

[6.2] J. Reggia, E. Ruppin, R. Berndt, Neural Modeling of Brain and Cognitive Disorders, World Scientific: Singapore, 1996.

[6.3] ABV. Apkarian, SN. Ayrapetian, Pain Mechanisms and Management, *IOS Press*, 1997.

[6.4] K. McCormack, "Signal transduction in neuropathic pain, with special emphasis on the analgesic role of opioids - Part I: The basic science of phenotype expression in normal and regenerating nerves," *Pain Reviews*, Vol.6, pp.3-33, 1999.

[6.5] LH. Finkel, “Neuroengineering models of brain disease,” *Annual Review of Biomedical Engineering,* Vol.2, pp.577-606, 2000.

[6.6] H. Fields, J. Levine, “Pain-Mechanisms and Management,” *West J Med*, Vol. 141, pp. 347-357, 1984.

[6.7] R. North et al., “Failed back surgery syndrome: 5-year follow-up after spinal cord stimulator implantation,” *J. Neurosurg*, Vol.28, pp.692-699, 1991.

[6.8] R. North et al., “Spinal cord stimulation for chronic, intractable pain: experience over two decades,” *J Neurosurg*, Vol. 32(3), pp.384-395, 1993.

[6.9] K. Burchiel et al., “Prospective, multicenter study of spinal cord stimulation for relief of chronic back and extremity pain,” *Spine*, Vol. 21,pp.2786-2794, 1996.

[6.10] T. Cameron, “Safety and efficacy of spinal cord stimulation for the treatment of chronic pain: a 20-year literature review,” *J. Neurosurg: (Spine 3)*, Vol.100,pp.254-67, 2004.

[6.11] E. Kandel, J. Schwartz, T. Jessell, Principles of neural science, New York: McGraw-Hill; 2000.

[6.12] P. Miller, J. Strang, and P. M. Miller, Addiction research method, Addiction Press, Willey-Blackwell, 2010.

BIOGRAPHICAL INFORMATION

Hung Cao was born in Haiphong, Vietnam. He received his Bachelor degree in Electronics and Telecommunications from Hanoi University of Technology, Hanoi, Vietnam in 2003. He received his Master of Science in Electrical Engineering from The University of Texas at Arlington in August 2007 with the thesis "Evaluation and Applications of Gas Sensors". From 2008, he joined The University of Texas at Arlington, pursuing his PhD degree in Electrical Engineering. He has been working as instructor/research/teaching associate and conducting various research projects at UT Arlington, UT Austin and UT Dallas.

His current research interests include MEMS, micro/nano fabrication, sensors and optics for biomedical applications. His PhD thesis topic is about fabrication and modification of long-term implantable probes used in studies of the nervous system.